Author:
Prouse, Lauren J

Title:
Evaluating CMIP6 simulations of historical Sahelian precipitation variability and potential links to future projections

Author:
Prouse, Lauren J

Title:
EVALUATING CMIP6 SIMULATIONS OF HISTORICAL SAHELIAN PRECIPITATION VARIABILITY AND POTENTIAL LINKS TO FUTURE PROJECTIONS

EVALUATING CMIP6 SIMULATIONS OF HISTORICAL SAHELIAN PRECIPITATION VARIABILITY AND POTENTIAL LINKS TO FUTURE PROJECTIONS

LAUREN PROUSE

JANUARY 2022

Presented as part of, and in accordance with, the requirements for the Final Degree of Masters by Research in Global Environmental Challenges, at the University of Bristol, Faculty of Science - School of Geographical Sciences, January 2022

University of BRISTOL
School of Geographical Sciences

CERTIFICATION OF OWNERSHIP OF THE COPYRIGHT IN A TYPESCRIPT OR MANUSCRIPT

Dissertation presented as part of, and in accordance with, the requirements for the Final Degree of Masters by Research at the University of Bristol, School of Geographical Sciences and the Cabot Institute for the Environment.

I hereby assert that I own exclusive copyright in the item named below. I give permission to the University of Bristol Library to add this item to its stock and to make it available for use and re-copying by its readers.

AUTHOR	LAUREN PROUSE
TITLE	EVALUATING CMIP6 SIMULATIONS OF HISTORICAL SAHELIAN PRECIPITATION VARIABILITY AND POTENTIAL LINKS TO FUTURE PROJECTIONS.
DATE OF SUBMISSION	21st JANUARY 2022

Signed:

…….....

Full name:
…….....LAUREN PROUSE.....

Date:
…….....21/01/22….....

ABSTRACT

The Intergovernmental Panel on Climate Change has recognised the Sahel region in Africa as a hotspot for the effects of climate change due to its economic and environmental vulnerability to changes. Its climate is driven by the West African Monsoon (WAM) which occurs during the June to September season, accounting for ~75% of annual precipitation. Modelling the WAM has many associated uncertainties, predominantly linked to precipitation and its occurrence on the sub-grid-scale. Previous projections for the Sahel have covered both extremes of wetting and drying, complicating policymaking, and reinforcing the need for confidence in projections. This study has examined the output from the sixth phase of the Coupled Model Intercomparison Project for monsoon season precipitation over the Sahel. Models were initially evaluated by comparing historical simulations to observations. No model well represented the wet period of the 1950s and the dry period of the 1970s. However, atmosphere-only models using prescribed sea surface temperatures performed much better with considerably higher correlation coefficients at decadal time scales. This suggests that representing ocean processes (and their coupling) remains a major limitation on simulating decadal precipitation over the Sahel. Projection anomalies revealed an inter-model range of +2mm/day to -1mm/day for SSP1-2.6 which increased to +4mm/day to -2mm/day for SSP5-8.5. Following this, these projections were analysed in the context of historical model performance. There is no clear link between historical model performance and their respective projections, but historical model behaviour partially explains the differences in projections. However, this study highlights the range of potential impacts for the Sahel should global warming not be limited. Although, there is no guarantee the climate system will behave the same way as it did in the past, improving historical model performance, specifically ocean representation and its coupling, could add confidence to projections for the Sahel.

WORD COUNT: 24703

AUTHOR DECLARATION

I declare that the work in this dissertation was carried out in accordance with the requirements of the University's Regulations and Code of Practice for Research Degree Programmes and that it has not been submitted for any other academic award. Except where indicated by specific reference in the text, the work is the candidate's own work. Work done in collaboration with, or with the assistance of, others, is indicated as such. Any views expressed in the dissertation are those of the author.

I completed the analysis and wrote up the thesis myself. Professor Paul Valdes and Dr Rachel James supervised this project and provided guidance during my degree. Paul contributed to the initial planning of this Masters by Research through helping me to develop a proposal that originated from my undergraduate dissertation and how to start a research degree. He also advised on the usage of the BluePebble server and using it to download observational datasets and how to handle the CMIP data. Rachel's expertise in African climate science helped me to understand key processes and which observational datasets to include. She also supported me in learning how to code using Python and how to navigate errors when they arose. Both provided feedback throughout which was helpful for restructuring the thesis.

SIGNED: 

DATE: 21/01/22

PERSONAL ACKNOWLEDGEMENTS

I would like to thank Professor Paul Valdes for agreeing to supervise me for a second time, helping me to develop this project and for his expertise this year – particularly in navigating the world of the Geography computer servers! Another thank you is to Dr Rachel James for being my secondary supervisor. Despite having only met in person twice, her guidance for using Python and knowledge on African climate science has been instrumental on this project.

I cannot begin to express my thanks to my family whose unwavering support got me through this degree – from being patient with me with working from home in Cornwall and knowing when to get me to take a break (even when I was in Bristol!) to bringing me everything I needed when I had Covid-19.

I am grateful to my friends for their support throughout the highs and lows of the last 18 months, the countless walks around Bristol and Zoom calls during lockdowns.

Thanks should also go to all of the staff members in the Geography department who have believed in me and provided helpful advice and guidance throughout my four, nearly five, years here.

A final thank you is to those who have agreed to be my examiners and assess my work, I really appreciate it.

TECHNICAL ACKNOWLEDGEMENTS

This work was carried out using the computational facilities of the Advanced Computing Research Centre, University of Bristol.

I acknowledge the World Climate Research Programme, which, through its Working Group on Coupled Modelling, coordinated and promoted CMIP6. I thank the climate modeling groups for producing and making available their model output, the Earth System Grid Federation (ESGF) for archiving the data and providing access, and the multiple funding agencies who support CMIP6 and ESGF. See Appendix 2 for the list of models from the Coupled Model Intercomparison Project 6 (CMIP6) that were used and their associated citations.

Observational datasets were downloaded from their respective locations and adapted to this study's requirements:

- **Climate Hazards group Infrared Precipitation with Stations (CHIRPS)** - provided by the University of California at Santa Barbara and the United States Geological Survey and downloaded from https://www.chc.ucsb.edu/data/chirps (Funk et al, 2019).
- **Climatic Research Unit Time-Series version 4.04 (CRU**) – provided by the University of East Anglia Climatic Research Unit and downloaded from https://catalogue.ceda.ac.uk/uuid/c26a65020a5e4b80b20018f148556681 (Harris et al, 2020; University of East Anglia Climatic Research Unit, 2020)
- **European Centre for Medium-Range Weather Forecasts Reanalysis Dataset 5 (ERA5)** – provided by the European Centre for Medium-Range Weather Forecasts. *Generated using Copernicus Climate Change Service Information [2021] and contains modified Copernicus Climate Change Service Information [2021]* (Hersbach et al, 2020).
- **European Centre for Medium-Range Weather Forecasts Reanalysis Dataset 5 Land (ERA5-Land)** – provided by the European Centre for Medium-Range Weather Forecasts. *Generated using Copernicus Climate Change Service Information [2021] and contains modified Copernicus Climate Change Service Information [2021]* (Muñoz-Sabater, 2019).
- **Global Precipitation Climatology Centre Full Data Reanalysis Product (GPCC)** – provided by the NOAA/OAR/ESRL PSL, Boulder, Colorado, USA, from their website at https://psl.noaa.gov/data/gridded/data.gpcc.html (Global Precipitation Climatology Center, 2020).
- **Hadley Centre Sea Ice and Sea Surface Temperature dataset (HadISST)** – provided by the Met Office Hadley Centre and downloaded from https://www.metoffice.gov.uk/hadobs/hadisst/data/download.html (Rayner et al, 2003).
- **Tropical Applications of Meteorology using Satellite data and ground-based observations (TAMSAT)** – provided by the University of Reading and downloaded from https://www.tamsat.org.uk/data (Maidment et al, 2014; Tarnavsky et al, 2014).

TABLE OF CONTENTS

LIST OF TABLES

LIST OF FIGURES

1. Introduction

Between 1901 and 2010, global surface air temperature (SAT) increased by an estimated ~0.07^{o}C each decade (Barry et al, 2018). Africa in particular has seen warming of at least 0.5^{o}C over the last 50 to 100 years, and by the end of the 21st century, temperatures could be up to 6^{o}C higher than the 20th century average temperature (Niang et al, 2014), depending on the scenario. Climate projections are generated through running simulations using general circulation models (GCMs) under a range of scenarios, the latest version being called Shared Socioeconomic Pathways in the Intergovernmental Panel for Climate Change's (IPCC) Sixth Assessment Report (AR6) (IPCC, 2021). These warming trends over the last 100 years can no longer be attributed to natural variability alone, so other factors are coming into play, associated with global warming (Niang et al, 2014). Radiative forcing due to anthropogenic greenhouse gases (GHGs) is increasing faster than the reduction in radiative forcing from anthropogenic aerosols, hence the warming from the GHGs outweighs the cooling from the reduced aerosols (Tebaldi et al, 2021).

The IPCC has recognised the Sahel region in Africa as a hotspot for the effects of climate change, signifying its economic and environmental vulnerability to potential changes (Niang et al, 2014; Sultan and Gaetani, 2016). The Sahel's climate is naturally highly variable, being susceptible to both droughts and flooding (Monerie et al, 2020). Over the last 50 years, observed temperatures have warmed in all seasons, with annual maximum temperatures increasing by 0.16^{o}C and annual minimum temperatures by 0.28^{o}C per decade – both statistically significant increases (Barry et al, 2018). The region's climate is driven by the West African Monsoon (WAM) which has a wet phase during June, July, August and September (JJAS) and a dry phase during January, February and March (JFM) (Quagraine et al, 2020). The JJAS wet phase is characterised by south-westerly winds and accounts for ~75% of West African annual precipitation, whereas the JFM dry phase has north-easterly winds (Akinsanola and Zhou, 2019; Quagraine et al, 2020). The principal driving force behind the change in wind is the land-sea temperature gradient between the Sahel and the equatorial Atlantic (Nicholson, 2013). Changes in the WAM can have detrimental impacts on the region, as seen with prolonged droughts which occurred during the 1970s and 1980s (Sultan and Gaetani, 2016). Since the vast majority of precipitation falls during the wet season, these droughts correspond to reduced precipitation during the wet season. The drought has been attributed to sea surface temperature (SST) anomalies, but 40 years later, the interaction between the different mechanisms behind the droughts are still being researched (Sultan and Gaetani, 2016; Monerie et al, 2020). Feedbacks being considered are linked to changes in SSTs, vegetation and aerosols (e.g. Haarsma et al 2005; Sheen et al, 2017; Giannini and Kaplan, 2019).

Projections show a range of potential outcomes for the Sahel, from intense drying to overwhelming wetting, with a subset of CMIP6 models suggesting an increase in the number of extreme hot days as well as extremely wet days (Vogel et al, 2020; Elagib et al, 2021). This lack of clarity makes policy making and mitigation planning more complicated (Sultan and Gaetani, 2016). There are also indications that by 2100, the Sahel could be over 5^{o}C warmer than other parts of the continent (James

et al, 2015). Temperature fluctuates within a narrow range over the Sahel, thus unprecedented climate changes are likely to occur earlier here compared to the global average (Niang et al, 2014). This will have knock-on impacts to local populations through affecting agriculture – the basis of their livelihoods (Bamba Sylla et al, 2016).

GCM performance is tested by comparing historical simulations to observations and the complex nature of Sahelian precipitation means models often struggle with reproducing the observations (Lau et al, 2006; Sheen et al, 2017; IPCC, 2021). Within the third and fifth phases of the Coupled Model Intercomparison Project (CMIP), the broad range of projections for the Sahel were partially attributed to the sensitivity of Sahel precipitation to global climate changes (Caminade and Terray, 2010; Biasutti, 2013; Sultan and Gaetani, 2016). Precipitation is hard to capture within models as it occurs on the sub-grid-scale, hence parameterisations are needed (Biasutti, 2013; Sultan and Gaetani, 2016). Also, Sahelian precipitation is connected to so many different circulation systems, both locally and globally (Figure 1.1), adding further complications to model representation (Sultan and Gaetani, 2016). The Sahel's warming projections imply improving simulations of past dry periods, like the 1970s and 1980s droughts, or the wetter period in the 1950s, is important for indications of how precipitation could behave with future warming (Sheffield and Wood, 2008). Should the model not capture the full scale of the drought or wet periods, confidence in their projections can be affected, as a potential extremity in projections is increased droughts with warming (Sheffield and Wood, 2008; Caminade and Terray, 2010; Sheen et al, 2017; Vogel et al, 2020). As a result, there is little consensus and confidence in projections for the 21st century under the differing emission scenarios (Niang et al, 2014; Sultan and Gaetani, 2016; Monerie et al, 2020).

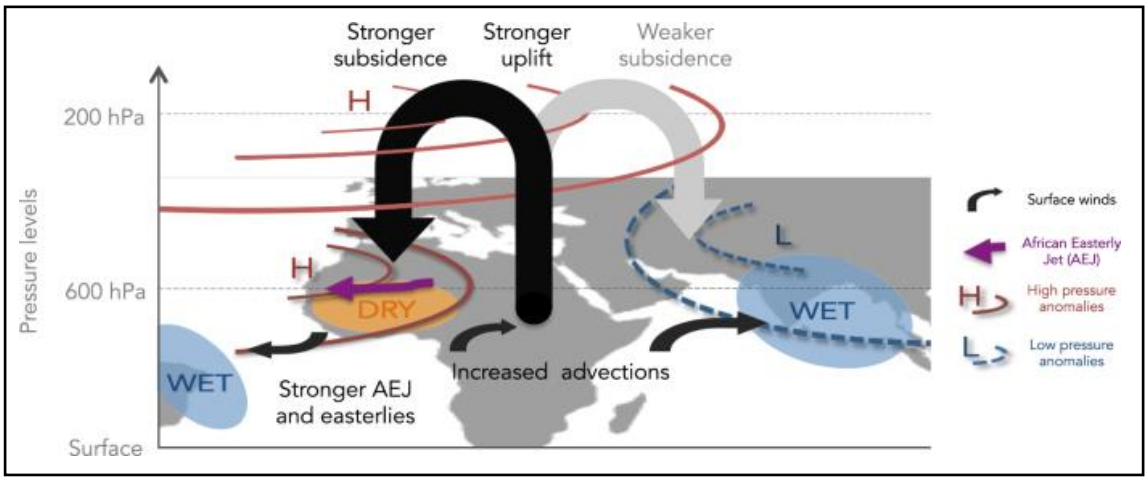

Figure 1.1: *From Vigaud and Giannini (2019, p.7046). Schematic showing the basic circulation of the WAM and teleconnections to other regions, whereby a drier WAM early in the season is associated with a stronger and wetter Indian Monsoon.*

This study aims to examine whether the newer CMIP6 models can reproduce the Sahelian droughts and wet periods and if their ability to do so impacts their future projections for the region. This will be achieved by evaluating historical simulations of Sahelian precipitation and comparing them to observations, exploring what factors affect precipitation representation in the models, and finally examining whether historical model performance informs understanding of future projections.

2. Literature Review

2.1. Sahel droughts

2.1.1. Observations

Approximately 75% of precipitation over the Sahel falls during June, July, August and September (JJAS) due to the West African Monsoon (WAM) (Quagraine et al, 2020). Hence any changes in annual mean precipitation are reflections of changes in the wet season, and droughts are equivalently reduced wet season precipitation. Most studies focus on changes in JJAS precipitation only. The WAM's south-westerly winds transport moisture into the Sahel from the through the Gulf of Guinea during JJAS, resulting in precipitation (Nicholson, 2013; Sultan and Gaetani, 2016). Precipitation changes over the Sahel have not been consistent over the last 50 to 100 years, with large interannual and interdecadal variability, linked into the WAM (Giannini et al, 2008; Vellinga et al, 2016; Kennedy et al, 2017; Barry et al, 2018). Despite the uncertainty, observations show the Sahel is undergoing strong and fast climate changes through the combination of warming and the WAM recovery, which has resulted in extreme climate events becoming more frequent (Sultan and Gaetani, 2016). Between 1901 and 1950s, precipitation was higher than today, but between 1960 and 1980, it was lower with droughts during the 1970s and 1980s (Niang et al, 2014; Kennedy et al, 2017; Monerie et al, 2020). Precipitation has been increasing since, however, it is still relatively low compared to the pre-drought values (Kennedy et al, 2017). The reason for the increasing precipitation is not conclusive, as it could be due to natural variability or anthropogenic climate change (Sultan and Gaetani, 2016; Barry et al, 2018). During the droughts, different areas in the region experienced different levels of reduced precipitation, ranging from a decline of 15% to over 30% (Barry et al, 2018). Paleoclimatic data has revealed that droughts of this extent have happened before in the Sahel and West Africa, so this is not an unusual event on these longer geological timescales (Biasutti, 2013).

2.1.2. Potential drivers of the drought

Many alternative processes that led to the droughts have been suggested. Among the frequently mentioned are changes in sea surface temperatures (SSTs) in the Atlantic and Indian Oceans (Mohino et al, 2011; Barry et al, 2018). SSTs can influence WAM variability though various feedbacks with the atmosphere. A stronger difference between the Northern and Southern Hemisphere is a key SST pattern associated with the drought (Folland et al, 1986). The temperature gradient between the Sahara and SSTs in the Gulf of Guinea has also been found to influence the WAM and Sahelian precipitation (Haarsma et al, 2005; Monerie et al, 2017). Land-atmosphere feedbacks can amplify changes in precipitation arising from SST variability (Giannini et al, 2003). Changes in tropical SSTs initiate Kelvin and Rossby waves that spread across the Equator, and upon reaching the Sahel they interact and alter the region's circulation (Lau et al, 2006; Sultan and Gaetani, 2016; Gaetani et al, 2017; Monerie et al, 2020). Increased convection over the oceans results in the convergence over the land weakening, reducing precipitation through there being less monsoonal moisture

(Giannini et al, 2003; Lau et al, 2006). Thus, moisture is reduced over land, affecting evaporation, exacerbating any drought periods (Giannini et al 2003; Lau et al, 2006).

Local SST feedbacks are important but Folland et al (1986) first showed that global feedbacks are also important in Sahelian precipitation variability. A comparison of the five driest and five wettest years between 1945 and 1985 found warmer SSTs in the Indian, South Atlantic and south-east Pacific Oceans, and cooler SSTs in the Mediterranean Sea, North Atlantic and North Pacific Oceans in the drier years (Folland et al, 1986). A subsequent study by Giannini et al (2003) reiterated the importance of both local and remote SST influences on Sahelian precipitation. Reduced precipitation over the Sahel was found to be associated with warmer SSTs in the tropical Pacific and Indian Oceans (Giannini et al, 2003). They attributed the variability in precipitation between the 1960s and 1980s to a warming trend in the Indian Ocean equatorial SSTs, with the impacts being amplified by land-atmosphere feedbacks, as discussed previously (Giannini et al, 2003; Lau et al, 2006).

Vegetation feedbacks have also been implicated in the droughts, for example, desertification has both natural and human causes and accentuates the impacts of decreased precipitation due to the reduced ability of the soil to take up moisture (Kucharski et al, 2013). Although over time, evidence has suggested desertification had a smaller role in the droughts that originally thought (Fensholt et al, 2017). Moreover, the Sahel region neighbours the Sahara which is an important dust source, and release of Saharan dust can interact with the WAM but there is limited research on its role in the drought (N'Datchoh et al, 2018; Bercos-Hickey et al, 2020). However, the effects of different feedbacks on climate variability in the Sahel makes it hard to draw robust conclusions on exactly how all the different drivers contribute (Martin and Thorncroft, 2014).

Some have questioned whether human activities caused the droughts. They most likely had an influence through global warming affecting feedback mechanisms between the land, ocean and atmosphere (Dong and Sutton, 2015; Sheen et al, 2017; Giannini and Kaplan, 2019). However, experiments forced by only GHGs do not show drying of the Sahel, suggesting that anthropogenic reflective aerosols played a more important role (Biasutti and Giannini, 2006). The interhemispheric SST gradient was adjusted by the Northern Hemisphere aerosol emissions dampening the warming from GHGs, leading to drying over the Sahel (Biasutti and Giannini, 2006). Although, it has also been suggested global warming contributed 10% to the changes in SSTs that supported drought conditions (Mohino et al, 2011).

Since the droughts, observations demonstrate a recovery in Sahelian and West African precipitation (Giannini et al, 2008; Kennedy et al, 2017). There are several possible reasons for this recovery, but published literature is not conclusive. One hypothesis is that the recovery is linked to SST changes: the difference between SSTs in Northern Hemisphere extratropics and tropics have driven the tropical rainbelt northward, bringing more precipitation to West Africa (Park et al, 2015). However, this influence is not very well understood, and there are many papers with conflicting results due to the numerous other factors that impact the gradient, such as cloud cover and changes in Arctic sea ice (Deser et al, 2015; Hwang and Frierson, 2013; Monerie

et al, 2020). Others argue precipitation has increased with increased atmospheric GHGs, resulting in a greater contrast in land and sea temperatures, but this has not been proven (Barry et al, 2018). It has also been suggested increased atmospheric GHGs has impacted the WAM through the initiation of thermodynamic feedbacks with regional warming, increasing precipitation (Dong and Sutton, 2015; Akinsanola and Zhou, 2019).

2.2. Circulation over the Sahel

Precipitation is typically found over the west Sahel, from 5ºN to 15ºN (Akinsanola and Zhou, 2019). Two of the maximum rainfall areas are found over the Guinea Coast region, where there is high topography, despite having a mini dry season of reduced rainfall at the same time as peak monsoon over the Sahel during August (Akinsanola and Zhou, 2019). The precipitation belt retreats south during October (Akinsanola and Zhou, 2019). The Inter-Tropical Discontinuity (ITD) is around 11ºN, and just south of 9ºN, where there are strong westerlies that converge at low levels at the Intertropical Convergence Zone (ITCZ), dividing the northern dry air and southern moist air (Lavaysse et al, 2010; Akinsanola and Zhou, 2019). The WAM takes place between late June and late September and accounts for ~80% of the annual rainfall (Sultan and Gaetani, 2016; Monerie et al, 2020). Alongside the previously discussed SSTs, the WAM's dynamics are inherently linked to other parts of Sahelian circulation, including African Easterly Jet (AEJ), African Easterly Waves (AEWs) and the West African Heat Low (WAHL) (Parker et al, 2005; Lavaysse et al, 2010; Vellinga et al, 2016; Brannan and Martin, 2018; Figure 2.1).

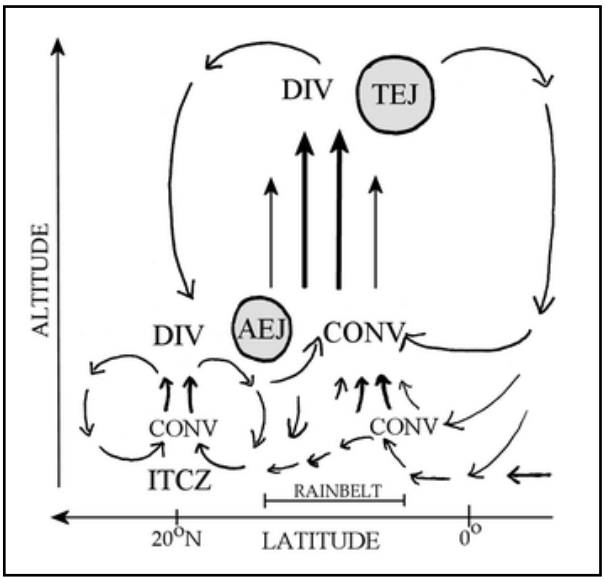

Figure 2.1: *A schematic diagram of the West African Monsoon, from Nicholson (2009, p.1167), with some key circulation elements. TEJ is Tropical Easterly Jet, AEJ is the African Easterly Jet, DIV is divergence of winds and CONV is convergence of winds.*

The AEJ is found at 15ºN in August, at ~600-700hPa in the mid-troposphere (Parker et al, 2005; Sultan and Gaetani, 2016). It is thought to be a foundation in maintaining the WAM's momentum balance, as it "is known to be in approximate

thermal-wind balance with the thermodynamic contrasts from the Guinea Coast to the Sahara" (Parker et al, 2005, p.2840). The AEJ impacts Sahelian weather systems, predominantly precipitation, as "the lower-tropospheric easterly component of wind shear with height is favourable for the generation of intense and long-lived cumulonimbus systems" (Parker et al, 2005, p.2840). The AEJ location and strength changes over the year but is usually strongest in summer, between 10^{o}N and 15^{o}N (Brannan and Martin, 2018).

AEWs have two tracks, one north of the AEJ and one south (Sultan and Gaetani, 2016; Brannan and Martin, 2018). AEWs have an influence on precipitation over the Sahel, but also on tropical cyclones that form off the continent and move westwards towards the Caribbean (Sultan and Gaetani, 2016; Brannan and Martin, 2018). They are disturbances on the synoptic scale that travel from North Africa to the Atlantic Basin, have 2000-4000km wavelengths on 2-10 day periods (Brannan and Martin, 2018). The northern track waves are strongest at around 850hPa and found close to the Sahara where there is less moist convection, which means northern track AEWs do not have as much influence on precipitation but do have a large role in Saharan dust transport (Lavaysse et al, 2010; Brannan and Martin, 2018). Southern track AEWs are found near the ITCZ, being strongest at ~600-700hPa, affecting tropical cyclones after leaving West African coast (Brannan and Martin, 2018). AEWs affect mesoscale convective systems, and AEWs that are longer in duration and more intense have been found to be associated with anomalously rainy summer seasons (Brannan and Martin, 2018).

The WAHL is a thermal depression at low levels over Northern Africa, affecting the WAM through its seasonal cycle, particularly preceding the monsoon season (Lavaysse et al, 2016). It impacts the WAM through its anticyclonic circulation in the mid-troposphere and helps maintain the AEJ through the temperature gradient between the WAHL and the rain belt (Lavaysse et al, 2010). During the summer, it is known as the Saharan Heat Low (SHL) as it is found primarily over the Sahara Desert (Lavaysse et al, 2016; Sultan and Gaetani, 2016). Satellite data revealed in the late summer of 2006, there was an event where the SHL weakened despite increased convective activity over the northern Sahel at the beginning of September (Lavaysse et al, 2010). It is thought the weakening was due to stronger easterly waves and influences from extratropical sources, such as one particularly detrimental one from Europe on 5th September (Lavaysse et al, 2010). There is some evidence of the connection between the WAHL/SHL and the WAM in various studies through the effect of dry air disturbing the circulation (see Covreux et al, 2010; Flaounas et al, 2012).

2.3. Climate Models

2.3.1. Coupled Model Intercomparison Project (CMIP)

The Coupled Model Intercomparison Project (CMIP) originally began 24 years ago "as a comparison of a handful of early global coupled climate models performing experiments using atmosphere models coupled to a dynamic ocean, a simple land surface, and thermodynamic sea ice" (Eyring et al, 2016, p.1938). It is now an international scale research effort with publicly available data and provides data for

the IPCC reports (Eyring et al, 2016). CMIP's objective is to "better understand past, present, and future climate change arising from natural, un-forced variability or in response to changes in radiative forcings in a multi-model context" (Eyring et al, 2016, p.1938). Over time, CMIP has become more complex in response to climate model developments, with the more recent phases beginning in 2008 (CMIP5) and the sixth phase – CMIP6 – in 2014 (Taylor et al, 2012; Eyring et al, 2016). CMIP6 aims to fill research gaps through examining the Earth's response to different forcings, the origin of systematic biases and the impact on models (Eyring et al, 2016). It also allows for investigation of how uncertainties and climate variability in models can affect future climate change (Eyring et al, 2016). To help address these, there are 21 Model Intercomparison Projects associated with CMIP6, including HighResMIP which analyses regional phenomena at high resolution and CORDEX which investigates how regional downscaling of various model output can advance scientific knowledge (Eyring et al, 2016). The models used have uncertainties and display a wide range of projections for various parts of the climate system, such as those shown over the Sahel in Figure 2.2. The strength of CMIPs is that they show the likely uncertainties due to model representations of key processes. However, a challenge of CMIPs is that the models all vary so much in structure and with parameterisations, therefore it is hard to attribute differences in results to specific elements of the models.

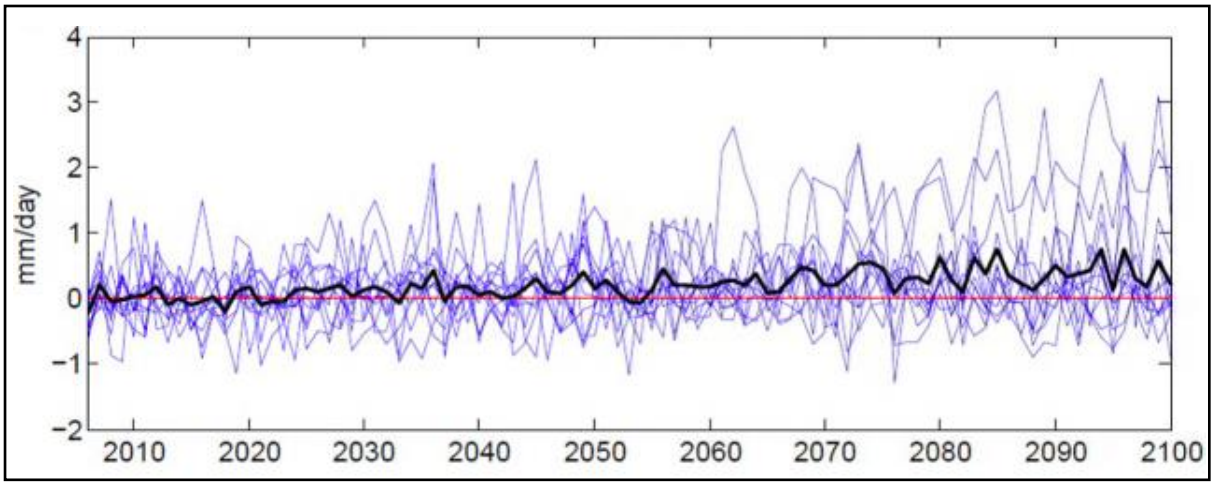

Figure 2.2: *Adapted from Sultan and Gaetani (2016). Projected changes in July to September monsoon season precipitation (mm/day), with the end of 21st century RCP8.5 projections calculated as the difference between the average of 2006-2015 and the 2081-2100 average, for 12 CMIP5 models. The black line reflects the average of the subset of models.*

2.3.2. Historical simulations over the Sahel

Precipitation over the Sahel varies on interannual and decadal timescales and is affected by various feedback mechanisms, making changes complicated to analyse (Akinsanola and Zhou, 2019; Monerie et al, 2020). There is limited agreement on the interactions between the drivers of precipitation variability and lots of models have biases which reduce confidence in conclusions (Biasutti, 2013). Factors involved include dynamic changes in wind strength and direction, thermodynamic changes in boundary layer specific humidity, SST variation impacting the Hadley Cell and tropical

precipitation, vegetation and dust feedbacks and moisture availability (Biasutti, 2013; Vellinga et al, 2016; Monerie et al, 2020). Vegetation and dust feedbacks associated with soil moisture are often missed in coupled models as SSTs influence these feedbacks through circulation, thus if the SSTs are incorrect, the feedbacks could be missed (Kucharski et al, 2013). Sultan and Gaetani (2016) argue models have improved with time, but they struggle with "large scale mechanisms which influence the regional atmospheric circulation" (p.4) and teleconnections associated with African climate. It has been suggested improving how models reproduce past observations could increase confidence in model projections for precipitation (Brannan and Martin, 2018). However, resolving past issues may not fully reduce uncertainties in projections because the climate system may not behave the same way as it did in the past (Sultan and Gaetani, 2016).

Evaluating CMIP3 and CMIP5 historical simulations revealed complications in understanding West Africa's response to climate change (Caminade and Terray, 2010; Biasutti, 2013). Complications are associated with precipitation's internal variability being strongly linked with feedbacks between the land, ocean and atmosphere, and the influence of GHGs on these (Caminade and Terray, 2010). Only one CMIP3 model was found to reproduce observations of the Sahel droughts well, having a correlation coefficient greater than 0.4, reflecting the limitations in models (Caminade and Terray, 2010). A similar study was conducted by Biasutti (2013) using CMIP5 models, which do reproduce the spatial drying trends over the Sahel in the 20th century, although displaced slightly south compared to observations. Nevertheless, biases that were present in CMIP3 are still retained in CMIP5 models (Biasutti, 2013). These include missing the Gulf of Guinea's cold tongue during the monsoon season – typically cooler SSTs than the surrounding oceans - and the incorrect location of the Sahelian precipitation band, along with circulation elements like the AEJ and AEWs (Biasutti, 2013). This is not helped by parameterisations of model elements and missing components like vegetation feedbacks (Biasutti, 2013).

Out of the 19 coupled GCMs included in Lau et al (2006)'s study, chosen from IPCC AR4 models used (CMIP3), only eight reproduced the Sahel droughts reasonably well and seven of them produced precipitation during the drought period. Even the most skilled model struggled with the start of the drought event and how long the event lasted for (Lau et al, 2006). Models were evaluated using the Standardised Precipitation Index (SPI) which is "a probabilistic type of drought monitoring index and is calculated via a nonlinear transformation that converts the precipitation data into a normally distributed, dimensionless random variable SPI" (Lau et al, 2006, p.3). The modelled SPI was compared to the observed SPI, with a drought being defined relative to the long-term historical precipitation trends (Lau et al, 2006). Correlation coefficients higher than 0.26 were classified as reasonable agreement (Lau et al, 2006), which is not that strong a coefficient, indicating the model struggles with simulating historical Sahelian precipitation. The authors concluded models need SSTs to be strongly coupled with Sahelian precipitation in both the Indian and Atlantic Oceans, alongside "a robust land surface feedback with strong sensitivity of precipitation and land evaporation to soil moisture" (Lau et al, 2006, p.9), to represent the droughts well.

However, even with numerous developments since CMIP3, models are still struggling with some of these elements through the interconnected nature of Sahelian circulation (Monerie et al, 2020).

Models have struggled representing the WAM and its precipitation on all timescales (Parker et al, 2005; Paxian et al, 2016). More recent research has tried to address this using Regional Climate Models (RCMs) to resolve biases, but these have had mixed results (Paxian et al, 2016). Monsoon precipitation tends to be from "organized convection, such as squall lines and large mesoscale convective systems", however this is usually missed by model resolution (Vellinga et al, 2016, p.326). In many GCMs, Sahel precipitation is underestimated when compared to observations, which has been improved by downscaling and using RCMs, but the positive bias over the Guinea Coast has been enhanced (Paxian et al, 2016). RCMs with coupled atmosphere and ocean components have helped reduce the precipitation biases associated with Atlantic SSTs and the WAM, but these are not yet fully resolved (Paxian et al, 2016).

RCMs have revealed the importance of the multiscale connections between convection and circulation, elements signifying the need for higher model resolution when examining the Sahel, as GCMs have previously missed these (Vellinga et al, 2016). It has been found increasing model resolution did improve representation of precipitation observations due to convective precipitation being more strongly coupled with circulation in higher resolution models (Vellinga et al, 2016). This study used the Met Office UM atmosphere model at 25km resolution which when compared to the lower resolution 130km model, could generate precipitation twice as efficiently, originating from the large-scale circulation providing more moisture (Vellinga et al, 2016). Circulation changes were analysed through prescribing historical SSTs in the models for the period 1984 to 2008, as this is when precipitation recovery began over the Sahel (Vellinga et al, 2016). It was found that changes in East Pacific and Atlantic SSTs cause an anomalous Walker circulation in the models forced by SSTs compared to their equivalent that were not (Vellinga et al, 2016). Changes seen include westerlies from the Atlantic below 850 hPa, easterlies above 700 hPa and AEJ intensification (Vellinga et al, 2016). More moisture was brought into the Sahel, corresponding with an increase in precipitation (Vellinga et al, 2016). The AEJ strengthened, promoting stronger moisture divergence, which could reduce precipitation, but the synoptic AEWs disturbed the AEJ, leading to low-level convergence and convective precipitation (Vellinga et al, 2016). This modelled feedback evolved from prescribing SSTs, exemplifying the importance of accurate representation. Overall, they concluded to accurately represent Sahelian precipitation, high resolution models are needed in combination with the correct model physics, although this requires lots of computational power and expense (Vellinga et al, 2016).

Comparing CMIP5 models to a multi-reanalysis mean showed a lot of CMIP5 models can represent the AEWs' seasonal cycle but underestimate their frequency and intensity (Brannan and Martin, 2018). Biasutti (2013) found the CMIP5 models often do not represent the AEWs well. Model resolution and parameterisations are among the likely causes of historical biases (Biasutti, 2013; Brannan and Martin,

2018). The evolution and strength of AEWs is influenced by parameterisations of the planetary boundary layer and convection, and the AEJ's simulation which tends to be better in higher resolution models (Brannan and Martin, 2018). Higher resolution models had the least bias for northern track AEWs, most likely due to them being drier and having weaker convection, thus not as affected by parameterisations (Brannan and Martin, 2018). Conversely, southern track AEWs are associated with higher levels of moisture and convection, hence parameterisations strongly influence their model misrepresentation (Brannan and Martin, 2018). Despite an initial hypothesis that increasing model resolution would improve AEW representation, it was found increasing resolution alone will not solve the problem, as further understanding is needed for precipitation, convection, and latent heat (Brannan and Martin, 2018).

Models tend to have different uncertainties which feed into Sahel precipitation, so to investigate this Monerie et al (2020) took 29 simulations from CMIP5 and 11 from CMIP6 for comparison. A good insight was provided despite more CMIP5 simulations being included than CMIP6 ones (Monerie et al, 2020). Precipitation changes in the chosen models were smaller compared to the overall spread of changes, indicating uncertainties (Monerie et al, 2020). There are more uncertainties associated with dynamic changes in response to climate change – mainly atmospheric circulation – than thermodynamic changes (Monerie et al, 2020). Uncertainties are also amplified by parameterisations as precipitation occurs on a scale smaller than the typical model grid box, which then feeds into the dynamic changes in atmospheric circulation (Brannan and Martin, 2018; Monerie et al, 2020). SSTs also play a role in these dynamic changes, with the temperature gradient in the Northern Hemisphere oceans being particularly influential on Sahelian precipitation (Barry et al, 2018; Monerie et al, 2020). Furthermore, Martin and Thorncroft (2014) found that CMIP5 models which had prescribed SSTs in the nearby Atlantic and Indian Oceans performed better in representing Sahelian precipitation than those that had not been. Overall, there were very little changes in uncertainties between CMIP5 and CMIP6 (Monerie et al, 2020).

2.3.3. Projections for the Sahel

All future precipitation trends over the 21st century in CMIP5 GCMs are significant, but there are some key differences (Biasutti, 2013; Sultan and Gaetani, 2016; Figure 2.2). About half agree precipitation is likely to increase over the Sahel, but a quarter of them suggest precipitation will decrease (Biasutti, 2013; Sultan and Gaetani, 2016; Figure 2.2). This is likely due to the biases associated with SSTs in the models, which has knock-on impacts to the WAM's variability (Sultan and Gaetani, 2016). Also, the model's response to carbon dioxide (CO_2) projections affects regional surface warming and global SSTs (Sultan and Gaetani, 2016).

Based on the ensemble mean of a subset of CMIP5 models, there are statistically significant projections of increased precipitation over east Sahel of 0.2-1mm/day and a decrease over west Sahel – stronger with higher Representative Concentration Pathways (RCPs) (Akinsanola and Zhou, 2019). Preceding the WAM, precipitation is projected to decrease by 0.2-0.5mm/day but increase afterwards by 0.4-0.6mm/day, with this increase being linked to "increased surface evaporation and

enhanced atmospheric moisture convergence" (Akinsanola and Zhou, 2019, p.1029). A similar study using an ensemble of models from the UK Met Office also found throughout the 21st century, the western Sahel is projected to dry by over 2mm/day (James et al, 2015). The decline in precipitation is contradicted by monsoon flow amplification, with increased moisture convergence and stronger uplift near the surface of the west Sahel (James et al, 2015). There are several potential reasons for the stronger WAM. Global warming could lead to changes in the inter-hemispheric SST gradient (Park et al, 2015), increased differences in temperature between the land and ocean (Barry et al, 2018), or the SHL deepening (Sultan and Gaetani, 2016), so theoretically should result in a wetter Sahel. The stronger monsoon could also have a role in the drier Guinea Coast and Congo Basin (James et al, 2015). The mechanism behind this contrast has previously been explained through a wetter Sahel and dry Guinea Coast coexisting as the monsoon circulation shifted north (James et al, 2015). However, there is a lack of data on the response of precipitation and the WAM to climate change to support this conclusion (Akinsanola and Zhou, 2019).

80% of CMIP5 model projections for the 21st century agree there will be a "dryer onset season in West Africa and an intensification of the late rainy season throughout the Sahel", with GHGs being a factor in this (Biasutti, 2013; p.1621-1622). Seasonal variation of SSTs and the response of convection to changes in the stability of the troposphere and surface energy budget have been implicated in these projections (Biasutti, 2013). Additionally, within CMIP6 data, all regions with monsoon systems have large uncertainties in future projections; North Africa/Sahel in particular has the largest at ~31.88% under the Shared Socioeconomic Pathway (SSP) 5-8.5 scenario (Chen et al, 2020). Nearly all scenarios for North Africa/Sahel do indicate an increase in mean precipitation compared to the 1995-2014 climatology, however, the 10th to 90th range bars get larger with time, showing the uncertainty, and the lower end of the range does extend into decreased precipitation (Chen et al, 2020; Figure 2.3).

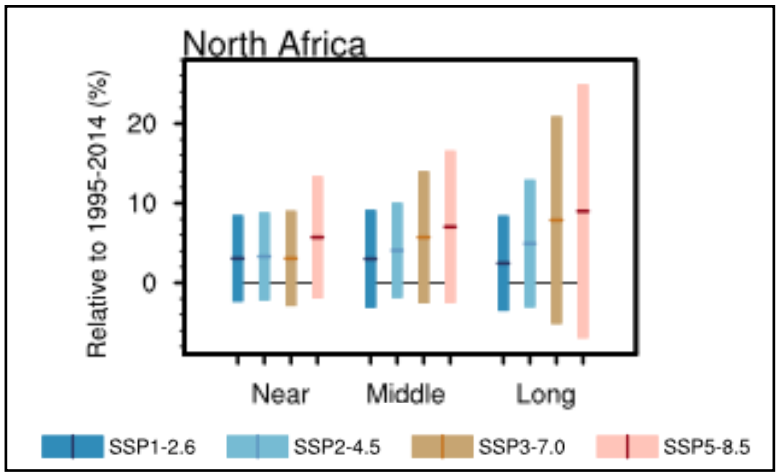

Figure 2.3: *Adapted from Chen et al (2020). Projections of monsoonal precipitation over North Africa monsoon region (defined as over the Sahel) under the differing scenarios. Near is 2021-2040, middle is 2041-2060 and long is 2080-2099. These projections are relative to the average climatology over 1995-2014, calculated as a percentage. The bars are the 10th to 90th percentiles, with the thick line representing the CMIP6 multi-model ensemble mean.*

Projections of meteorological droughts in CMIP6 were analysed by Ukkola et al (2020), defined as droughts that are caused by a lack of precipitation. CMIP6 models predict meteorological droughts in south and west Africa are likely to intensify and increase in duration, from two to four months (Ukkola et al, 2020). Robustness has been defined as the size of the future change being larger than the standard deviation between the models (Ukkola et al, 2020). Results in western Africa are amongst the strongest and most robust when compared to other regions across the globe, increasing confidence in the projections (Ukkola et al, 2020). CMIP6 results tend to be more robust compared to CMIP5 (Ukkola et al, 2020). However, models generally do not agree well with observations when simulating drought events across the globe, reducing the skill level for reproducing drought intensity (Ukkola et al, 2020). Models need to be able to simulate average precipitation and its variability, but there are systematic biases involved, especially with the variability in monthly precipitation where models tend to underestimate the average in humid regions (Ukkola et al, 2020). There has not been much change in this between CMIP5 and CMIP6 (Ukkola et al, 2020), indicating continuing uncertainty for future projections.

Moreover, a study that included both models from CMIP5 and CMIP6 found a link between Sahelian precipitation and the projected warming of the North Atlantic Ocean, with a warmer ocean corresponding with a wet Sahel (Monerie et al, 2020). Interannual variation in monsoon season precipitation has been found to be related to tropical ocean SSTs, but on multidecadal timescales, there is a teleconnection with extratropical ocean SSTs (Sultan and Gaetani, 2016). This again shows that to improve future projections, how important it is to accurately represent SSTs in models because of their impact on precipitation and the WAM.

The SHL impacts precipitation throughout the monsoon season, with a clear connection between a strong SHL phase and the eastern Sahel being wetter than usual and the west drier (Sultan and Gaetani, 2016). Compared to the rest of Africa and surrounding oceans, the west Sahel is projected to have decreased precipitation that corresponds with a strong increase in temperature (James et al, 2015). This results in the sea level pressure lowering, implying a stronger SHL, thus strengthening the WAM too (James et al, 2015). This study's results correspond with Sultan and Gaetani (2016)'s findings of a stronger SHL with a drier west Sahel and shows potential for WAM intensification despite the Sahel drying (James et al, 2015). However, the SHL behaviour in relation to Sahelian precipitation could be dependent on where the maximum warming is found because different locations could have different effects on the SHL itself (Vizy et al, 2013).

WAM projections are associated with changes in AEWs (Sultan and Gaetani, 2016). CMIP5 models suggest pre-monsoonal AEWs may reduce with warming but could increase significantly during the monsoon season (Sultan and Gaetani, 2016). Northern AEWs are predicted to increase in intensity and frequency by 1.5 waves a year by end of the 21st century (Brannan and Martin, 2018). Southern AEWs are more uncertain, with models lacking agreement on frequency, strength and precipitation, but there are indications of increased intensity and shift of timing to later months (Brannan and Martin, 2018). Model resolution leads to variation in projections for

AEWs (Sultan and Gaetani, 2016). Higher resolution models show increased frequency of strong AEWs, by ~12% per decade, but this is not seen in the lower resolution models, with the link between AEWs and precipitation being less clear or not even shown at all (Vellinga et al, 2016).

AEWs' locations are likely to change should the AEJ migrate, further adjusting their characteristics (Brannan and Martin, 2018). With warming, the AEJ could strengthen and migrate northwards from its current position, nearer the Sahara Desert, and the Tropical Easterly Jet (TEJ) could weaken, particularly over the Indian Ocean where it originates from (Akinsanola and Zhou, 2019). CMIP5 models have shown a stronger AEJ could dry some parts of the western Sahel (Sultan and Gaetani, 2016; Vellinga et al, 2016). Potential feedbacks on the AEJ may originate from surface warming in the western Sahel, potentially leading to more dry convection in the northern Sahel, strengthening the SHL, affecting the AEJ and WAM (James et al, 2015). The stronger AEJ results in stronger moisture divergence and can reduce precipitation further (Vellinga et al, 2016). Although, synoptic AEWs disturb the AEJ, resulting in convergence at lower atmospheric levels and convective rainfall (Vellinga et al, 2016). The SHL may also impact the AEJ through a drier west Sahel and warming reducing humidity and lowering pressure relative to the Guinea Coast (James et al, 2015). The AEJ may therefore also migrate southwards and could reduce Sahelian precipitation (James et al, 2015).

The WAM's circulation dynamics can further be altered through the aerosol feedback (Zhou et al, 2016; Giannini and Kaplan, 2019). The land/sea temperature gradient, and/or hemispheric SST gradients, can be altered by aerosols increasing the albedo and the amount of radiation reflected (Zhou et al, 2016). As previously discussed, the land/sea temperature gradient can affect the WAM's strength, and a smaller gradient could lead to a weaker WAM, thus less Sahelian precipitation (Haarsma et al, 2005; Monerie et al, 2017; Giannini and Kaplan, 2019). One reason that SSPs were developed for CMIP6 is that the aerosol concentrations in CMIP5 RCPs are now thought to have been underestimated, as all four pathways assumed there would be a dramatic decrease in aerosols, which is unlikely (Tebaldi et al, 2021). There are eight SSPs considering a wider range of more realistic aerosol pathways, are consistent with projected GHG emissions and account for the implementation of climate policies for atmospheric aerosols (Tebaldi et al, 2021). Various climatic feedbacks across the globe, including the WAM, will see differing impacts under these new SSPs (Zhou et al, 2016; Tebaldi et al, 2021). Research is lacking on the future impact of aerosols on WAM projections, and it has been recognised the feedback needs to be evaluated further (e.g. Lee and Wang, 2014). Scannell et al (2019) examined 40-year precipitation projections for subset of CMIP6 models using SSP2-4.5 for West Africa which assumes a reduction in aerosol emissions. Models produced a range of results, with some suggesting drying and others wetting over West Africa, leading the authors to speculate whether this is associated with SST changes (Scannell et al, 2019). This combined with the suggested influence of the aerosol feedback on SSTs during the Sahel droughts means the aerosol feedback needs to be considered when examining projections of Sahelian precipitation.

2.4. Research Questions

Reviewing the existing literature highlighted the many uncertainties and struggles associated with analysing the West African climatology in relation to the droughts in the 1970s and 1980s. Moreover, very few studies have also focussed on the wetter (than present) conditions during the 1950's. Various studies used different observational datasets to analyse the data which will impact any conclusions drawn, as it is unlikely the observational datasets are the same. As the CMIP6 data has only recently been published, there are less studies using the data than CMIP3 and CMIP5, hence it will be useful to compare CMIP6 models and to see how the models vary within CMIP6 in relation to the drought period. Improving historical simulations often helps to increase confidence in model projections, and it could be likely that if the models have different representations of the Sahelian droughts that this will feed into their projections. Moreover, model resolution has appeared frequently in the literature as a factor that affects model behaviour, through struggling to represent precipitation but also circulation over Africa. Average model resolution is increased within CMIP6 and will relate to the historical simulations of Sahel droughts and the projections for precipitation over the region. Hence if resolution is a dominant process, we might hope to see overall improvements in CMIP6 models. The literature shows circulation over the Sahel is complex with many associated feedbacks, but due to time constraints, more focus will be placed on investigating precipitation variability. To investigate these issues, the following research questions were devised:

1. Can CMIP6 models simulate observed interdecadal precipitation variability over the Sahel?
2. What factors relate to model representation of precipitation variability?
3. Does evaluation of past variability inform understanding of future change?

3. Methodology

In this chapter, the methods for the thesis will be discussed. The geographical study location and drought time period will be defined, alongside a summary of the various observational and reanalysis datasets that will be compared to the model simulations. The spatial and time series analysis methods will also be outlined.

3.1. Study Region

Following an examination of the literature, it was found there is a lot of variation on how the drought period is defined and what region it affected (Table 3.1). The study region of 18ºW to 20ºE and 10ºN to 20ºN was chosen and the drought period was defined as 1970 to 1983 (Figure 3.1; Figure 3.2; Table 3.1). This produces a region which minimises the area of ocean whilst covering the Sahel in West Africa. It is also the location of the WAM during the wet months of June, July, August and September (JJAS), thus JJAS was chosen to be analysed. As can be seen, it is very similar to many other studies (Table 3.1).

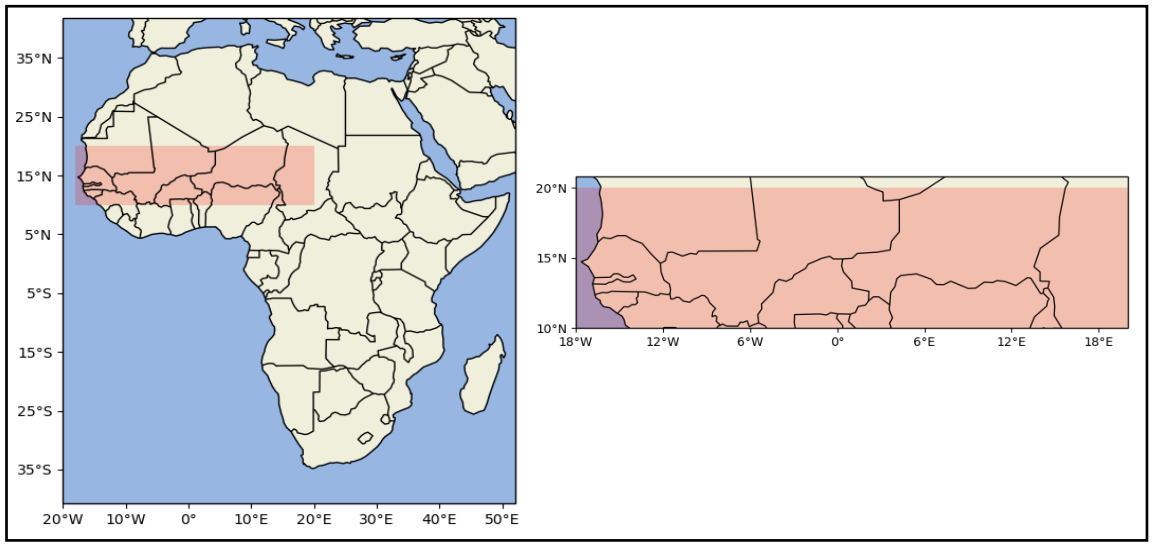

Figure 3.1: *Left - Map of Africa showing the study region which is highlighted in red. Right - Map of the study region itself.*

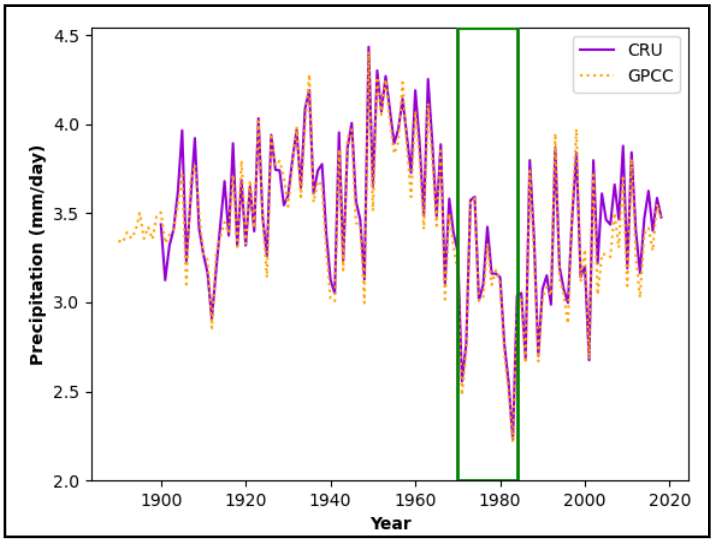

Figure 3.2: *Time series of observed monsoon season precipitation over the Sahel (mm/day). The green box depicts the time period defined as the drought.*

Table 3.1: *Definition of the Sahelian drought in academic literature, in terms of location, timing and duration, and how the data was analysed.*

Paper	Drought Location	Drought Timing and Duration	Months	Absolute values or anomalies
Binns (1990)	Savanna-Sahel = Mauritania to Sudan: 10°N-25°N, 18°W-35°E	1968-1974, 1979-1984	N/A – discusses desertification	N/A
Dai et al (2004)	10°N-20°N, 20°W-20°E	Early 1970s to late 1980s	JJAS	Anomaly relative to 1920-2003 long term mean
Lau et al (2006)	10°N-20°N,20°W-40°E	1970-1980s	JAS	Absolute
Giannini et al (2008)	10°N-20°N, 20°W-35°E West Sahel = 13°N-20°N, 15°W-20°E	1970s to mid 1980s	JJAS	21 year running mean, annual anomalies
Biasutti (2013)	3°N-20°N, 20°W-30°E	1970s and 1980s	JAS	Anomalies
Nicholson (2013)	Sahel = 14°N-18°N, 20°W-25°E	1970s-1980s	JJAS	Varies
Bamba Sylla et al (2016)	10°N-20°N, 15°W-15°E	N/A – looking at climatic zones	N/A	N/A
Vellinga et al (2016)	10°N-20°N,15°W-30°E	Lifted in 1984 – year when Sahelian rainfall recovered from the drought	JAS	Absolute
Sultan and Gaetani (2016)	7°N-20°N, 15°W-30°E (west = west of 5°W and east = east of 5°E)	1970s-1980s	JAS	Absolute
Barry et al (2018)	West Africa = 5°N to 20°N, 20°W-15°E	Between 1970 and 1980	N/A – looking across all years	N/A
Akinsanola and Zhou (2019)	West Africa = 0-20°N, 20°W-20°E	N/A – did not go in depth about the past	JJAS	Anomalies compared to historical period of 1980-2005
Andrews et al (2020)	12.5°S-17.5°N, 15°W-37.5°E West Africa = 0-10°N, 20°W-10°E	1970s-1980s	N/A - Annual	Absolute and decadal anomalies
Monerie et al (2020)	Western Sahel = 10°N-20°N, 20°W-5°W Central Sahel = 10°N-20°N, 5°W-20°E	N/A – analysing model uncertainty, does not mention drought in depth	JAS	N/A

3.2. Observational, satellite, and reanalysis datasets

3.2.1. Precipitation

This study used five observational, satellite, and reanalysis datasets to compare model results to: Tropical Applications of Meteorology using satellite data and ground-based observations (TAMSAT), Climate Hazards group Infrared Precipitation with Stations (CHIRPS), Climatic Research Unit Time-Series version 4.04 (CRU), European Centre for Medium-Range Weather Forecasts Reanalysis Dataset 5 Land (ERA5) and the Global Precipitation Climatology Centre Full Data Reanalysis Product (GPCC) (Table 2.1). These datasets are compiled using different methods thus results in a range of estimates of Sahelian precipitation.

Table 3.2: *Summary of the observational, satellite and reanalysis datasets used in this study.*

Full Name	Developers	Duration	Resolution	Reference	Data Type
Climatic Research Unit Time-Series version 4.04 (CRU)	University of East Anglia	1901 - 2019	0.5^{o} x 0.5^{o}	University of East Anglia Climatic Research Unit (2020)	Gauge
Tropical Applications of Meteorology using Satellite data and ground-based observations (TAMSAT)	University of Reading	1983 - 2020	0.0375^{o}	Maidment et al (2014)	Merged gauge and satellite
Climate Hazards group Infrared Precipitation with Stations (CHIRPS)	University of California at Santa Barbara and the United States Geological Survey	1981 - 2020	0.05^{o}	Funk et al (2015)	Merged gauge and satellite
European Centre for Medium-Range Weather Forecasts Reanalysis Dataset 5 (ERA5)	European Centre for Medium-range Weather Forecasts (ECMWF)	1981 - 2020	0.25^{o}	Hersbach et al (2020)	Reanalysis
Global Precipitation Climatology Centre Full Data Reanalysis Product (GPCC)	Global Precipitation Climatology Center	1891 - 2019	0.25^{o}	Global Precipitation Climatology Center (2020)	Gauge

TAMSAT was developed by the University of Reading and was originally an algorithm to estimate precipitation from satellite data for West Africa but was eventually extended to the rest of Africa, from 1983 to present day, with a 0.0375^{o} resolution

(Maidment et al, 2014; Tarnavsky et al, 2014; Dembélé and Zwart, 2016). The algorithm has been calibrated for the period 1983 to 2010 due to data availability associated with ground-based rain gauges (Tarnavsky et al, 2014; Dembélé and Zwart, 2016). TAMSAT estimations themselves are not affected by biases from the number of gauges as it uses Thermal Infrared imagery (TIR) which took samples every 30 minutes up to July 2006, and then every 15 minutes after that (Tarnavsky et al, 2014; Maidment et al, 2014). TIR is most useful because African precipitation tends to come from deep convective systems (Maidment et al, 2014), although, the signal does not penetrate the clouds fully, and consequently struggles with quantifying the exact amount of precipitation (Dembélé and Zwart, 2016). Precipitation is estimated "by applying the predetermined calibration parameters to cold cloud duration (CCD) fields calculated from TIR data", assuming most African precipitation is produced by cold clouds (Maidment et al, 2014, p.3). This data is used with rain gauge observations to provide information; however, the number of rain gauges has decreased over time hence the satellite data has become dominant (Maidment et al, 2014; Tarnavsky et al, 2014). Evaluation of the estimates produced by TAMSAT found Africa specific datasets tend to perform better than a subset of a global dataset as it accounts for local climatologies within the algorithm (Maidment et al, 2014).

CHIRPS has been derived by the University of California at Santa Barbara and the United States Geological Survey, covering 50ºS to 50ºN, with a resolution of 0.05º (Funk et al, 2015). It aims to fill a gap by being a high-resolution dataset that has a higher temporal coverage with a low bias and goes back further in time than other available datasets (Funk et al, 2015). The dataset was "mainly designed for drought monitoring […] in regions with complex topography, changing observation networks and deep convective precipitation systems that correspond reasonably well with CCD estimates" (Funk et al, 2015, p.17). Its algorithm uses satellite information over areas that lack gauge data alongside estimates of precipitation from CCD data from 1981 to present day (Funk et al, 2015). This is merged with available World Meteorological Organization's Global Telecommunication System (GTS) gauge data (Funk et al, 2015). The database has been validated and shown to perform well in relation to drought monitoring, thus supporting the United States Agency for International Development Famine Early Warning Systems Network well (Funk et al, 2015). Using 28 stations in the Sahel region, it has been shown that the wet season bias in CHIRPS is lower than other datasets as it includes weather station data (Funk et al, 2015). However, CHIRPS still overestimates precipitation compared to gauge data, but there is a strong correlation coefficient for data from 1998 to 2010 before the data is averaged to monthly resolution (Sacré Regis et al, 2020). During the monsoon season, CHIRPS overestimates precipitation by an average of 14mm/month (Sacré Regis et al, 2020). Despite this, studies such as Badr et al (2016) deemed CHIRPS to be among the best of observational datasets for Africa due to its "higher resolution, better station coverage over Africa, improved statistical approaches and updated temporal coverage" (p.9029).

The CRU TS.04 precipitation dataset is a gridded gauge dataset, which retrieves observations from different sources and combines them (Maidment et al,

2014). It was initially released in 2000 and has since been updated on many different occasions to refine the dataset and implement new variables (Harris et al, 2020). There is a high temporal coverage, so it is useful for analysing long term climate changes (Maidment et al, 2014). However, there is the potential for large errors because gauges are sparsely and unevenly distributed across Africa (Maidment et al, 2014). The grids in the CRU datasets are 0.5º x 0.5º, and provide monthly data from 1901 to 2019, derived from National Meteorological Services' daily or sub-daily observational data (University of East Anglia Climatic Research Unit, 2020). There are a total of 10 variables, including precipitation, cloud coverage, temperature and evapotranspiration (University of East Anglia Climatic Research Unit 2020). The time series was created by angular-distance weighting interpolation (University of East Anglia Climatic Research Unit, 2020). Gaps in observational data are filled using published climatology for the region (Harris et al, 2020). For Africa in particular, the CRU dataset has been recognised as one of the most trustworthy providers of historical observational data (Zebaze et al, 2019).

GPCC is a gridded gauge dataset like CRU (Maidment et al, 2014; National Center for Atmospheric Research Staff, 2020). The World Meteorological Organization uses the datasets provided by the GPCC 'through the Global Telecommunication System (GTS) on near-real-time basis' (Akinsanola et al, 2017, p.671). The data for the GPCC began to be compiled in 1989, and now there is data from 85,000 stations across the globe and a temporal coverage of over 100 years (Becker et al, 2013; Global Precipitation Climatology Center, 2020; Table 3.2). For a station to be used, there has to be a 10-year minimum length, which results in over 65,000 stations being used to calculate annual climatologies (Becker et al, 2013). However, it should be noted that between 1983 and 2010, the number of gauges across Africa has decreased up by to 80%, adding uncertainty to the data despite the rigorous quality control process (Becker et al, 2013). Every one to three years, the gridded products are released, with spatial resolutions of 0.25º, 0.5º, 1.0º and 2.5º (Becker et al, 2013; Global Precipitation Climatology Center, 2020). This study will use the 0.25º spatial resolution dataset. Akinsanola et al (2017) calibrated GPCC over West Africa for the time period January 1990 to December 2008, comparing to observational data from 81 West African meteorological stations that have been quality control checked. They used a monthly dataset at 0.5º spatial resolution and found that GPCC did manage to reproduce the WAM annual cycle but underestimated Sahelian precipitation (Akinsanola et al, 2017). Despite this, they stated that GPCC was one 'of the most outstanding datasets' in their study, along with an earlier version of CRU TS.04 (Akinsanola et al, 2017, p.687). Over the Sahel, GPCC had a Pearson's value of 0.96 and over the whole of West Africa the resultant value is 0.94 (Akinsanola et al, 2017), indicating just how well it performed compared to the observations.

ERA5 provides data from 1950 to present day, with a resolution of 31km and using the 4D Variance assimilation scheme (Hersbach et al, 2020). ERA5 is "produced by combining a numerical weather prediction model with observational data from satellites and ground observations" (Gleixner et al, 2020, p.4). It provides hourly data at a 0.25º spatial resolution from 1979 to present day (Gleixner et al, 2020). ERA5

matches precipitation observations better than the previous version ERA-Interim (Gleixner et al, 2020; Quagraine et al, 2020). The monsoon season wet bias over West Africa was reduced by up to 60% in ERA5 compared to ERA-Interim, which suggests the overall cycle of precipitation across the year is better represented, as well as the extreme precipitation distribution (Gleixner et al, 2020; Quagraine et al, 2020). The peak monsoon values produced by ERA5 are lower than the gauge data though, and the WAM precipitation band is placed more south in ERA5 compared to observations, however, this has also been seen in other reanalysis datasets (Quagraine et al, 2020). It has been found that ERA5 is able to represent the spread of West African precipitation across the year and the interannual variability well (Quagraine et al, 2020). This study uses ERA5-Land which was produced by taking the land component from ERA5 and refining its accuracy through a range of improvements, predominantly by an increased resolution of 9km rather than ERA5's 31km resolution, on a grid of 0.1^{o} by 0.1^{o} (Muñoz-Sabater et al, 2019).

3.2.2. Circulation

Circulation over the Sahel has been linked to changes in precipitation, such as through the WAM (Parker et al, 2005; Nicholson and Klotter, 2021), thus it has formed part of the analysis in this study. Due to limitations with observational circulation data availability over the Sahel (Nicholson and Klotter, 2021), circulation data has been taken from the ERA5 reanalysis dataset - discussed previously (Hersbach et al, 2020). It is important to note due to this lack of continuous records of upper-air stations in the Sahel region, reanalysis datasets like ERA5 have not been properly validated (Nicholson and Klotter, 2021). However, reanalysis circulation data is trusted more than precipitation estimates (Hersbach et al, 2020). ERA5 itself has a slightly lower resolution than the ERA5-Land dataset used for precipitation data (0.25^{o} vs 0.1^{o}); and a back-dated version has been released that covers 1950 to 1979 which will be merged with the version that covers 1979 to 2021 (Hersbach et al, 2020) to maximise the temporal coverage. It is constructed using the same methods as ERA5 (Hersbach et al, 2020). The u and v components of wind variables will be used to examine changes in wind speed and compare to the surface zonal and meridional wind speeds in the CMIP6 models. The study area has been extended to 25^{o}W to 20^{o}E and 0^{o}N to 20^{o}N to capture the winds that feed into the Sahel region.

3.2.3. Sea Surface Temperatures (SST)

The sea surface temperatures (SST) variable from the Met Office Hadley Centre's sea ice and sea surface temperature version 1 (HadISST) dataset was used (Rayner et al, 2003). It has a spatial resolution of 1^{o} x 1^{o}, and a temporal coverage of 1870 to 2016 (Rayner et al, 2003). Building on previous datasets, interpolation was undertaken to fill more gaps of missing data (Rayner et al, 2003). Again, the lack of available observational data adds uncertainty to this dataset as it cannot be fully validated, nevertheless, the interpolated data performs well when compared to other published datasets (Rayner et al, 2003). To aid analysis for this study, all missing data values were set to be 'land' rather than -1000.0. The data was remapped to a regular 360^{o} by

180^{o} grid using Climate Data Operators (CDO). Data was plotted as global maps, rather than specifying an area related to West Africa, because the ocean's influence on West African precipitation is not limited to just one area, for example, both the Indian and Atlantic oceans affect the WAM (Sultan and Gaetani, 2016).

3.3. Models

All coupled models within CMIP6 with historical runs were analysed. The lowest numbered ensemble member was taken (see 3.4 for discussion about ensemble choice). Details are in Table 3.3., using information from Eyring et al (2016). For detailed information of model set-up, see Appendix 2.

As well as these, the equivalent simulations in the historical atmosphere only experiments with prescribed SSTs (AMIP-Hist) and the coupled Historical-Natural experiments (Hist-Nat) were examined to evaluate the coupled historical experiments (Table 3.3.). The Hist-Nat simulations hold GHGs at pre-industrial levels and do not include land-use changes, which removes the impact of humans. However, they do not include all natural forcings (e.g. natural forest fires) (Eyring et al, 2016). The historical version of AMIP was analysed because those experiments cover 1870 to 2014 (Eyring et al, 2016), encompassing all of the drought period. It needs to be noted that a lot fewer modelling groups ran AMIP-Hist experiments compared to AMIP (16 versus 42) (Eyring et al, 2016).

Five Shared Socioeconomic Pathway (SSP) projections were examined: 1-2.6, 2-4.5, 3-7.0, 4-6.0 and 5-8.5. These were chosen as they build on the Representative Concentration Pathways in the fifth IPCC report and CMIP5 models (Monerie et al, 2017). SSP3-7.0 was also included because it is a new baseline scenario that has been developed assuming no further mitigation policies are put in place, continuing on the current trajectory, with higher levels of aerosols too (Tebaldi et al, 2021).

Table 3.3: *Details of the experiments used in this study, their duration, and the number of models in the experiment.*

Experiment	Years	Number of Models
Coupled (CMIP)	1850 – 2014	49
Atmosphere Only Historical (AMIP-Hist)	1870 - 2014	16
Coupled Historical-Natural (Hist-Nat)	1850 - 2014	14
Shared Socioeconomic Pathways (SSPs) projections	2015 - 2100	34 (at least one SSP)

3.4. Analysis Methods

Analysis was undertaken on the BluePebble server using Python through the Linux operating system on the computational facilities of the Advanced Computing Research Centre at the University of Bristol (2021).

The lowest numbered ensemble member run by each modelling group was used. This was decided on after examining CanESM5 – a model which was run for 65 different experiments in the historical category, by the Canadian Centre for Climate Modelling and Analysis (Swart et al, 2019). Within the CanESM5 ensemble members, the average range between the different members amounts to 1.17mm/day for the interannual variability and decreases to 0.38mm/day with the 20-year running mean (Figure 2.3). There is likely to be a larger difference between the different modelling groups rather than the different ensemble members within a modelling group, as seen with past CMIPs like CMIP5 (Sultan and Gaetani, 2016). The subset of CMIP5 models in Sultan and Gaetani (2016)'s work had an inter-model range of ~4mm/day, nearly four times larger than what is seen within CanESM5. In addition, this means the multi-model mean is not going to be weighted towards models with more ensemble members, with previous studies using similar methodologies (e.g. Santer et al, 2009; Monerie et al, 2012; Gaetani et al, 2017).

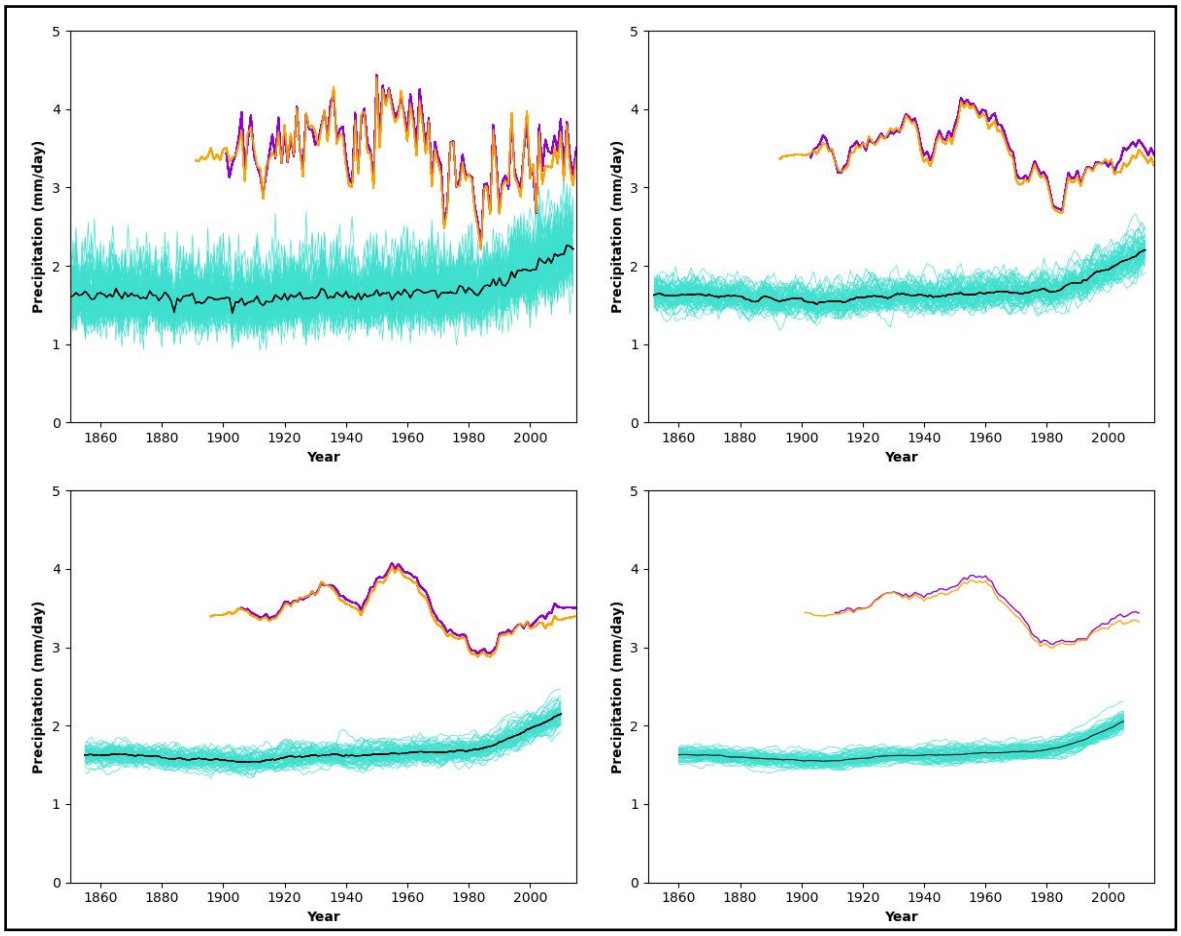

Figure 3.3: *Time series of each ensemble member of the CanESM5 model by the Canadian Centre for Climate Modelling and Analysis (mm/day). Interannual (top left), five year running mean (top right), 10 year running mean (bottom right) and 20 year running mean (bottom left). The multi-model mean is the black line, CRU is the purple line and GPCC is orange.*

3.4.1. Time series analysis

For time series analysis, models were averaged over the study region, producing one value for each timestep, using CDO. All models and observations need to be mm/day, so the relevant conversions will be completed. TAMSAT was already in mm/day. CHIRPS, GPCC and CRU were converted from mm/month to mm/day by dividing by 30.5, as that is the average number of days in the months of JJAS. ERA5-Land and ERA5-Backdated were converted from m/day to mm/day by multiplying by 1000.

3.4.2. Spatial analysis

For spatial analysis, models were averaged over the chosen time periods (Table 3.4) producing one value per grid point, using CDO. Model resolution varies, so for spatial comparison to the observations, the models were re-gridded to match the respective observational grid through using CDO bi-linear interpolation. This allowed for the correct calculations to take place and model bias to be evaluated. Additionally, models have been grouped into three categories approximately equal in size according to their nominal resolution: higher resolution (<160km), medium resolution (160km-250km) and lower resolution (>250km) (Figure 3.4).

Table 3.4: *Details of time periods to be analysed in this study. The common period is the overlapping time period between the coupled historical model runs and the observations.*

Time Period Name	Years in Time Period
Drought	1970 - 1983
Wet Period	1950 - 1963
Recent Period	2001 - 2014
CRU common period	1901 - 2014
GPCC common period	1891 - 2014

LOWER RESOLUTION	
Model	**Nominal Resolution (km)**
AWI-ESM-1-1-LR	268
BCC-ESM1	402
CanESM5	402
CanESM5-CanOE	402
CESM2-FV2	305.6
CESM2-WACCM-FV2	305.6
GISS-E2-1-G	315.5
GISS-E2-1-G-CC	315.5
GISS-E2-1-H	315.5
IITM-ESM	271.5
IPSL-CM6A-LR	262.4
MCM-UA-1-0	417.3
MIROC-ES2L	402
MPI-ESM-1-2-HAM	268
MPI-ESM1-2-LR	268
NESM3	268
NorESM2-LM	305.6

MEDIUM RESOLUTION	
Model	**Nominal Resolution (km)**
ACCESS-CM2	217.5
ACCESS-ESM1-5	216.9
BCC-CSM2-MR	160.8
CAMS-CSM1-0	160.8
CAS-ESM2-0	201
CNRM-CM6-1	201
CNRM-ESM2-1	201
FGOALS-f3-L	157.7
GFDL-ESM4	157.7
HadGEM3-GC31-LL	217.5
INM-CM4-8	244.5
INM-CM5-0	244.5
KACE-1-0-G	217.5
MIROC6	201
MRI-ESM2-0	160.8
UKESM1-0-LL	217.5

HIGHER RESOLUTION	
Model	**Nominal Resolution (km)**
AWI-CM-1-1-MR	134
CESM2	152.8
CESM2-WACCM	152.8
CNRM-CM6-1-HR	71.5
E3SM-1-0	142.9
E3SM-1-1	142.9
E3SM-1-1-ECA	142.9
EC-Earth3	100.5
EC-Earth3-Veg	100.5
FIO-ESM-2-0	152.8
HadGEM3-GC31-MM	96.7
MPI-ESM1-2-HR	134
NorESM2-MM	152.8
SAM0-UNICON	152.8
TaiESM1	152.8

Figure 3.4: *Model resolution groupings.*

3.4.3. Statistical testing

To quantify the differences between the models and the observations and the different time periods, statistical testing was carried out. Anomalies were calculated across the varying timescales and time periods (Table 3.4). Projection anomalies were calculated by subtracting the average of the recent period from each timestep in the projection time period.

Running means of various lengths were applied to filter out the interannual variability and analyse the long-term variations in precipitation. For comparison, the interannual variability and five- and 10-year running means were analysed. A longer period in the running mean was considered but the standard deviation of applying one that is longer than 10 years drops to less than 50% of the interannual standard deviation, smoothing out too much of the variation (Figures 3.3/3.5). The 10-year running mean allows for some variation to still exist as well as a distinguishable signal (Figure 3.5).

Pearson's R correlation coefficients were computed to help with the understanding of how well the models represent the historical observations. There was also analysis of the variation within the historical time series by standardising them. These was calculated by subtracting the long term mean from each timestep and dividing by the long-term standard deviation.

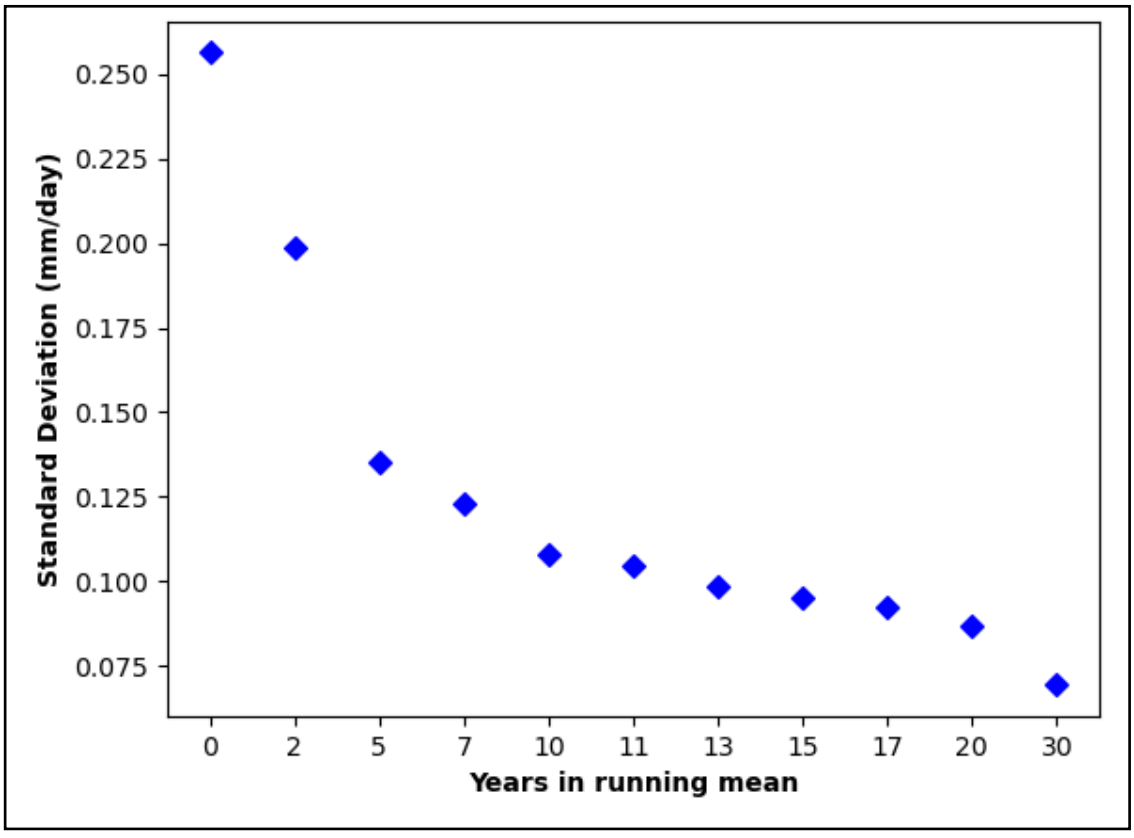

***Figure 3.5**: Standard deviation of the long term means (mm/day) for differing number of years in the running mean for the r1i1p1f1 ensemble member of CanESM5.*

4. Results and Discussion

To investigate the ability of the CMIP6 models to simulate the Sahel droughts, and whether there is a relationship with their future projections, three research questions were devised after examining the literature:

1. Can CMIP6 models simulate observed interdecadal precipitation variability over the Sahel?
2. What factors relate to model representation of precipitation variability?
3. Does evaluation of past variability inform understanding of future change?

4.1. Can CMIP6 models simulate observed interdecadal precipitation variability over the Sahel?

There have been huge improvements in climate models over time (Eyring et al, 2016). Despite these improvements, there are still discrepancies between models and observations for Sahelian precipitation that have yet to be fully resolved.

4.1.1. Observations

Figure 4.1.1. illustrates Sahelian precipitation over time from observed, satellite, and reanalysis datasets. Precipitation has been averaged over JJAS, and GPCC has the best temporal coverage, closely followed by CRU. TAMSAT, CHIRPS and the reanalysis data of ERA5-Land start in the early 1980s, hence do not cover the entire drought period. ERA5-Backdated is similar to ERA5-Land but is a coarser resolution and covers a longer time period.

GPCC and CRU agree quite well across their available coverage, with ERA5-Backdated's fluctuations aligning with the other two but has lower values. For the datasets which cover the drought period, preceding the drought, there is a wetter period of high precipitation values during the 1950s and early 1960s (Figure 4.1.1). Following this, there is a clear decrease in precipitation around 1970 and remains low for about 13/14 years. Precipitation recovers around 1983/1984 and continues to increase, albeit at different rates between datasets. In the more recent years, all the datasets agree quite well, with there being ~1mm/day between all of them. This can be attributed to the ERA5 data not quite having the same level of recovery in precipitation following the drought period compared to the other four datasets. It has been found reanalysis datasets tend to underestimate Sahelian precipitation compared to datasets such as CRU, CHIRPS and GPCC, linked to factors like parameterisations and relationships between earth system elements (Quagraine et al, 2020). Also consistent across some reanalysis datasets, including ERA5, is the WAM's band of precipitation is often being located too south, hence reducing precipitation over the Sahel (Quagraine et al, 2020). Thus, ERA5 is not expected to represent Sahelian precipitation well but it is useful for comparison to the other available datasets.

The spatial representation of the drought for the two long timeseries (GPCC and CRU) will be shown later (in Figures 4.1.5 to 4.1.10). GPCC and CRU resemble each other, with the only difference linking to the generation of their data – CRU has smoother contours than GPCC. The values across the study region are consistent in both datasets.

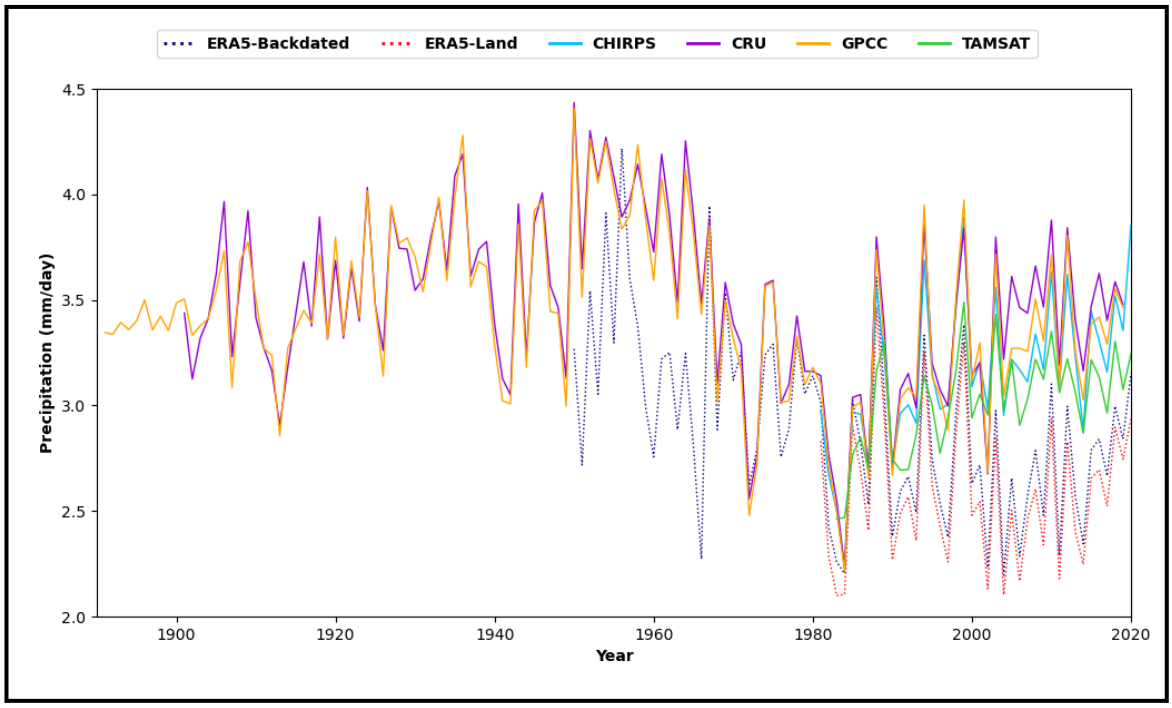

Figure 4.1.1: *Time series of mean JJAS precipitation (mm/day) over the Sahel study region for the observational datasets. Note that only GPCC, CRU and ERA5-Backdated cover the entire drought period.*

4.1.2. Evaluation of models

Deciding which models have the best and worst representation of precipitation over the Sahel depends on the method used. This study uses three methods to help examine model performance: comparison of temporal correlations, spatial comparison using difference maps and model biases.

Temporal correlations have been derived using the Pearson's *r* correlation test between the modelled and observed time series. This method tests whether the models capture the long-term variability that has been observed, however, the models may perform well here despite not having the right magnitude of change. For example, the modelled fluctuations could mirror the observed fluctuations but instead of being around 3mm/day, they are around 1mm/day. Developing this further, Lau et al's 2006 study defined reasonable agreement between models and observations to be significant when coefficients at the 95% confidence interval are higher than 0.26 and reasonable disagreement being -0.26 or lower, with neutral models in between. These were computed for the time series that came out of the Standardised Precipitation Index (SPI) (Lau et al, 2006). This study did not use the SPI, but the time series have been standardised which is a very similar method (see Methodology).

The second method of comparison was to compare the spatial distribution of precipitation averaged over the different time periods, a visual method of comparison rather than numerical. It assesses the model's ability to capture the magnitude of change across the Sahel and not the variability like the temporal correlation coefficients do. Using this method of analysis may result in different models being classed as the 'best' performers compared to the temporal correlations. Model performance will be defined by representation of the anomalies between the drought and wet periods because models tend to perform better with the anomalies between the drought and recent periods, limiting the distinctions.

Additionally, as a third method of comparison, model biases can be calculated both temporally and spatially through creating an average over the drought period and subtracting the observations from the models. The larger the bias, the more uncertainty there is in the model.

4.1.2.1. Method 1: Temporal Correlations

Figure 4.1.2 shows Sahelian precipitation over time in observations and CMIP6 models. There are a wide range of results within CMIP6 historical simulations, with an average of 4.5mm/day between the minimum and maximum models with no running mean implemented, decreasing to 4.2mm/day with a 10-year running mean. This is over 3mm/day larger than the range of different ensemble members of CanESM5 (Figure 3.4.1). Every available historical simulation was plotted for the lowest ensemble member, apart from CIESM2, as these results were out by a factor of approximately 100, thus the model was removed from the analysis. The multi-model mean (MMM) does not seem to capture the wet (1950-1963) or drought (1970-1983) periods in any of the plots, in fact it suggests there is a slight increase in precipitation during the drought (Figure 4.1.2).

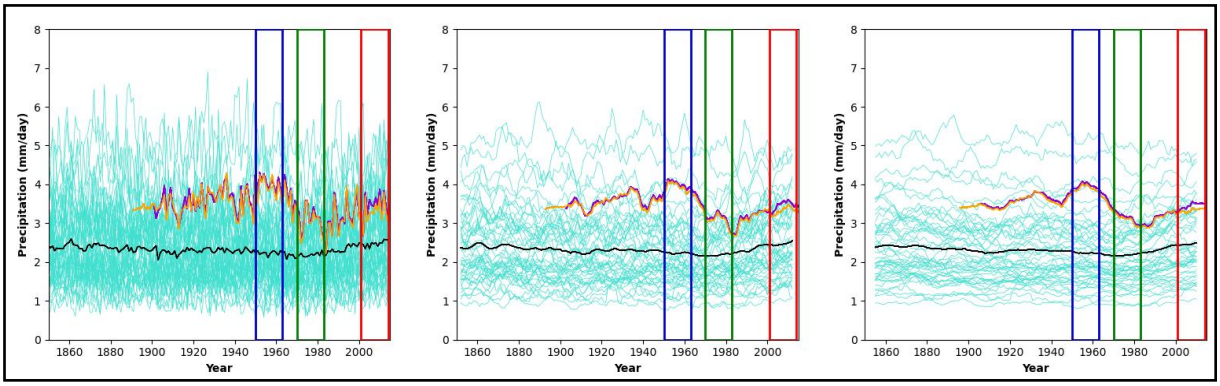

Figure 4.1.2: *Time series of mean JJAS precipitation (mm/day) over the study region for the lowest numbered ensemble member for each historical run (1850-2014). From left to right: interannual time series, five-year running mean and 10-year running mean. The black line is the multi-model mean, purple is CRU and orange is GPCC. The blue box represents the wet period, green the drought and red the recent period.*

Previous studies have focused more on the spatial changes in precipitation over the Sahel or conducting ensemble mean analysis instead of explicitly examining the time series data (Akinsanola and Zhou, 2019; Monerie et al, 2020). There are uncertainties associated with using the ensemble mean; it often risks being an

oversimplification, especially when examining precipitation due to its variable nature (Daron et al, 2021). Narrower ranges of projections were interpreted when participants were shown the ensemble mean instead of the whole range (Daron et al, 2021). This is reflected in these results, as there is not even a 1mm/day change between 1850 and 2014, compared to the 4.5mm/day inter-model range, and it does not show the same variations as observations (Figure 4.1.2). However, it is useful for an insight into the overall behaviour of modelled precipitation when used in context of the full range.

Upon inspecting the individual models, there is little indication that they reproduce the observed interdecadal variability: a wetter period in the 1950s, a long term drought in the 1970s, and then a recovery. However, despite apparently struggling to represent the wet and drought periods, CMIP6 models do show a wetting trend in the recent period over the Sahel (Figures 4.1.2/4.1.3). Some studies have attributed recent increases in precipitation (or the drought recovery) to GHGs (Dong and Sutton, 2015), so it is interesting the models show recent increases, which may also be due to rising GHGs.

It is a little challenging to evaluate individual models' representation of the wet and dry periods from Figure 4.1.2. Models have different mean precipitation and magnitude of variability, hence standardising the modelled and observed time series was appropriate, so changes could be analysed relative to the long term means of each model. This results in the interannual variability being the same in each model and allows for analysis of whether the models have relative drought and wet periods compared to their long-term mean. The time series were standardised by subtracting the long term mean from each timestep and dividing by the long-term standard deviation, for each model. This method is similar to the Standardised Precipitation Index (SPI) (Lau et al, 2006; Mishra and Singh, 2010). However, the SPI adjusts the precipitation variance to have a Gaussian distribution so that drought frequency statistics are appropriate. It was decided to not use this approach and keep the standardisation simpler, and comparable to that used for phenomena such as El Niño.

There is still a lot of scatter within the data and the MMM shows some similarity to the observations in the wet period and the recent period, but not the drought period (Figure 4.1.3). The models being able to capture the variability in the recent period suggests they have been able to depict the influence of rising GHGs on the Sahel, even if slightly overestimated compared to the observations (Dong and Sutton, 2015).

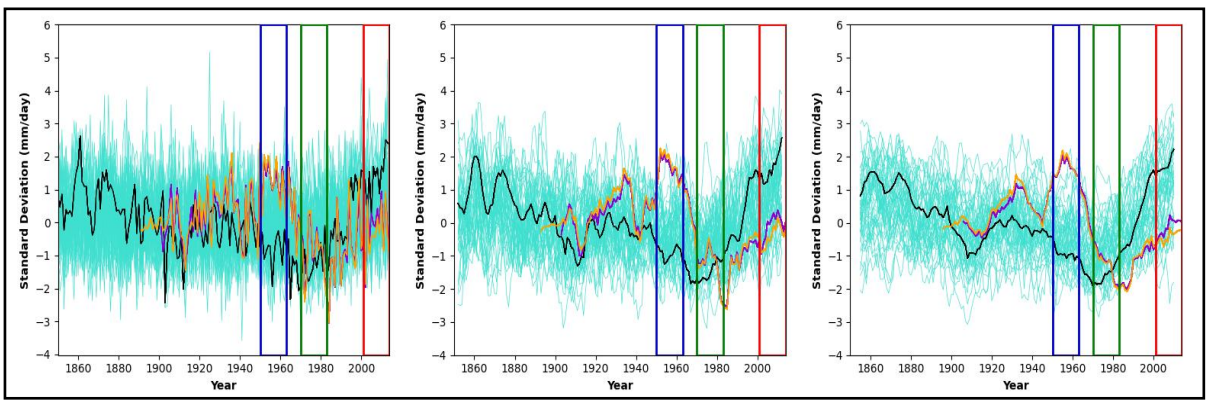

Figure 4.1.3: *As Figure 4.1.2, but for the standardised time series instead.*

It is possible that the models are able to simulate long term wet and dry periods, but they are not simulating them at the same time as in observations. Following this logic, the standardised time series (Figure 4.1.3) were analysed further to examine whether the models were able to simulate a drought period, regardless of the years it occurred in. A ‘dry’ or ‘wet’ year was defined as a year where the dry/wet anomaly is more than one times standard deviation (SD). A ‘drought’ or ‘wet’ period were classified by three or more consecutive years with the anomaly being more than one times the SD (Appendix 1.1a/1b).

Surprisingly, the observations do not have a sustained drought period during the defined time period of 1970-1983. GPCC has six years that are below 1SD and CRU has five in the drought period (Appendix 1a). There are 26 models which have sustained drought periods, with nine models having consecutive years falling within the defined drought period. In particular, E3SM-1-1 has seven ‘dry’ years within the defined drought period, closely followed with HadGEM3-GC31-LL having six. However, the fact 26 can simulate consecutive dry years implies the models are able to be dry enough for a drought to occur, despite being out of sync with the observations. This can be explained by years in coupled simulations not being expected to correspond with specific years in observations because models produce their own unforced interannual variability.

The observations have eight out of the 13 years in the wet period defined as ‘wet’ years, with two sustained wet periods, but no years fall in the recent period. 24 models have prolonged ‘wet’ periods across the whole historical time period. Only two models – IITM-ESM and MCM-UA-1-0 – have three or more wet years in the wet period. 10 models have sustained ‘wet’ years during the recent period. Significant models include CanESM5-CanOE with 10 ‘wet’ years and EC-Earth3-Veg with seven all in the defined recent period. Despite E3SM-1-1 capturing a large proportion of the drought period, it struggles with the wet periods, having no ‘wet’ years falling in either the wet period or recent period.

The overall long term mean and the magnitude of changes across the historical time period will have affected whether a year is deemed ‘dry’ or ‘wet’. It has been suggested the wet period that preceded the drought was anomalous instead of the drought, which may feed into the observations lacking ‘wet’ years in the recent period, despite a clear indication that recent years have become significantly wetter. Kennedy et al (2017) recognises that precipitation has been recovering since the drought but notes that the current values are lower than the pre-drought levels, implying the wet period is anomalous, which could explain these patterns.

Pearson's *r* correlation coefficients were computed for each model with both observational datasets to assess whether they can capture the long-term variability. The resulting coefficients with GPCC are consistent with those of CRU (Appendix 1.2a-2c). Lau et al (2006) conducted an analysis of a subset of CMIP3 models and their ability at representing the Sahel droughts. They deemed a sufficient representation to be a Pearson's *r* correlation coefficient of 0.26, and disagreement at -0.26 (Lau et al, 2006). These thresholds were applied to the correlation coefficients for the historical CMIP6 simulations, to evaluate whether models were able to simulate observed variability. The number of models meeting the threshold for agreement with observed variability increases with the implementation of the running mean, from one model agreeing with the original time series (EC-Earth3, *r* = 0.31) to 13 models agreeing with a 10-year running mean. It also must be noted that there are six (five-year running mean) and 10 (10-year running mean) models that demonstrate significant disagreement with the observational datasets.

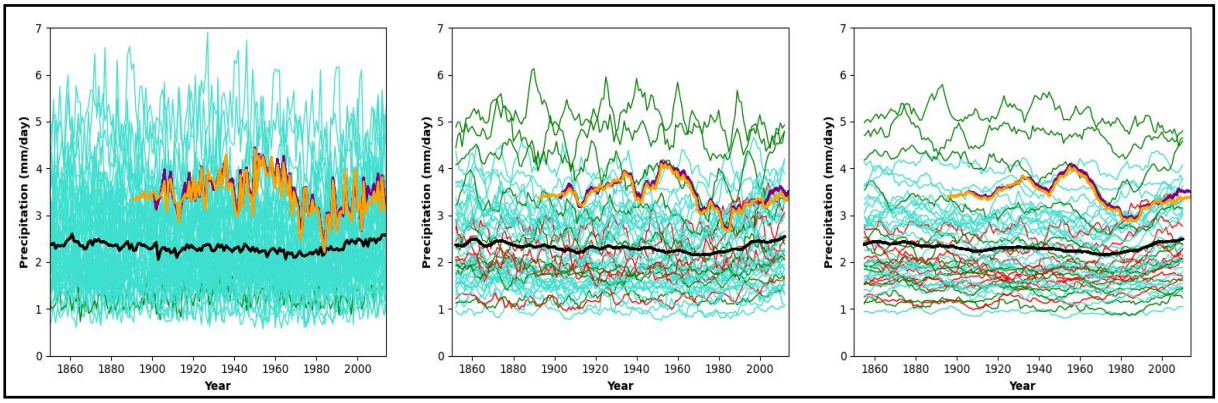

Figure 4.1.4: *As Figure 4.1.2, with models coloured according to Lau et al (2006)'s thresholds where green is a Pearson's r value greater than 0.26 (agreement) and red is less than -0.26 (disagreement) with GPCC.*

4.1.2.2. Method 2: Spatial comparisons

Figures 4.1.5 to 4.1.10 are anomaly maps showing the differences between the observations and the models between either the drought period and wet period or the drought period and the recent period, grouped according to resolution. For the drought and wet period anomalies, E3SM-1-1 visually best represents the observations in the higher resolution grouping. There is a similar area 0.5-1mm/day drier in the drought than the wet period in both the model and the observations (Figure 4.1.5). In the medium resolution grouping, MIROC6 has a band across the southern Sahel with areas in the drought period up to 1.5mm/day drier, but compared to observations, this is only about one third of the areal extent of drying (Figure 4.1.7). The lower resolution models appear to have very marginal differences between the drought and wet periods (Figure 4.1.9). Interestingly, a lot of the models across all three groupings have drought periods wetter than the wet period. However, this is consistent with the interannual variability multi-model means in both Figure 4.1.2 and 4.1.2, where there appears to be a slight increase in precipitation over the drought period - higher than the preceding wet period. Furthermore, this also suggests there are many models that

struggle to get the volume of precipitation that has been observed in the wet period.

Across all three groupings, more models better represent the observations for the drought and recent period anomalies compared to the drought and wet period. Although, it is not the same models with the best representation in both. EC-Earth3-Veg suggested the drought period was wetter than the wet period (Figure 4.1.5) but represents the observations well for the differences between the drought and recent periods (Figure 4.1.6). In the medium resolution models, there are some which do capture some of the same differences as the observations, however, there are a few, for example MIROC6, which have a larger difference between the drought and recent period than the observations (Figure 4.1.8). There is a similar pattern in the lower resolution models, but, again, a few models show a larger dry difference compared to the observations (Figure 4.1.10).

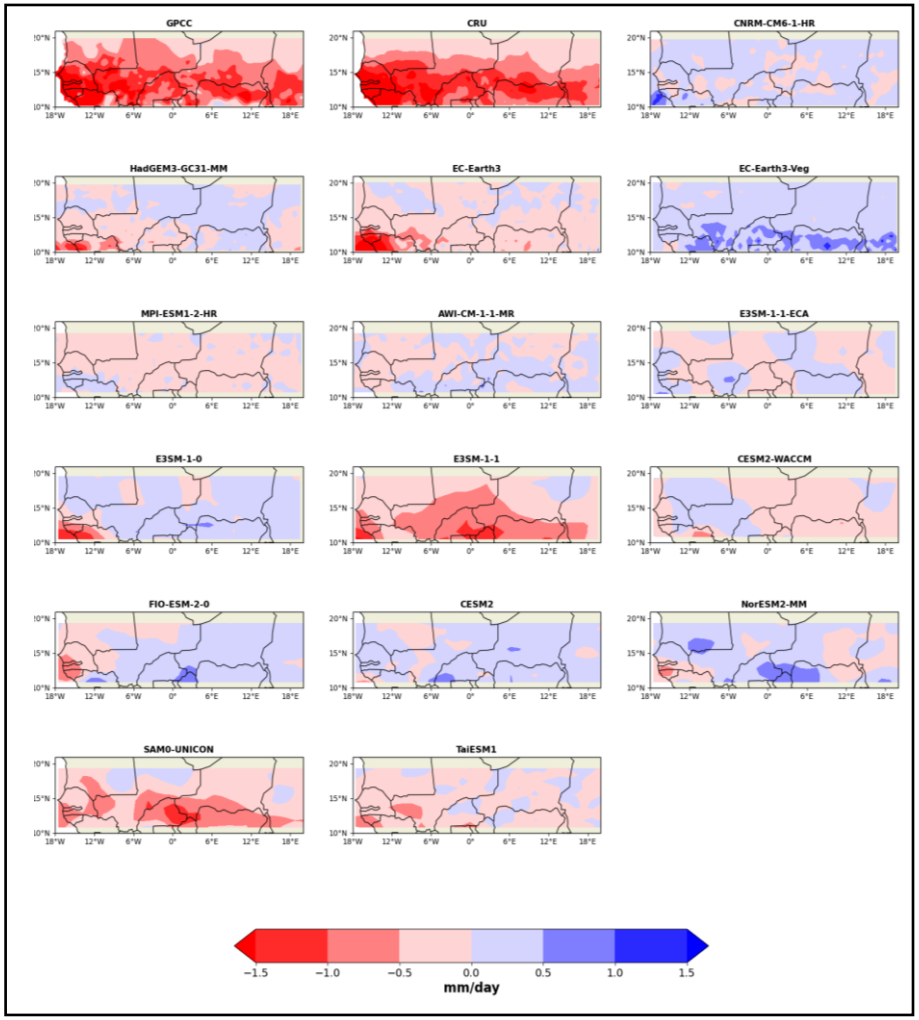

Figure 4.1.5: *Maps displaying the difference (mm/day) between the average of the drought period (1970-1983) and the wet period (1950-1963) for all the models and the two observational datasets, for the higher resolution models. Negative (positive) numbers represent the drought period being drier (wetter) than the wet period.*

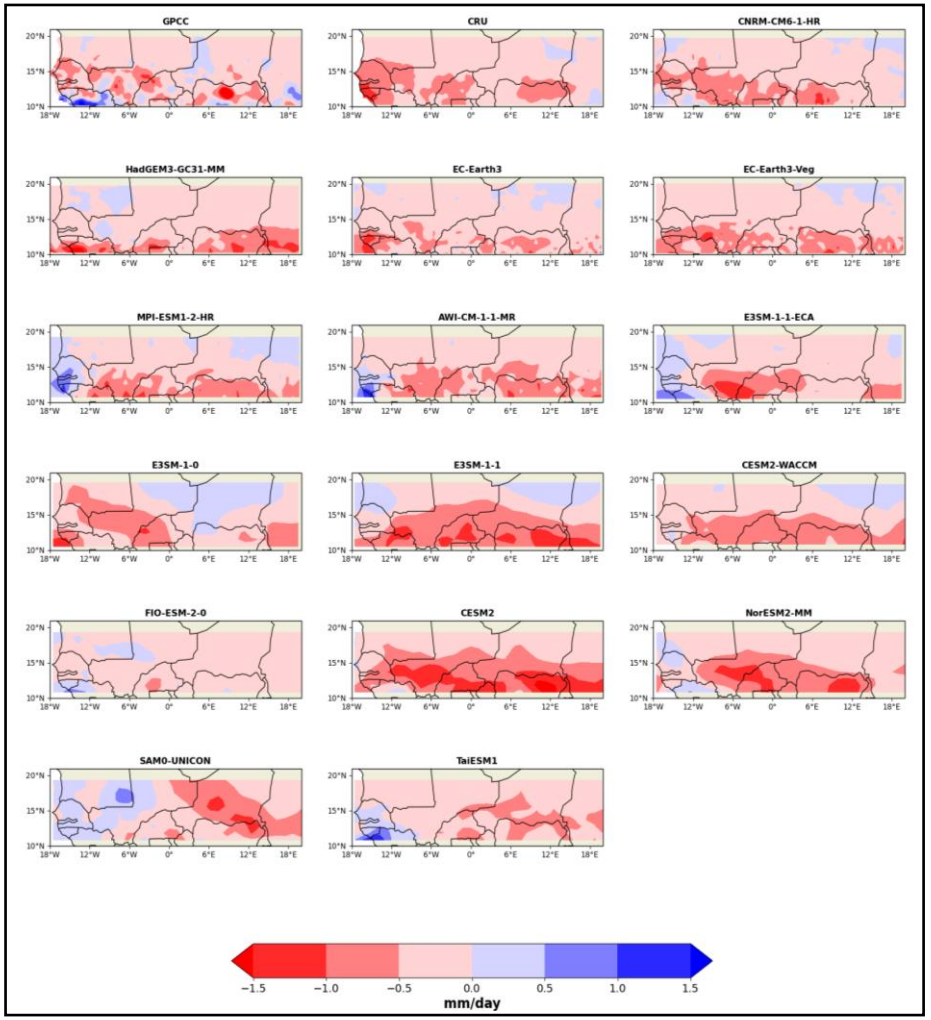

Figure 4.1.6: *Maps displaying the difference (mm/day) between the average of the drought period (1970-1983) and the recent period (2001-2014) for all the models and the two observational datasets, for the higher resolution models. Negative (positive) numbers represent the drought period being drier (wetter) than the recent period.*

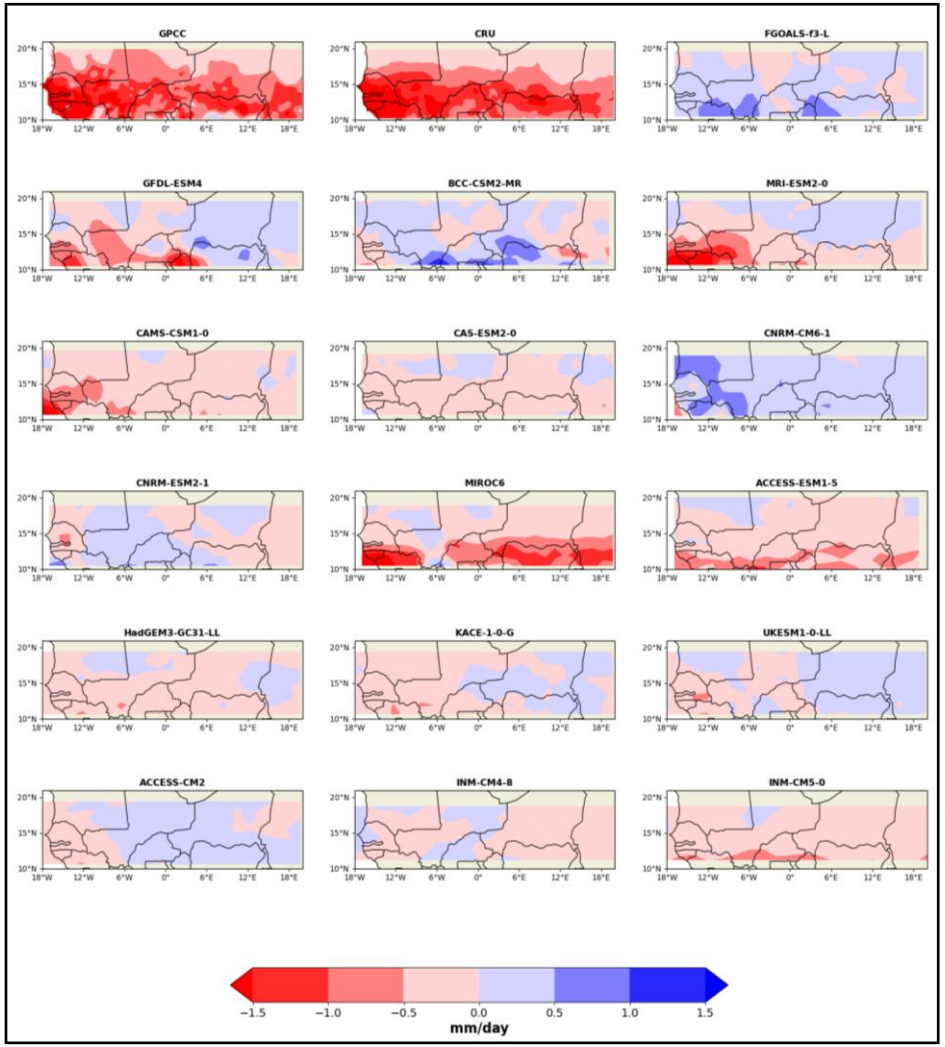

Figure 4.1.7: *As Figure 4.1.5, but for the medium resolution models.*

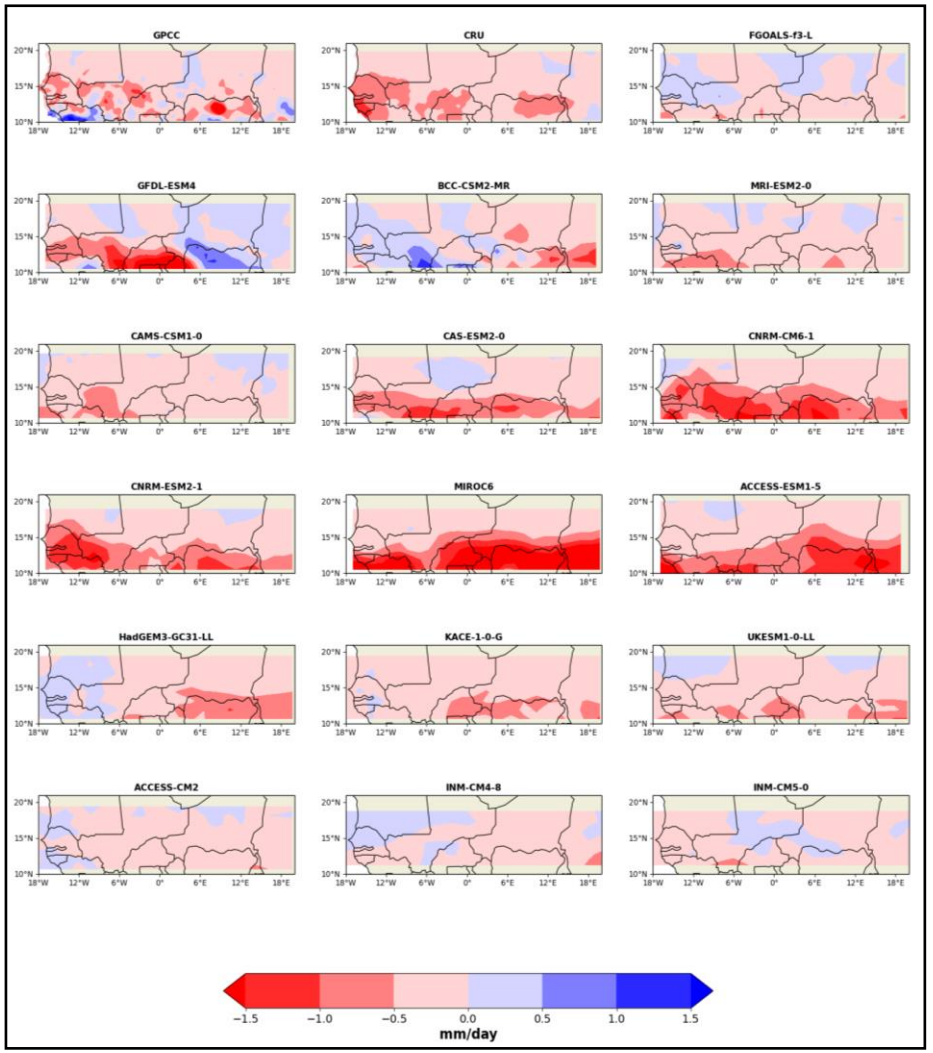

Figure 4.1.8: *As Figure 4.1.6, but for the medium resolution models.*

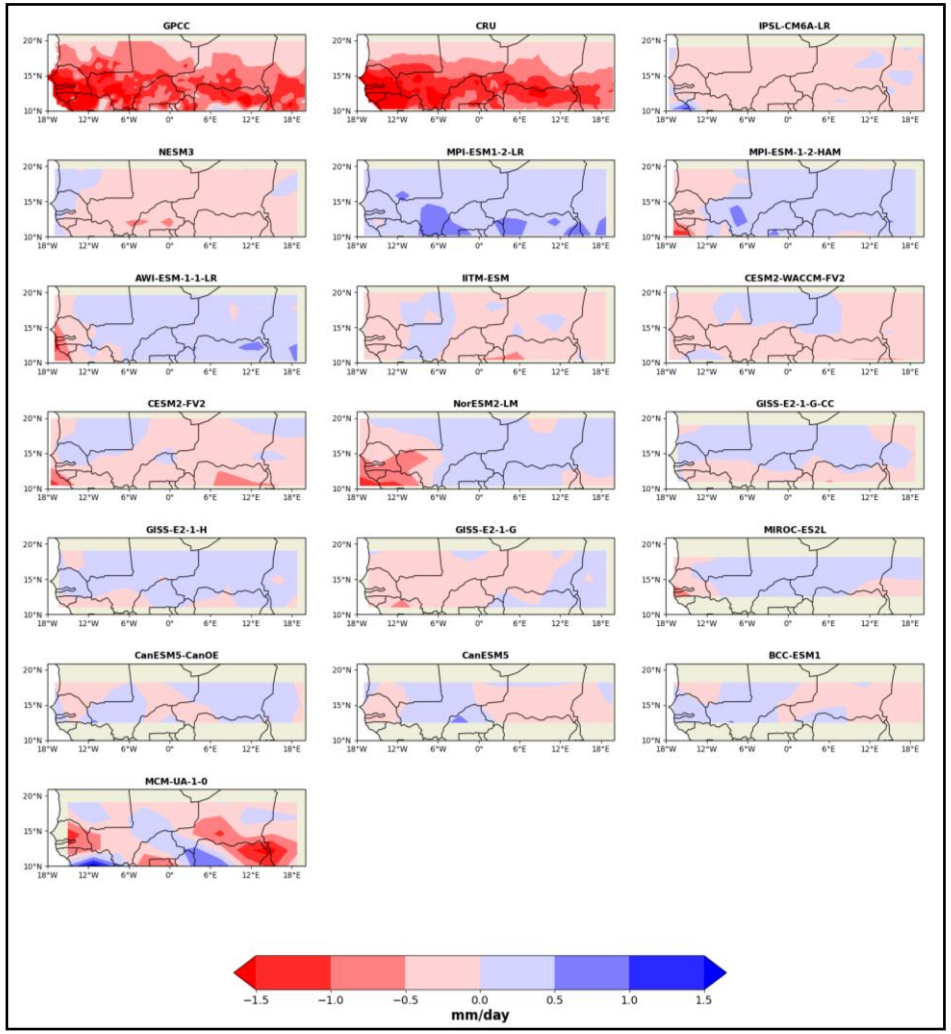

Figure 4.1.9: *As Figure 4.1.5, but for the lower resolution models.*

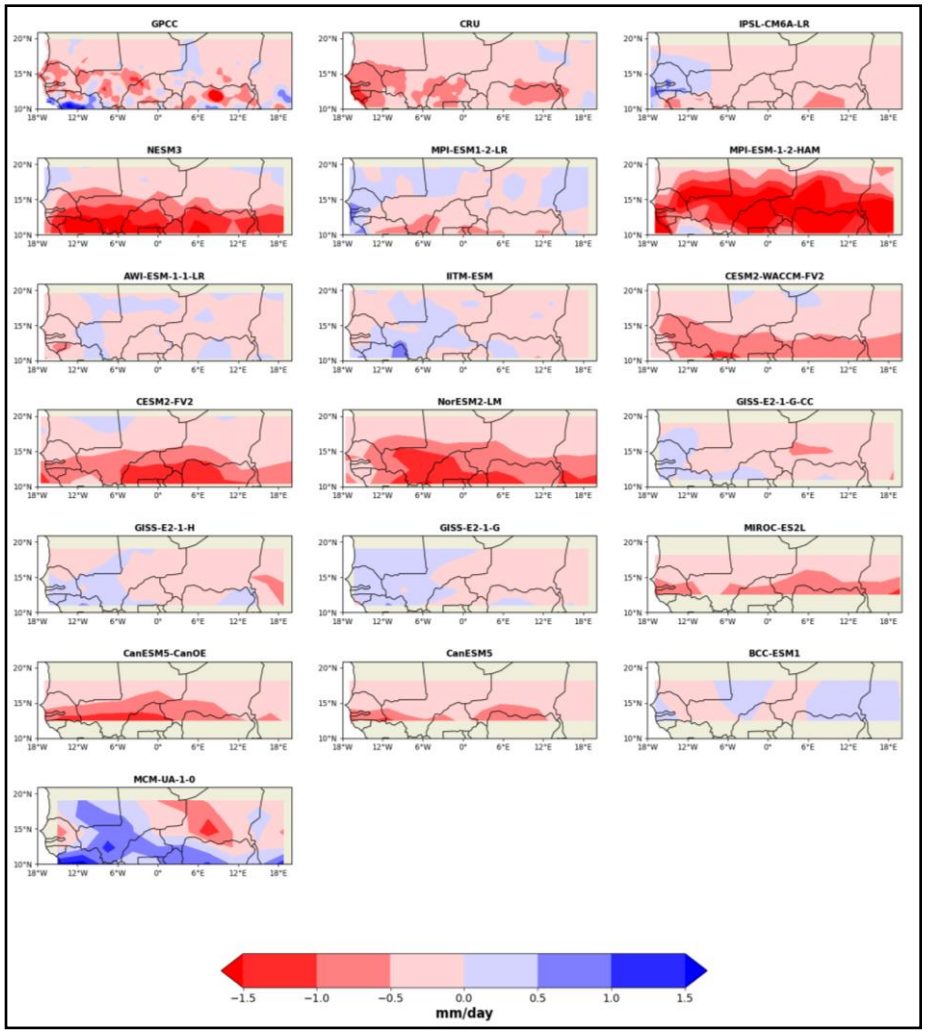

Figure 4.1.10: *As Figure 4.1.6, but for the lower resolution models.*

4.1.2.3. Method 3: Model bias during the drought period

Model biases were calculated for the drought period, as another route to evaluating the models' ability to simulate the drought, using both the time series (Figure 4.1.11) and spatial data (Figures 4.1.12 – 4.1.14). These are the difference between the average precipitation during the modelled drought period and the observations.

According to the time series data, five models overestimate precipitation, with the rest underestimating (Figure 4.1.11). The relationship with resolution was also considered. There was no consistency between model resolution and bias (Figure 4.1.11). MCM-UA-1-0 is the lowest resolution model and has the strongest overestimation of nearly 2mm/day, which is significant when analysing low precipitation periods as this bias could hide the overall signal. ACCESS-CM2 has the strongest underestimation bias the same magnitude of MCM-UA-1-0 but is a medium resolution model.

Most models have a dry spatial bias of over 2mm/day, however, there are some which are wetter than the observations, for example, SAM0-UNICON has areas which are over 4mm/day wetter (Figures 4.1.12 – 4.1.14). Regardless of the direction of bias, the strongest differences are seen in the south-west Sahel, over the Guinea Coast, suggesting this is a region where model representation still needs to be improved – an uncertainty that has persisted across CMIPs (Paxian et al, 2016). A subset of CMIP5 models revealed many struggled to capture the observed magnitude of change in Sahelian precipitation, with the Guinea Coast seeing the largest overestimation of differences (Paxian et al, 2016). The E3SM models have a relatively small bias compared to the other models in the higher resolution group, with most of the Sahel being ±1mm/day than the observations (Figure 4.1.12). The medium resolution models are generally drier than the observations, except for GFDL-ESM4, MIROC6 and the two CNRM models (Figure 4.1.13). The lower resolution models tend to have a smaller bias compared to the other two resolution groupings, apart from MCM-UA-1-0 which has a strong wet bias over a large area (Figure 4.1.14). However, the temporal bias calculations do provide different results compared to the spatial biases, for example, SAM0-UNICON has a temporal bias of ~1.5mm/day (Figure 4.1.11) but an average spatial bias of ~3mm/day (Figure 4.1.12), highlighting how the perspective taken can affect how well the models behave in comparison to each other.

The location of precipitation biases over the Sahel is influenced by the modelled ITCZ (Monerie et al, 2017). For example, Monerie et al (2017) found that if the ITCZ is displaced south, the Gulf of Guinea tends to have a wet bias whereas western Africa has a dry bias. In these results, south-west Sahel has a dry bias in most models and the Gulf of Guinea is not in the study region, but this could indicate the ITCZ is incorrectly located within the models. Alongside this, Ukkola et al (2020) researched meteorological droughts in the region and deemed a result robust when the standard deviation between the models was smaller than the magnitude of the change itself. In the results here, most models have a bias that is larger than the difference between the various time periods, suggesting the results are not robust.

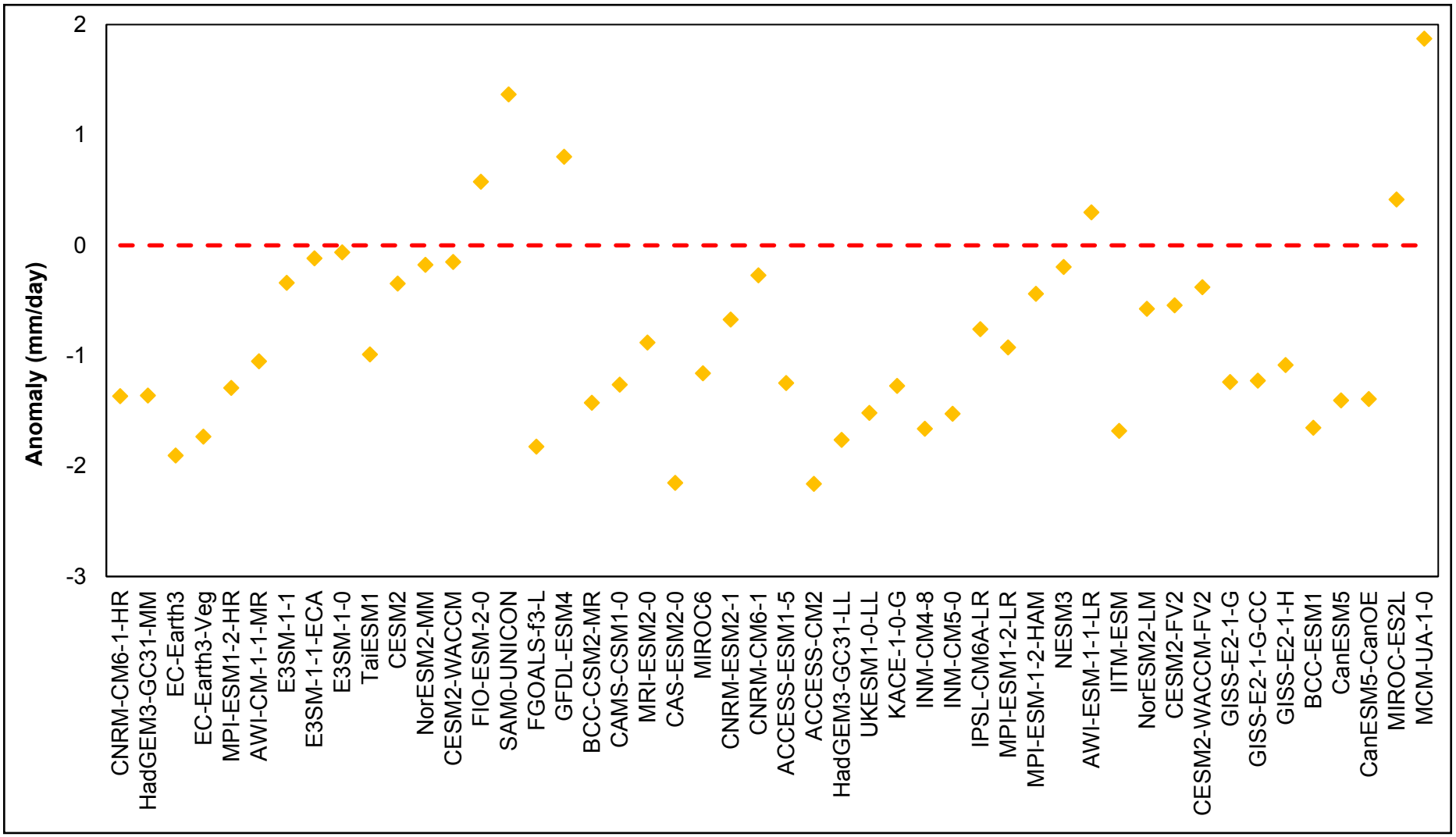

Figure 4.1.11: *Temporal biases (mm/day) between the time series data for the modelled drought period (1970-1983) and the observed drought period in the GPCC dataset, organised by nominal resolution, with the highest resolution on the left and the lowest on the right. The CRU anomalies are consistent with GPCC.*

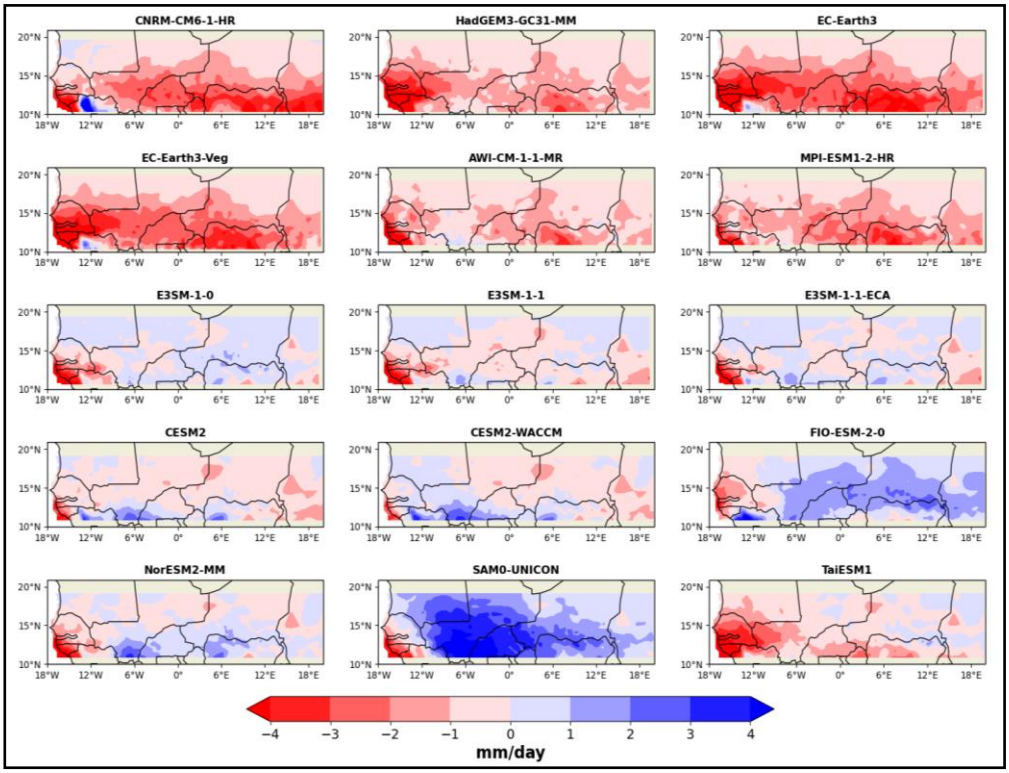

Figure 4.1.12: *Maps displaying the difference (mm/day) between the average of the drought period (1970-1983) in the highest resolution models and GPCC. Negative (positive) numbers represent the model being drier (wetter) than GPCC. The difference with CRU is consistent with those displayed for GPCC.*

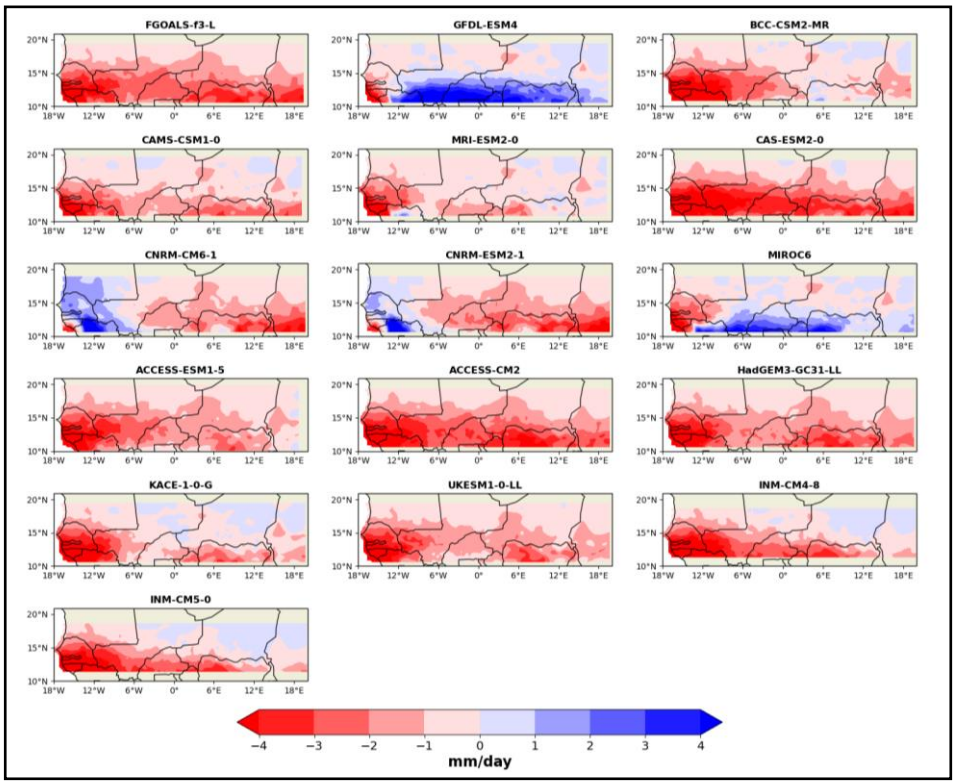

Figure 4.1.13: *As Figure 4.1.12, but for the medium resolution models.*

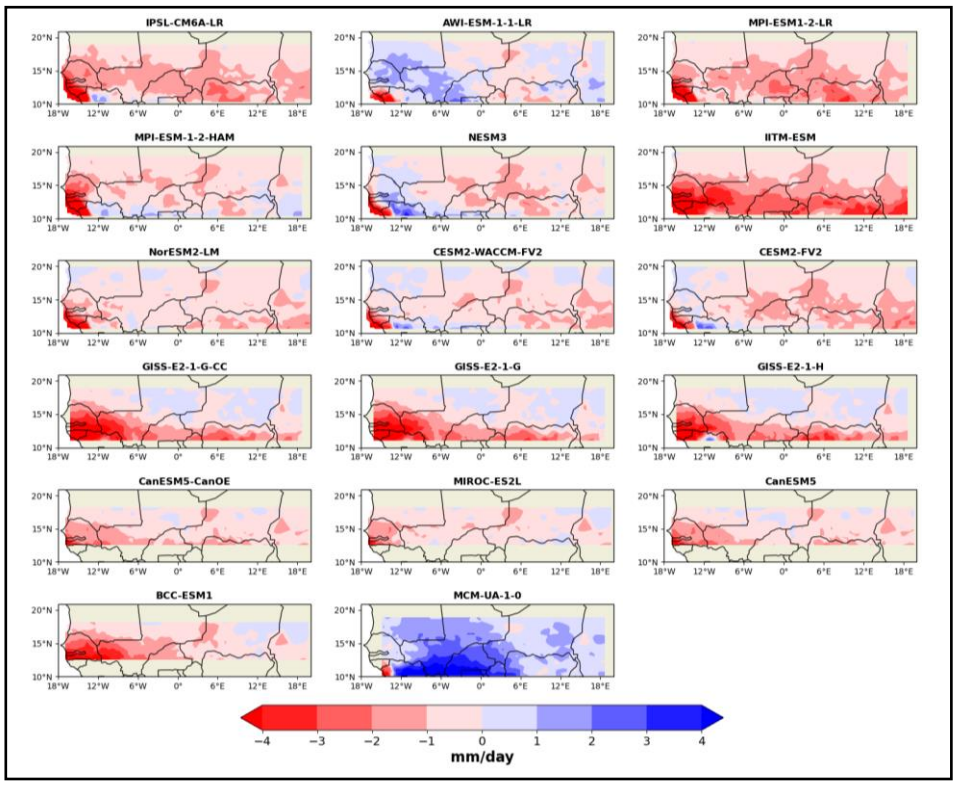

Figure 4.1.14: *As Figure 4.1.12, but for the lower resolution models.*

4.1.3. Summary

Whether a model is judged to be able to simulate observed interdecadal variability in precipitation depends on the method used for assessment. Regardless of the method used, it is clear most CMIP6 models fail to capture the interdecadal variability and the magnitude of the wet and dry periods.

According to temporal correlations, EC-Earth3 is one of the best performing models and one of the worst is HadGEM3-GC31-MM – both in the higher resolution model grouping. Going by the spatial representation of the differences between the drought and wet periods, E3SM-1-1 (higher resolution; Figure 4.1.7) is one of the best performers and the worst is MPI-ESM1-2-LR (lower resolution; Figure 4.1.9).

Spatially through visual analysis, the best model appears to be MIROC-E2SL in the lower resolution grouping, where the bias is mainly 1mm/day with some small areas of slightly higher dry numbers (Figure 4.1.14). Both worst models are in the higher resolution grouping (Figure 4.1.12). The worst dry bias model is EC-Earth3 with most of the bias being up 3mm/day drier than the observations below 15ºN, and above this it ranges from 0-2mm/day. SAM0-UNICON is the worst model for the wet bias, which is mainly +1-3mm/day, with a small dry area over Guinea of 3mm/day. According to the temporal bias, the best model is E3SM-1-0 (-0.06mm/day; higher resolution) and the worst models are ACCESS-CM2 (-2.16mm/day; medium resolution) and MCM-UA-1-0 (+1.87mm/day; lower resolution).

4.2. What factors relate to model representation of precipitation variability?

Various factors have been implicated for the varying representations of historical precipitation over the Sahel in CMIP models. Higher resolution models should in theory capture more of the small-scale precipitation systems, but this can be affected by other aspects such as the role of aerosols and other anthropogenic influences which either directly change precipitation or indirectly via changes in sea surface temperatures.

4.2.1. Resolution

Figure 4.2.1. shows there is a wide range in the strength of correlation coefficients between the models and GPCC, using either a five-year or 10-year running mean, from 0.6 to -0.5 and nearly 0.8 to -0.7 respectively. The correlations strengthen with more years in the running mean. The interannual coefficients were not plotted because no correlation is expected on this timescale, as seen in Figure 4.1.4. Figure 4.2.1. illustrates the relationship between correlation coefficients and model resolution. On the whole, the higher positive correlation coefficients are found in the higher resolution models. However, outside of this, there is no clear link between model resolution and representation of precipitation variability, with some of the lowest resolution models having higher correlation coefficients than the higher resolution models. A similar pattern is seen with the model biases, for example, E3SM-1-0 has the smallest bias but is not the highest resolution model (Figure 4.1.11-4.1.14).

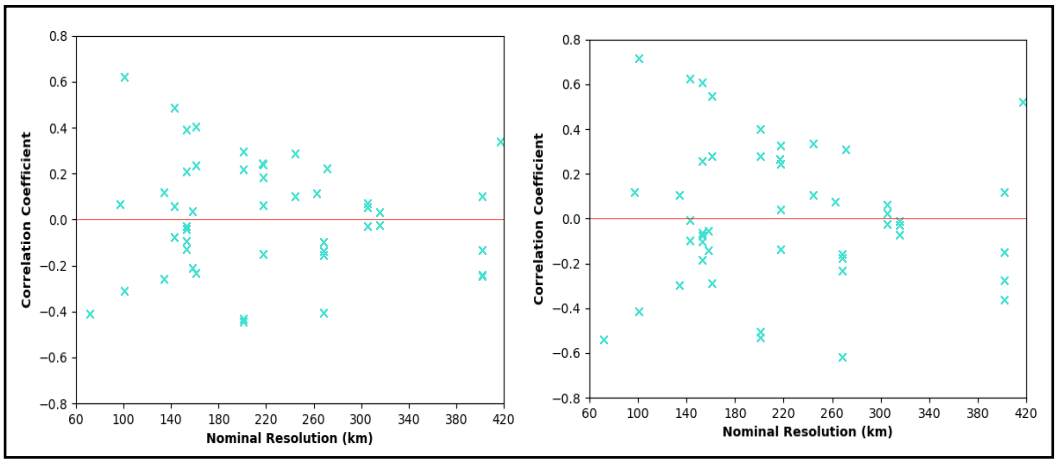

Figure 4.2.1: *Scatterplots of the GPCC Pearson's r correlation coefficients and the model's respective nominal resolution (km). Left: five-year running mean. Right: 10-year running mean. correlation coefficients with CRU are consistent with those with GPCC.*

Vellinga et al (2016) found increasing model resolution in three versions of the Met Office UM atmosphere model had a positive impact on the representation of Sahelian precipitation. They inferred this to be due to the higher resolution model being able to depict fine circulation elements better than the low-resolution models, thus can generate precipitation more efficiently (Vellinga et al, 2016). However, the model also needs to have accurate physics to improve performance (Vellinga et al, 2016). It must be noted that this study only focused on one model so is not representative of all models that have participated in CMIP6, and that it was an earlier version of HadGEM3. Later versions, as used in CMIP6, did not show such a clear improvement with resolution (Vellinga, pers. comm).

4.2.2. Anthropogenic influence

The Historical-Natural (Hist-Nat) simulations are still coupled but hold CO_2 and other GHGs at pre-industrial levels and only includes natural aerosols (Eyring et al, 2016). There are no land-use changes so removes the impact of humans, although do not include all natural forcings, such as natural forest fires (Eyring et al, 2016).

Figure 4.2.2 shows the time series data for the Hist-Nat simulations. On the whole, there is less variation compared to the historical simulations, signifying the influence humans have had on precipitation across time. It also suggests the recent increase in precipitation seen in the coupled historical simulations towards the end of the 20th century is linked to human actions (Figure 4.1.2/4.1.2), due to the Hist-Nat simulations not having a corresponding increase (Figure 4.2.2). The data is plotted on the same scale as the historical simulations, indicating the Hist-Nat simulations have less spread than the full historical runs. However, fewer models performed this simulation so this result could be influenced by a smaller sample size.

Dong and Sutton (2015) specifically focused on the radiative forcings associated with greenhouse gases (GHGs) to investigate the anthropogenic influence towards the end of the 20th century on Sahelian precipitation. They concluded nearly 75% of the observed changes in Sahelian precipitation is associated with the rise in GHGs, hence indicating GHGs might have a positive impact in this region (Dong and Sutton, 2015). However, another study by Giannini and Kaplan (2019) hinted conclusions like this may only hold when the impact of aerosol cooling is outweighed by GHG warming. They implicated the aerosol feedback on SSTs in the Sahel droughts through the balance of tropical oceans warming by increased GHGs and the North Atlantic cooling from aerosols (Giannini and Kaplan, 2019). In the late 20th century, environmental policies were introduced to limit aerosol emissions, thus the GHG warming began to outweigh aerosol cooling and coincided with the precipitation recovery over the Sahel (Giannini and Kaplan, 2019). These studies suggest aerosols played a bigger role in the drought whereas GHGs played a bigger role in the recovery, implying they potentially have opposite influences on Sahelian precipitation (Giannini and Kaplan, 2019).

As with the historical simulations, correlation coefficients were computed to assess whether the Hist-Nat simulations represent observed variability. No models agree with the observations on the interannual timescale (Appendix 1.3). On the five-year timescale, only ACCESS-CM2 and CESM2 agree. On top of these two, HadGEM3-GC31-LL, ACCESS-ESM1-5 and IPSL-CM6A-LR agree with the observations on the 10-year running mean, but only just over the threshold. CNRM-CM6-1 disagrees with the observations with the 10-year running mean, with correlations of -0.25 (GPCC) and -0.27 (CRU), again, just over the threshold. The coupled historical simulations tend to have better correlations, which is reassuring as it implies the models can better capture the anthropogenic influence and supports the existing research base.

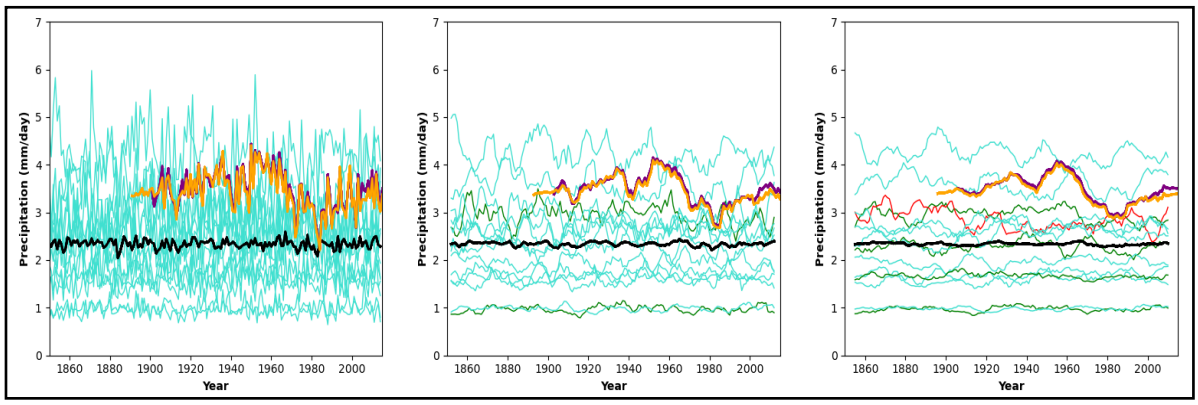

Figure 4.2.2: *Time series of JJAS precipitation (mm/day) over the study region for the lowest numbered ensemble member for each Historical-Natural run. From left to right: interannual timescale, five year running mean and 10 year running mean. The black line is the multi-model mean, purple is CRU and orange is GPCC. The models are coloured according to Lau et al (2006)'s thresholds where green is a Pearson's R value greater than 0.26 (agreement) and red is less than -0.26 (disagreement).*

The spatial pattern of change was also investigated in the Hist-Nat simulations (Figures 4.2.3 – 4.2.4). Despite the removal of the variation in CO_2 and other anthropogenic influences, CESM2 and GFDL-CSM4 still capture an area of significant drying that resembles the observations between the wet and drought periods (Figure 4.2.3). The other models have more muted differences, mainly between ±0.5mm/day, which is to be expected following the smaller variations seen in the time series. Nearly every model apart from CESM2 has an area where the drought is modelled at least 0.5mm/day wetter than the wet period (Figure 4.2.3).

Again, GFDL-CM4 and CESM2 have large areas with a negative difference of between 0.5mm/day and 1.5mm/day between the drought and recent periods (Figure 4.2.4). More models capture the drought being drier than the recent period, however, a few, for example IPSL-CM6A-LR and NorESM2-LM have large areas wetter in the drought period than the recent period, although, this is mostly +0.5mm/day.

Despite the more muted differences seen between the different time periods, it is clear model biases still exist (Figure 4.2.5). Generally, the highest uncertainties are found in the southern part of the study region, and a small concentration of high uncertainty over the Guinea Coast, regardless of the direction of bias of ±3mm/day.

ACCESS-CM2 has a similar bias to its historical equivalent, and so does ACCESS-ESM1-5, bar the added slight wet bias of 0.5mm/day on the eastern border of the Sahel. BCC-CSM2-MR, CanESM5, CNRM-CM6-1, GISS-E2-1-G, MIROC6 mirror their historical equivalent. CESM2's bias has been slightly reduced, as well as HadGEM3-GC31-LL. Whereas, IPSL-CM6A-LR's bias has been significantly reduced but now has a small area of wet bias, up to +3mm/day.

FGOALS-g3 has no historical equivalent, but its nearest comparison is FGOALS-f3-L and the bias for each model is very much the same. GFDL-CM4's nearest equivalent is GFDL-ESM4 and the model biases in the Hist-Nat simulations are a smaller magnitude than the historical model. Whereas, NorESM2-LM has a larger area of a slightly wet bias of up to 0.5mm/day, but in the historical equivalent, it is mostly a dry bias of 0.5mm/day in the now wetter areas.

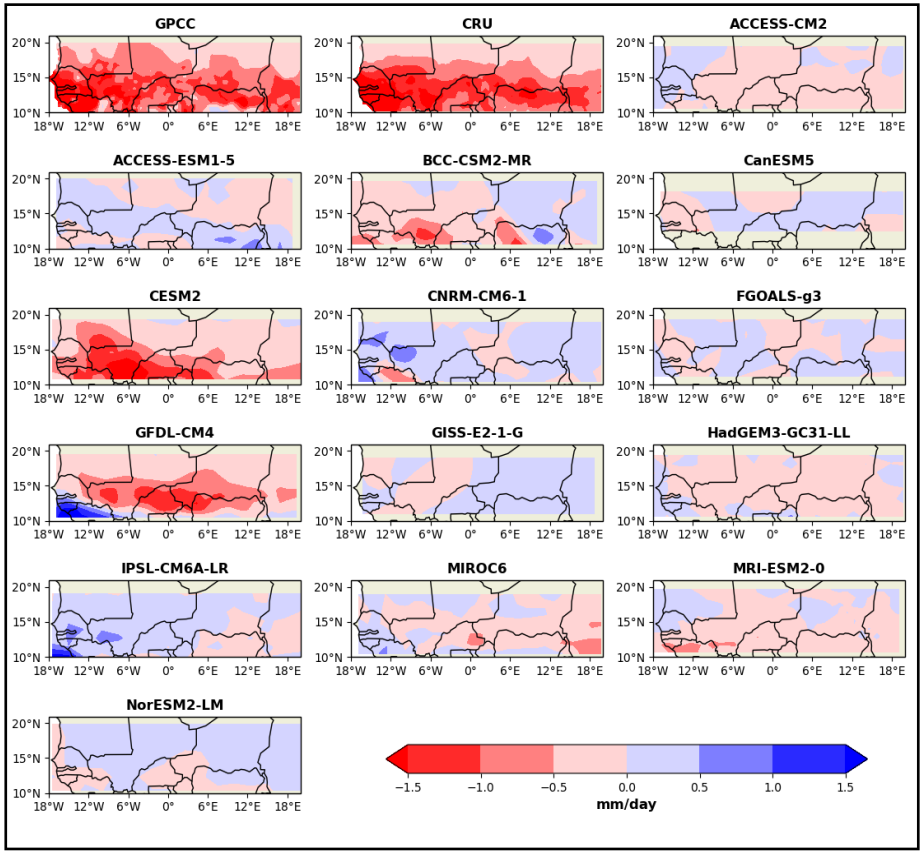

Figure 4.2.3: *Maps displaying the difference (mm/day) between the average of the drought period (1970-1983) and the wet period (1950-1963) for all the available Historical-Natural models and the two observational datasets. Negative (positive) numbers represent the drought period being drier (wetter) than the wet period.*

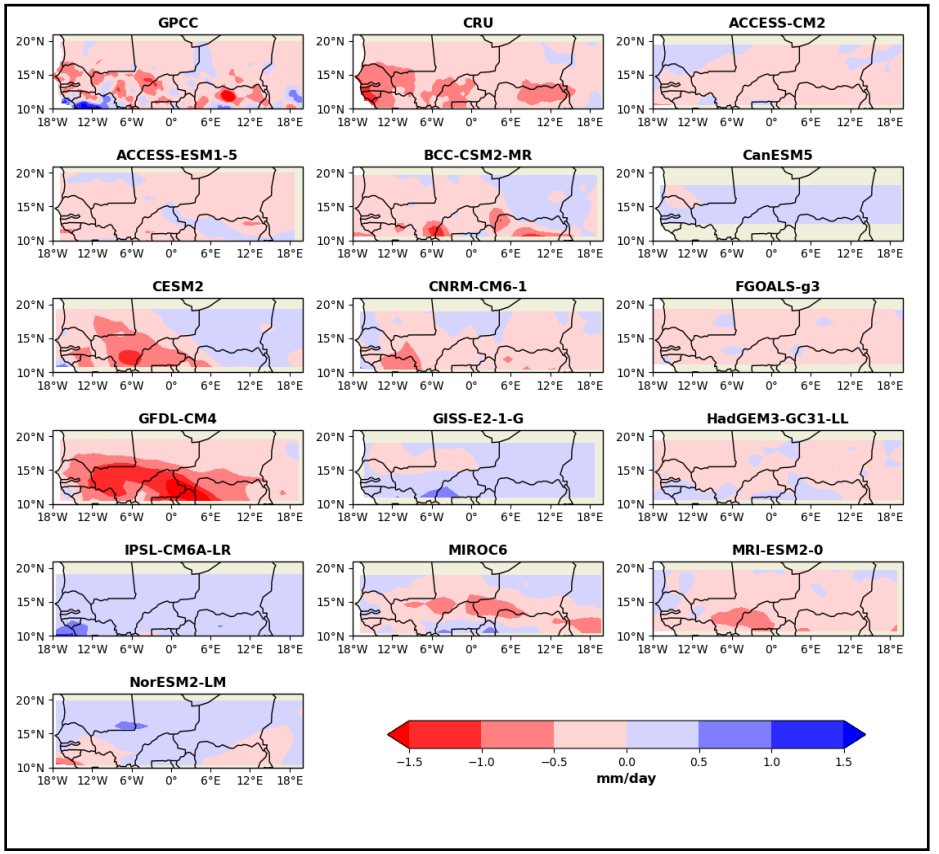

Figure 4.2.4: *As Figure 4.2.3 but for the average of the drought period (1970-1983) and the recent period (2001-2014).*

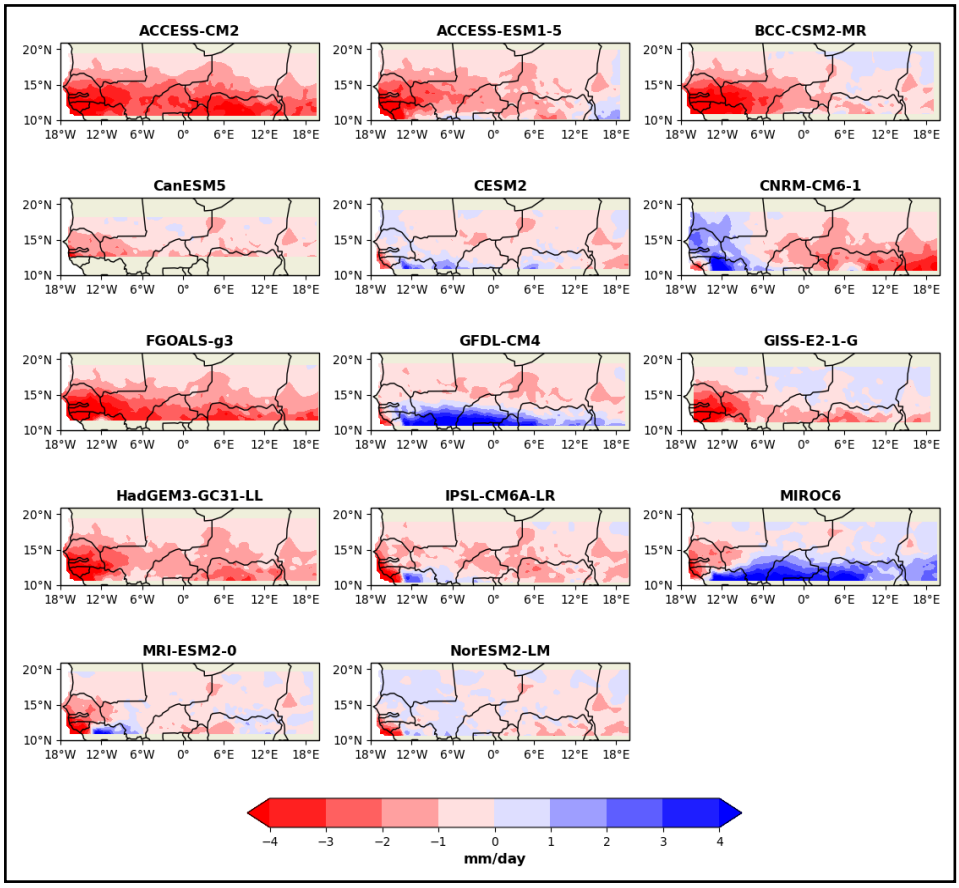

Figure 4.2.5: *Difference maps of the models and GPCC of JJAS precipitation (mm/day) averaged over the drought period (1970-1983) for the Historical-Natural simulations. Negative (positive) numbers represent the model being drier (wetter) than the observations. Note: only GPCC is presented because the differences are consistent with CRU.*

4.2.3. Interactive oceans (AMIP-Historical)

The atmosphere-only simulations have prescribed oceans, rather than dynamic, which forces modelled interannual variability to align with the observations (Eyring et al, 2016). AMIP-Hist simulations cover 1870 to 2014 (Eyring et al, 2016) - including the full drought period. These simulations were examined to evaluate whether models can reproduce the drought when forced with the observed SSTs. The range of precipitation timeseries is slightly narrower compared to the coupled historical simulations (Figure 4.2.6). The MMM is also more consistent with the observations, showing similar long-term variations, albeit ~1mm/day drier (Figure 4.2.6). There is a clear decrease in modelled precipitation in the drought period across all three plots, however particularly in the 5-year running means, the MMM increases and peaks in the recent period, then decreases again (Figure 4.2.6).

68% of the models in AMIP-Hist strongly agree with the observations and are statistically significant on the interannual timescale (Appendix 1.4) – a substantial increase from 2% in the coupled historical simulations (Figure 4.2.7). There are no models in AMIP-Hist which disagree. This is consistent with other studies which have found atmosphere-only models to simulate the annual cycle of precipitation better than coupled models, having higher correlations (Sow et al, 2021). This is likely linked to

coupled models having their own simulated interannual variability as they are not forced by observations.

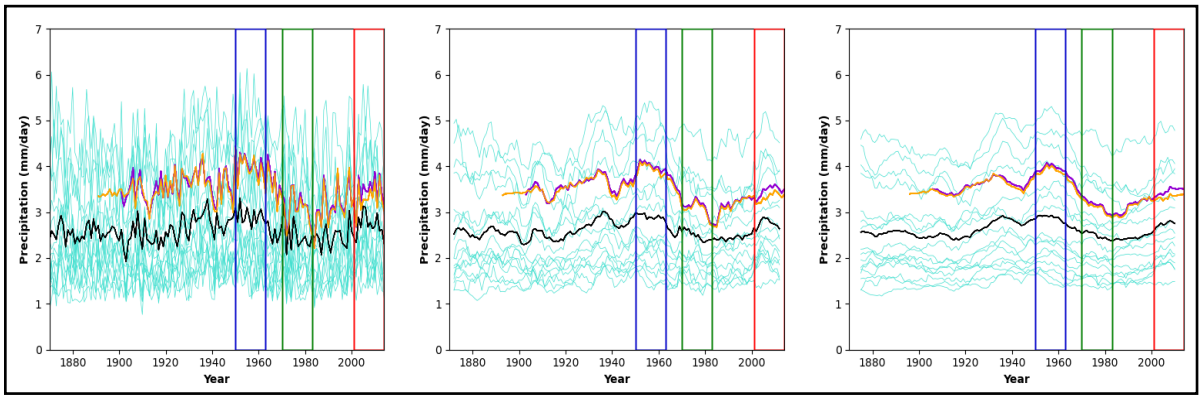

Figure 4.2.6: *Time series of JJAS precipitation (mm/day) the lowest numbered ensemble member for each AMIP-Hist model run (1870-2014). From left to right: interannual timescale, five-year running mean and 10-year running mean. The multi-model mean is the black line, CRU is the purple line and GPCC is orange. The blue box denotes the wet period, the green the drought and the red the recent period.*

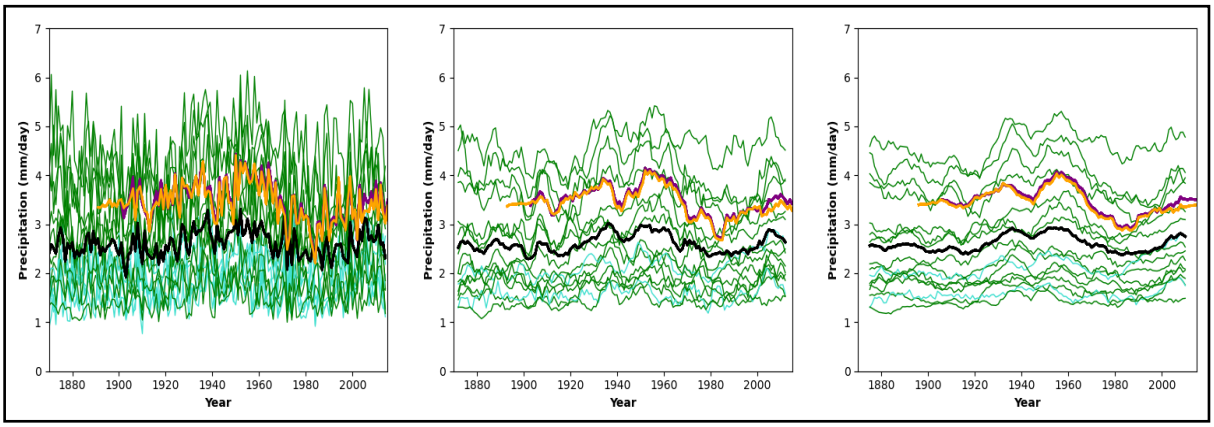

Figure 4.2.7: *As Figure 4.2.6 but the models are coloured according to Lau et al (2006)'s thresholds where green is a Pearson's r value greater than 0.26 (agreement) and red is less than -0.26 (disagreement).*

The decrease in precipitation in the recent period (Figure 4.2.6) is reflected in the difference maps between the drought period and wet period and drought and recent period. The differences between the drought and wet periods are larger than the drought and recent period, although for both anomaly calculations there are still models suggesting large areas are wetter in the drought period than both the wet and recent periods (Figures 4.2.8 and 4.2.9). The CNRM models show more similarity to the observations in the drought minus recent period maps but struggle in the drought minus wet period maps. CESM2 appears to capture the observations well in both sets of differences, closely followed by TaiESM1. MIROC6 is interesting because it has a dry band corresponding to the observations between 10ºN and 15ºN in the drought minus wet period map, but in the drought minus recent it shows the whole study region being up to 0.5mm/day wetter in the drought period.

In terms of model bias, the differences are larger, with the colour bar being ±4mm/day rather than ±1.5mm/day, highlighting how the model biases are greater than the changes shown by the models (Figure 4.2.10). There is no consistency across

the models for the direction of bias, with some being drier than the observations and others being wetter. However, as seen with the coupled simulations, the highest uncertainty tends to be in the southern part of the study region, regardless of the direction of the difference. As well, there are more models with a wet bias over west Africa, implying the modelled ITCZ could be located correctly, as seen in Monerie et al (2017)'s study.

Compared to the coupled simulations, there are changes in the extent and direction of the bias. MRI-ESM2-0, TaiESM1, CESM2, BCC-CSM2-MR, CAMS-CSM1-0, CanESM5 and FIO-ESM2-0 have wetter biases in the AMIP-Hist simulations, with some models having a complete change in bias direction than in the coupled simulations (Figure 4.2.10). MIROC6, IPSL-CM6A-LR, FGOALS-f3-L, CNRM-ESM2-1 and CNRM-CM6-1 all have slightly lower biases in AMIP-Hist, and despite GFDL-CM4 not having a direct equivalent coupled model, the bias has been reduced here too. IITM-ESM's bias has reduced in some areas, and become wetter in others, whereas CNRM-CM6-1-HR has remained relatively the same in both coupled and atmosphere only simulations across the whole Sahel.

Thus, the atmosphere only simulations indicate the coupled models struggle to represent the patterns of SST change and/or the interaction between SST patterns and the atmosphere. This is because prescribing the oceans has improved the model relationship with the observations. The model bias compared to observations has been improved slightly, however, model bias is still larger than the changes seen between the different periods in the models.

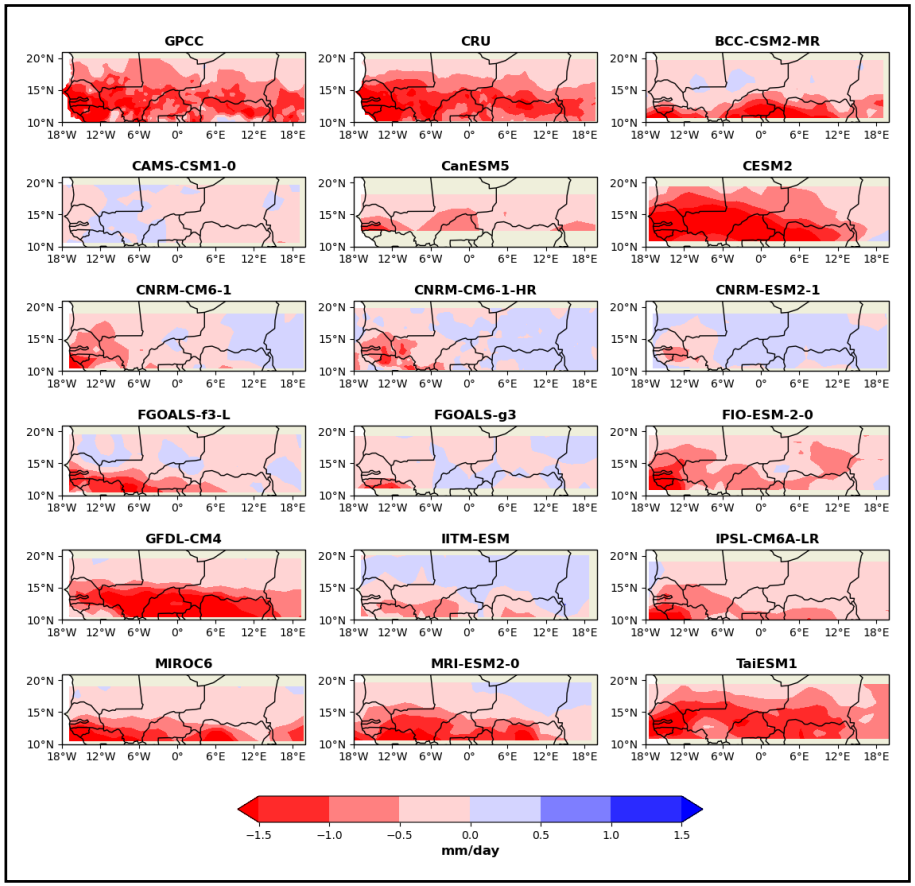

Figure 4.2.8: *Maps displaying the difference (mm/day) between the average of the drought period (1970-1983) and the wet period (1950-1963) for all the available AMIP-Hist models and the two observational datasets. Negative (positive) numbers represent the drought period being drier (wetter) than the wet period.*

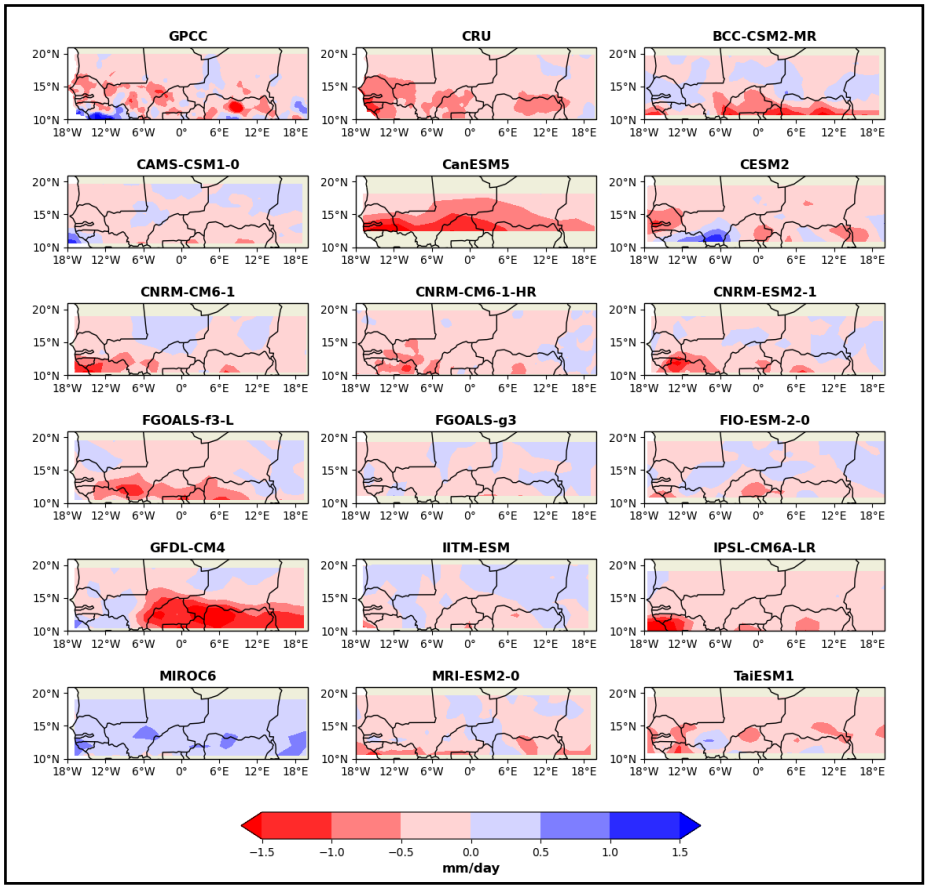

Figure 4.2.9*: As Figure 4.2.8, but between the average of the drought period (1970-1983) and the recent period (2001-2014).*

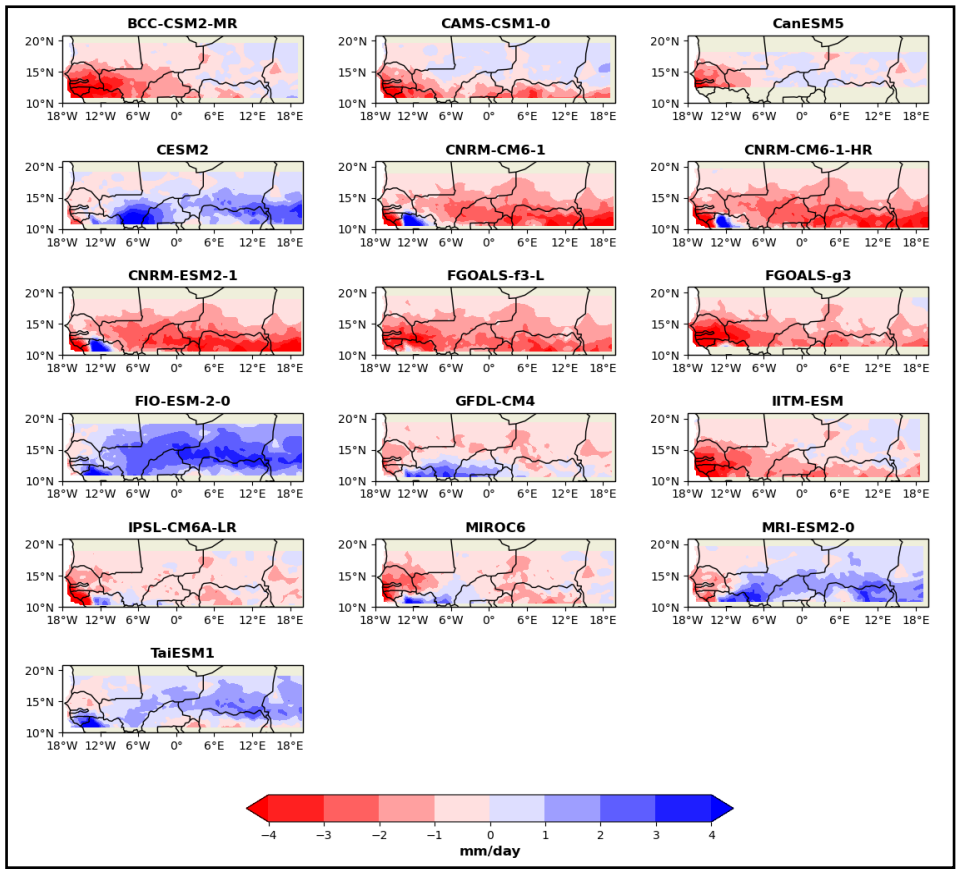

Figure 4.2.10: *Difference maps of the models and GPCC of JJAS precipitation (mm/day) averaged over the drought period (1970-1983) for the AMIP-Hist simulations. Negative (positive) numbers represent the model being drier (wetter) than the observations. Note: only GPCC is presented because the differences are consistent with CRU.*

The relationship between a models' performance in coupled mode and atmosphere-only mode was examined, to establish whether those models with better historical simulations also have better AMIP-hist simulations. 13 models have run both the CMIP historical simulations and the AMIP-Hist simulations (Figure 4.2.11). AMIP-Hist correlation coefficients are clearly stronger than the CMIP ones, with not even one negative coefficient, although CNRM-ESM2-1 (black square on Figure 4.2.11) is close to zero. Models by the CNRM group consistently have the lowest correlations across all pairings on the interannual timescale and the five-year running mean, suggesting even with removing the uncertainty of the oceans, there is still something affecting the representation in these models. They are amongst the models with the lowest correlations for the 10-year running mean. CNRM-CM6-1-HR is the highest resolution model in this study and the other two are medium resolution models (Figure 4.1.4), indicating resolution does not always have a large influence on representation. This contrasts with Vellinga et al (2016)'s conclusions for the Met Office UM. MRI-ESM2-0 has the highest CMIP correlation coefficients across all three timescales from ~0.2 to ~0.6, and the highest AMIP-Hist coefficient switches between CESM2 at ~0.5 on the interannual to MIROC6 at over 0.9 with the 10-year running mean.

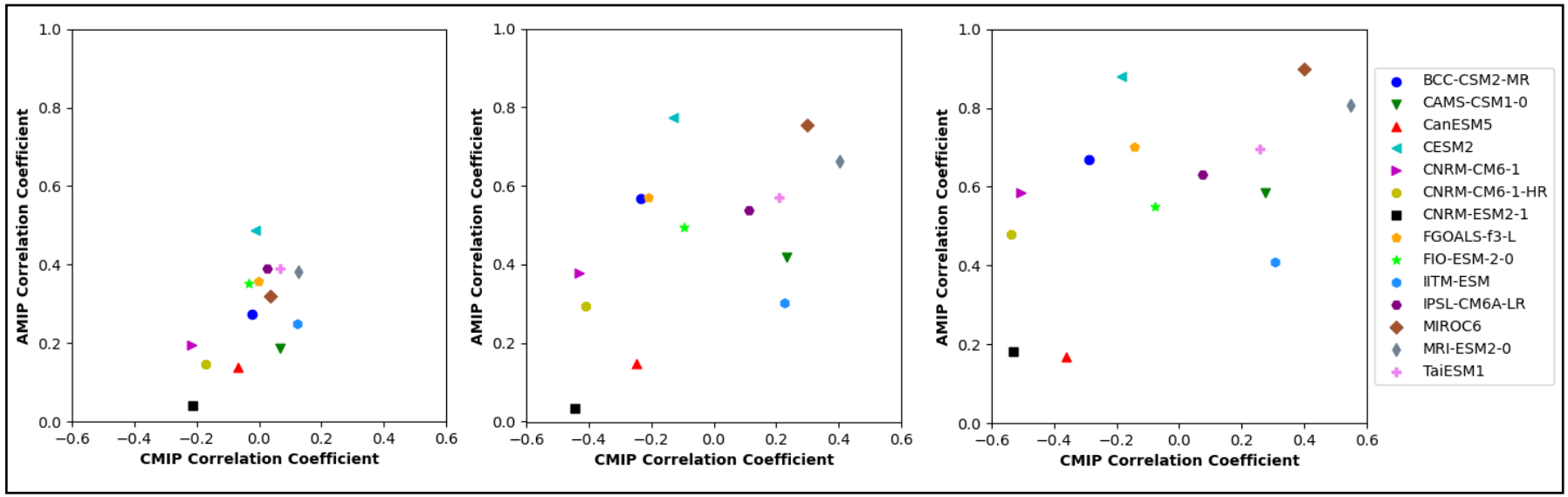

Figure 4.2.11: *Scatterplots comparing the Pearson's r correlation coefficients of CMIP models and AMIP models with GPCC. The correlation coefficients for CRU are consistent with those of GPCC. From left to right: interannual timescale, five-year running mean and 10-year running mean.*

4.2.4. Sea Surface Temperatures (SSTs)

Having shown the importance of SSTs for improving simulations of Sahel precipitation variability, they were examined in CMIP6 models in relation to the drought period. SSTs have been implicated as an influence on Sahelian precipitation through their connection to West African circulation (Nicholson, 2013). Previously, variations in modelled Sahelian precipitation have been linked to SSTs across a range of oceans; North Atlantic (Mohino et al, 2011), Indian (Bader and Latif, 2003) and the Mediterranean Sea (Polo et al, 2011). The North and South Atlantic dipole is a key influence on Sahelian precipitation (Mohino et al, 2011). Extratropical oceans have been found to influence precipitation on multidecadal timescales, with interannual variations linked to nearby oceans (Sultan and Gaetani, 2016). Also, tropical Pacific SSTs could induce Kelvin and Rossby waves that propagate across the equator and eventually interact over the Sahel, influencing precipitation in the region (Gaetani et al, 2017). This adds another level of complexity to understanding the role of SSTs in Sahelian precipitation.

The observations show the Northern Hemisphere SSTs are cooler by up to 1^{o}C and the Southern is warmer by 0.5-1^{o}C in the drought period compared to the wet period (Figure 4.2.12). The Indian Ocean is also warmer by 0.75^{o}C. These conditions are all linked to the Sahelian drought (Park et al, 2015; Zhou et al, 2016). Conversely, in the drought and recent period modelled differences, there is less of a clear distinction between the Northern and Southern Hemisphere oceans (Figure 4.2.13). Global warming has had a strong influence on SSTs, for most of the oceans are at least 0.5^{o}C colder in the drought period, with a large part of the Northern Hemisphere seeing SSTs that are over 1^{o}C colder (Dong and Sutton, 2015). Where there are warmer SSTs in the drought period, these are found in the Southern Hemisphere and are typically 0.5-1^{o}C warmer, although the predominant difference is the large negative difference between the drought and recent periods.

On the whole, the models struggle with capturing the difference in SSTs between the drought and wet periods. This is likely contributing to the models not having the high precipitation values that were observed in the wet period. As well as this, generally there are larger negative differences between the modelled drought and recent periods in the north Atlantic, linking to the upward trend in precipitation in recent years and global warming (Dong and Sutton, 2015), consistent across all models.

Where the models do capture the correct direction of change, the differences tend to be larger than HadISST. On the other hand, there are some models that are completely opposite to the observations. For example, EC-Earth3-Veg and HadGEM3-GC31-MM have modelled SSTs to be warmer in the North Atlantic (by over 1.5^{o}C and 0.5^{o}C-1^{o}C respectively) during the drought period than the wet period (Figure 4.2.12). It is expected to be the reverse, with the observations showing a lower temperature by up to 1.5^{o}C in the same location during the drought period (Figure 4.2.12). Although, these two models do perform better with the drought and recent period differences (Figure 4.2.13).

Changes in SSTs can increase Sahelian precipitation through a stronger

difference between the Sahara and the Gulf of Guinea SSTs (Haarsma et al, 2005; Monerie et al, 2017), and a stronger Atlantic dipole between the two hemispheres, with the latter having been seen in both CMIP5 and CMIP6 models (Park et al, 2015; Zhou et al, 2016; Monerie et al, 2017; Monerie et al, 2020). CMIP5 models that had been initialised with Atlantic and Indian Ocean SSTs performed better regarding Sahelian precipitation compared to those that were not (Martin and Thorncroft, 2014). In these CMIP6 results, E3SM-1-1 has one of the best representations of the observations for the drought and wet period precipitation anomalies (Figure 4.1.5). Its SSTs show an overestimation of the cooling in the Northern Hemisphere compared to HadISST, however, there is a clear difference between the two hemispheres so the resultant temperature gradient could have influenced the Sahelian precipitation, despite the overestimation (Figure 4.2.12).

An alternative theory is warmer SSTs resulting in a drier Sahel, comparable to the influence of ENSO, because of an associated increase in upper-level moist static energy, thus impacting the atmosphere's vertical stability (Giannini, 2010). EC-Earth3-Veg is one model with significantly warmer SSTs in the drought period compared to the wet period, opposite to the observations (Figure 4.2.12) and suggests this may be the cause of the drought period being much wetter than the wet period (Figure 4.1.5). For the drought and recent periods, the SSTs have a better resemblance of the observations, which feeds into the precipitation anomalies too. Despite not being the expected pattern, it can be inferred the warmer SSTs contributed to the higher modelled precipitation levels – the opposite to what has been suggested in the literature. Additionally, Monerie et al (2017) showed drought conditions in the west Sahel have been accompanied by a reduction in moisture convergence and increased subsidence by the winds, whereas the central Sahel being wetter is linked to Saharan warming and an increased gradient between the north and south Atlantic SSTs. So, whilst the concern remains that warmer SSTs could cause further droughts in the Sahel in the future, the current historical models suggest otherwise for past trends.

It has been found that the modelled ITCZ can be displaced south when the equatorial Atlantic have a warm bias and the north Atlantic colder, which has a knock-on impact to Sahelian precipitation (Monerie et al, 2017). The dry bias over west Africa implies the modelled ITCZ in these results could be displaced south. Following this, there are not many models with a warm bias for SSTs over the equatorial Atlantic, but there are larger cold biases in the North Atlantic which could feed into ITCZ displacement and Sahelian precipitation (Monerie et al, 2017).

As well, the West African Monsoon brings moisture into the Sahel and is linked with SSTs (Nicholson, 2013). The temperature gradient between the Sahara and the Gulf of Guinea is one of the main influences on the WAM (Nicholson, 2013). This gradient tends to be underestimated in models, resulting in the WAM being displaced south compared to observations (Nicholson, 2013; Monerie et al, 2017), thus also impacting precipitation.

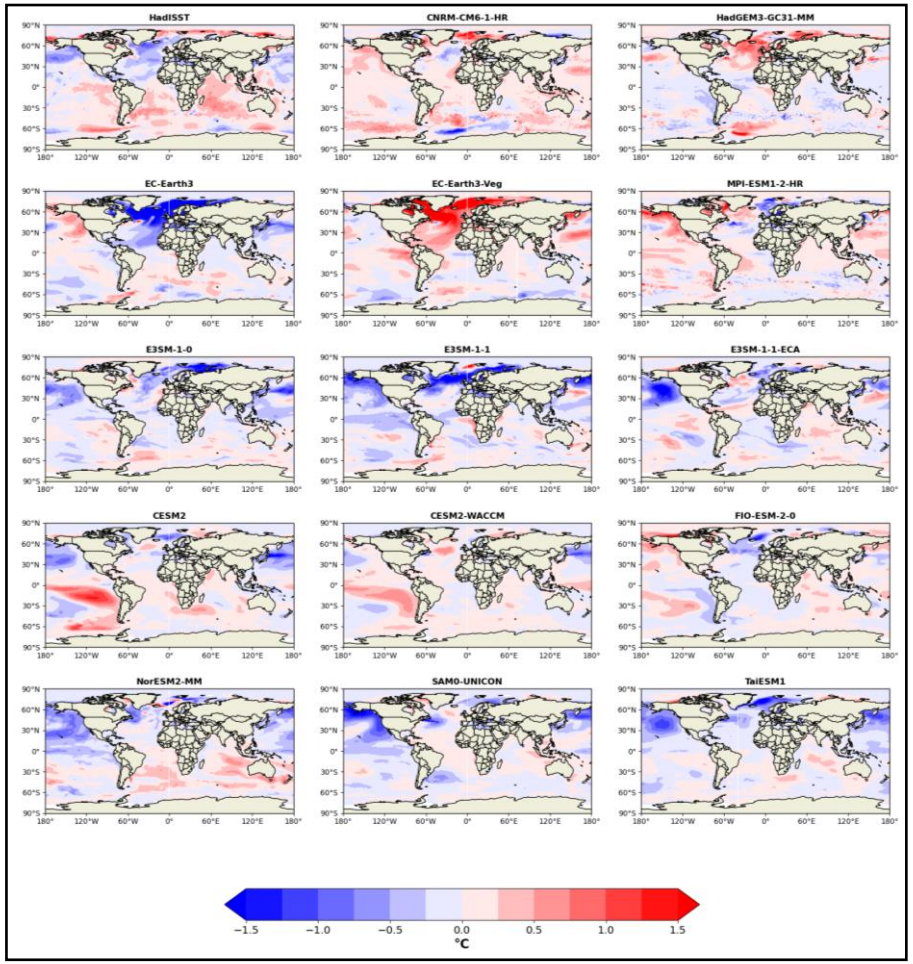

Figure 4.2.12: *Maps displaying the difference in sea surface temperatures (°C) between the average of the drought period (1970-1983) and the wet period (1950-1963) for the higher resolution models and HadISST, ordered by nominal resolution. Negative (positive) numbers represent the drought period being colder (warmer) than the wet period.*

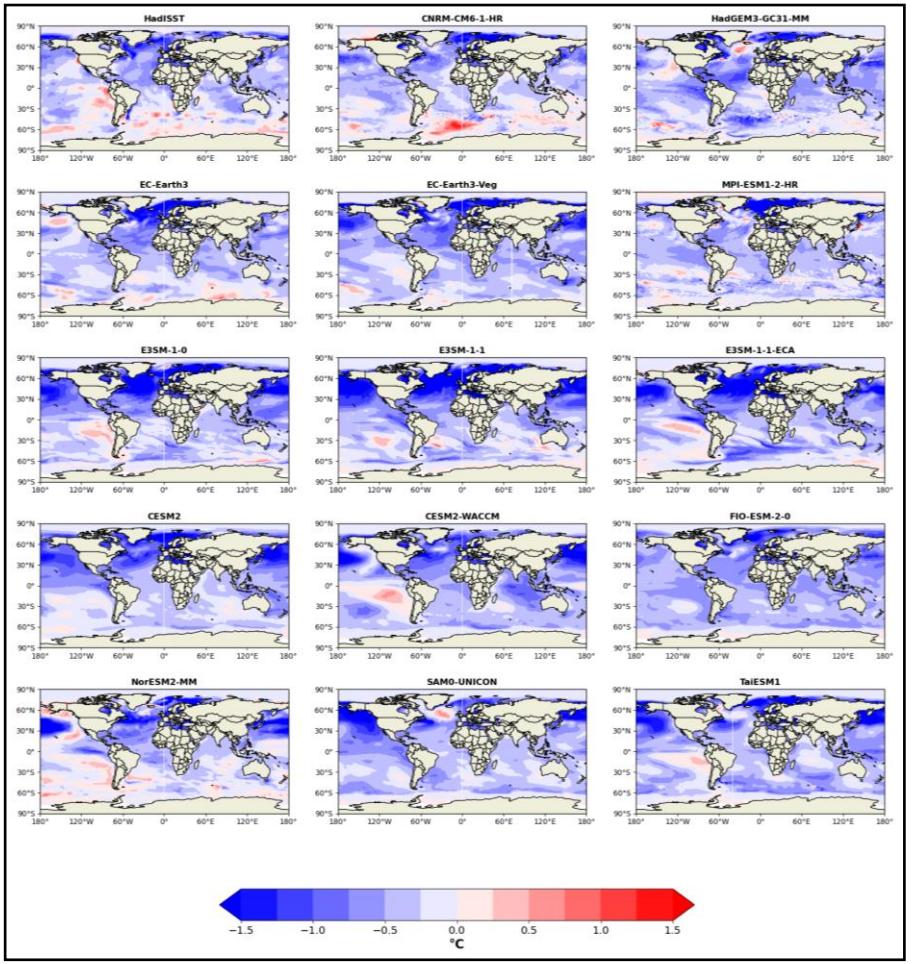

Figure 4.2.13: *Maps displaying the difference in sea surface temperatures (°C) between the average of the drought period (1970-1983) and the recent period (2001-2014) for the higher resolution models and HadISST, ordered by nominal resolution. Negative (positive) numbers represent the drought period being colder (warmer) than the recent period.*

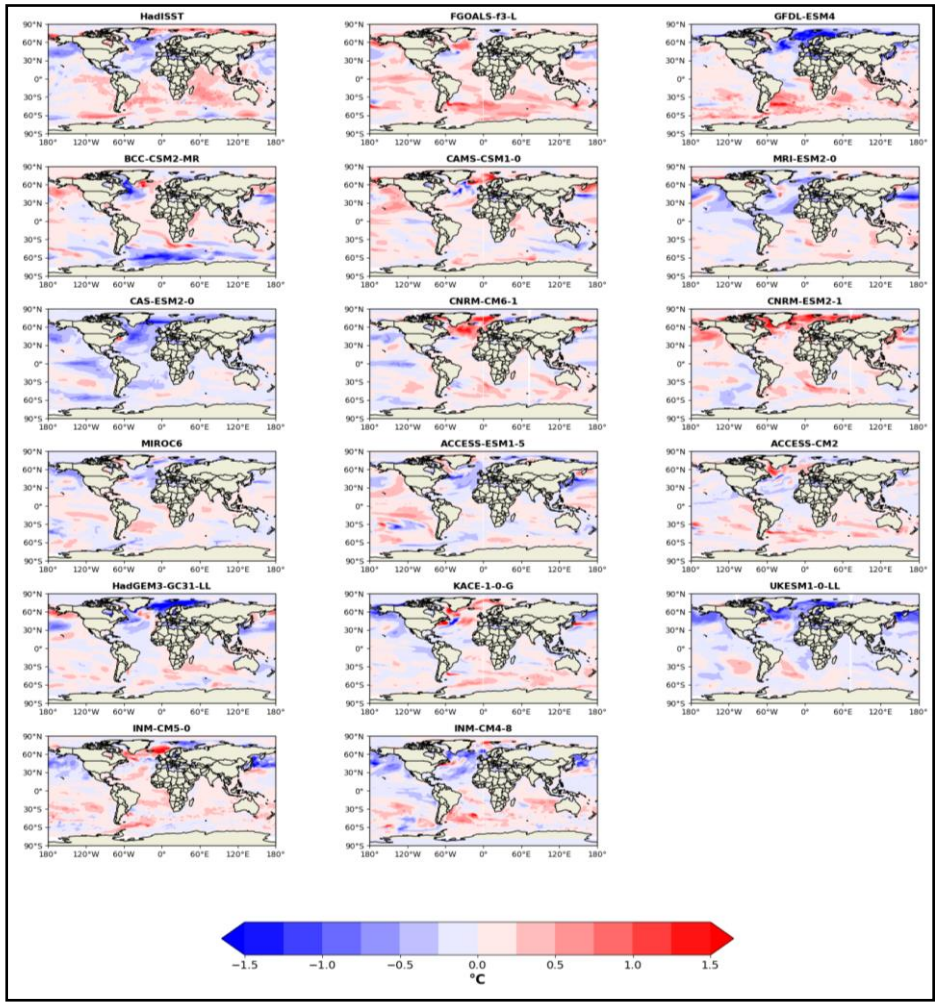

Figure 4.2.14: *As Figure 4.2.12 but for the medium resolution models.*

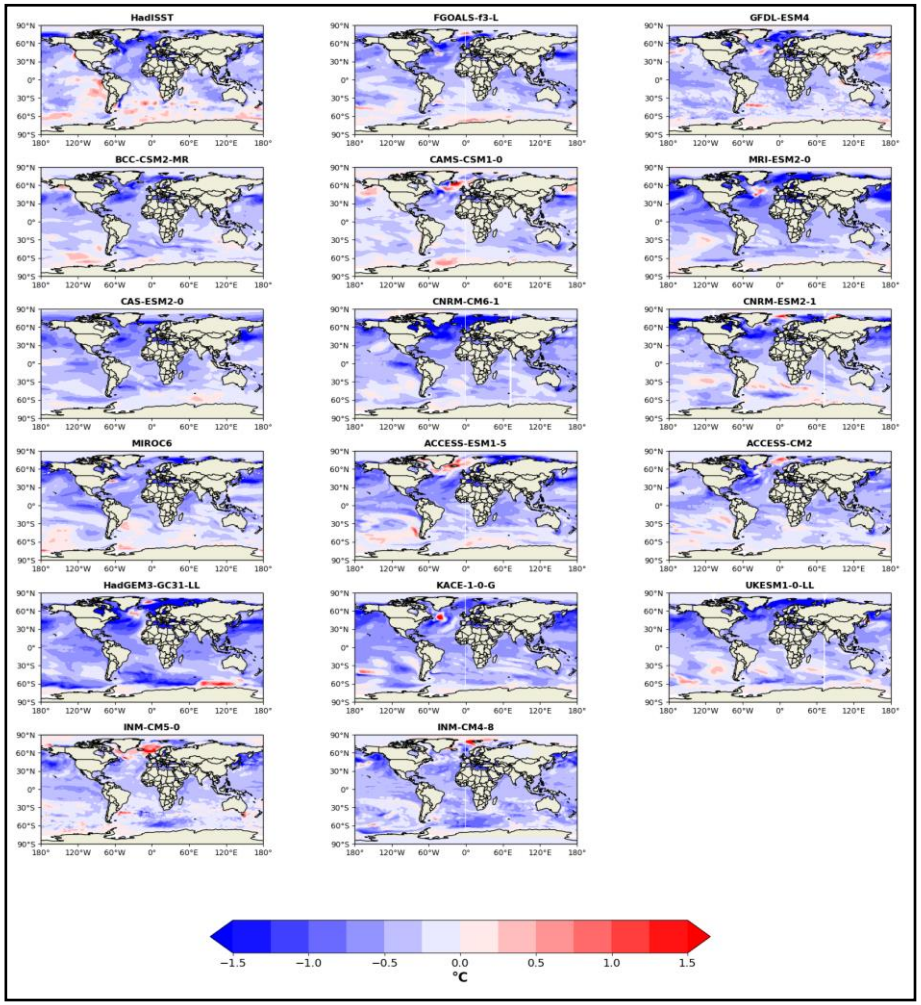

Figure 4.2.15: *As Figure 4.2.13 but for the medium resolution models.*

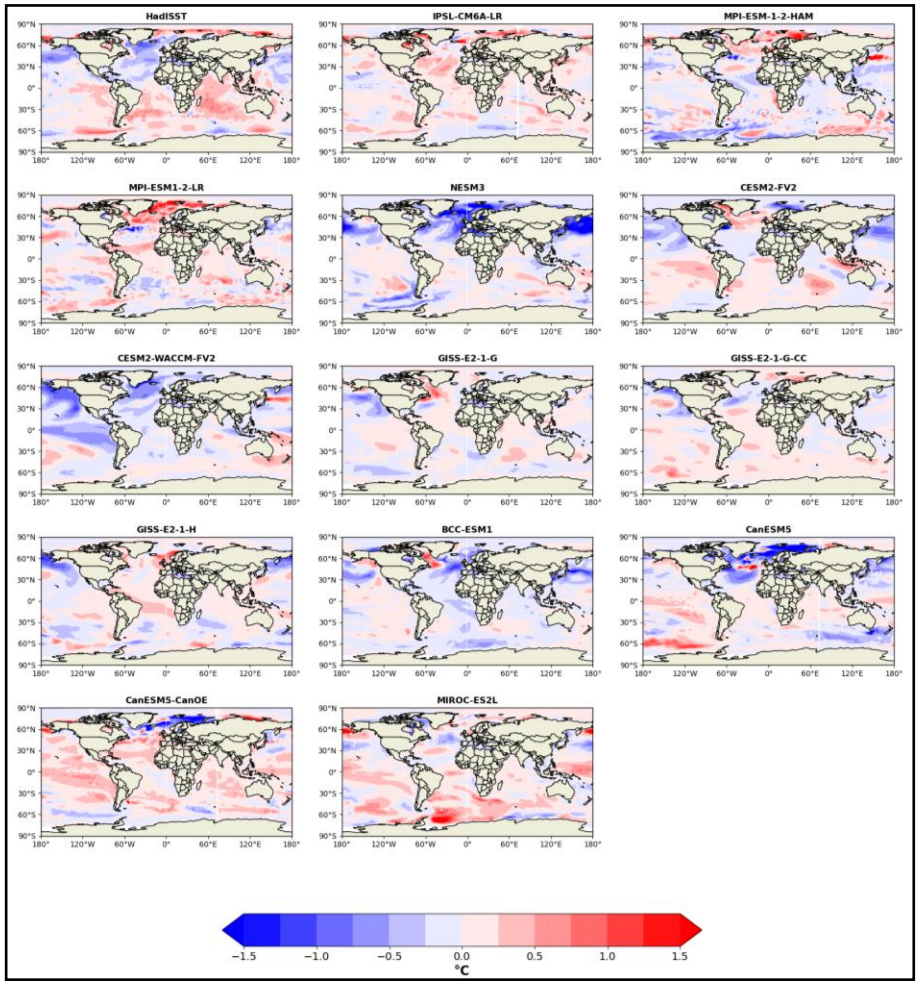

Figure 4.2.16: *As Figure 4.2.12 but for the lower resolution models.*

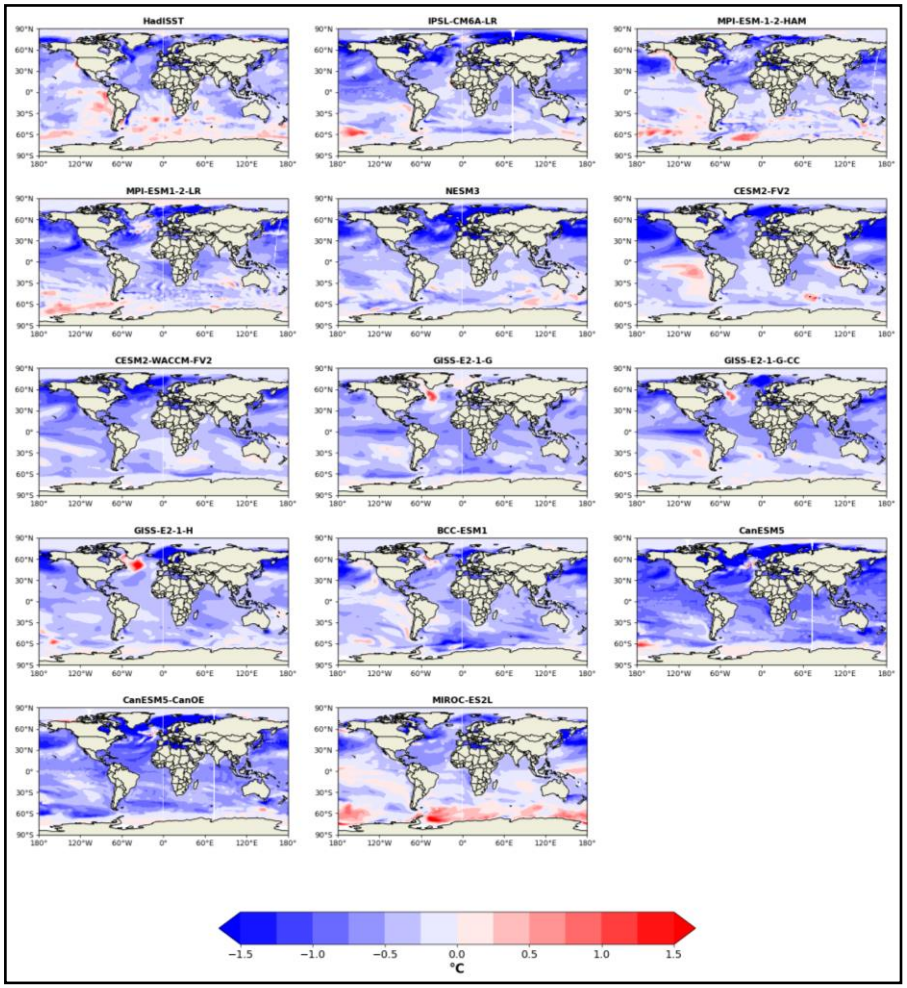

Figure 4.2.17: *As Figure 4.2.13 but for the lower resolution models.*

4.2.5. Circulation

It has been seen the coupled historical models are able to capture the recent trend with the increased precipitation, but struggle with the wet period that preceded the drought, hence analysis of the circulation over the Sahel and the surrounding area was undertaken. Three models were chosen: EC-Earth3 for having the best time series correlation coefficients, HadGEM3-GC31-MM for the worst and E3SM-1-1 for having a better visual representation of the differences between the drought and the wet period (Figures 4.2.18/4.2.19). HadGEM3-GC31-MM and E3SM-1-1 were re-gridded to EC-Earth3's resolution for ease of comparison. 850hPa was chosen as most key circulation elements either originate or exist near the top of the atmospheric boundary layer, such as zonal winds associated with the Walker Circulation and meridional ones linked to the Hadley cell (Sheen et al, 2017).

The vector plots for drought minus recent period (Figure 4.2.19) have a better representation of the observations than the drought minus wet periods (Figure 4.2.18). This is interesting because the absolute plots for the drought and wet periods appear to capture the general circulation shown by the ERA5 observations, whereas the recent period absolute plots are slightly more dissimilar. Despite this, the models have quite a good resemblance to one another in the structure of the flow over West Africa and the surrounding ocean, for both sets of comparisons.

ERA5 observations help explain how the circulation played a role in the drought period, for the comparison between the drought and the wet period shows a weakening of the West African Easterly Jet which brings moisture onto the continent (Figure 4.2.18). All three models do not have a good representation of this flow and show little changes in winds between the two periods, which is intriguing for E3SM-1-1 due to its representation of the observed precipitation. As a result, it can be argued that E3SM-1-1 could be getting the precipitation right for the wrong reasons, from the circulation perspective.

Over the Guinea Coast, the winds seem to be westerly in the absolute plots for the drought and the recent period, but the anomaly plots suggest the flow has become weaker between the two periods due to the easterly vectors (Figure 4.2.19). The West African Monsoon (WAM) originates from the south, with south-westerly winds over the Gulf of Guinea bringing moisture from the ocean into the Sahel (Parker et al, 2005; Biasutti, 2013; Vellinga et al, 2016). Thus, weaker westerlies would indicate a weakening of the WAM and a reduction in precipitation over the Sahel. As well, over the eastern Sahel, EC-Earth3 and HadGEM3-GC31-MM and the observations show a strengthening in some north-easterly winds which would originate from the Sahara. These winds are going to be much drier compared to the moist ocean winds (Brannan and Martin, 2018), so combined with a weakening in the moist ocean winds, there is enhanced drying over the Sahel in the drought period compared to the recent period. This results in the spatial distribution of precipitation in the models showing more similarities to the observations for the drought and recent periods.

SSTs and Sahelian circulation are interlinked (Biasutti, 2013; Nicholson, 2013). Drought conditions in the west Sahel have been accompanied by a reduction in moisture convergence and increased subsidence by the winds, whereas the central

Sahel being wetter is linked to Saharan warming and an increased gradient between the north and south Atlantic SSTs (Monerie et al, 2017). Furthermore, temperature gradients between the land and ocean and between the North and tropical Atlantic and stronger winds in the lower and mid-levels have been implicated as some of the main reasons for the differences between models (Monerie et al, 2017). EC-Earth3 and E3SM-1-1 have a stronger Atlantic dipole for the anomalies between the drought and recent period; the drought period SSTs are up to 1.5^{o}C cooler in the North Atlantic than the recent period (Figure 4.2.13). HadGEM3-GC31-MM also has a clear Atlantic dipole but not to the same extent as the other two models. This links into the 850hPa vector plots, as EC-Earth3 and E3SM-1-1 are alike between 5-15^{o}N over the Atlantic Ocean of increased easterlies, indicating weaker westerlies (Figure 4.2.19). HadGEM3-GC31-MM also has increased easterlies in the drought and recent period, although this is not as consistent as the other two models, relating back to the cooler SSTs in the drought period not being the same areal extent and magnitude. There are smaller differences in SSTs between the drought and wet periods for EC-Earth3 and E3SM-1-1, and HadGEM3-GC31-MM suggests a part of the North Atlantic is warmer in the drought period than the wet period (Figure 4.2.12). These smaller SST changes can help explain the corresponding vector plots, for there are little differences between the drought and wet period 850hPa winds.

Consequently, it can be implied that SSTs are an uncertainty that affect Sahelian precipitation in CMIP6 due to their relationship with the region's circulation and precipitation (Biasutti, 2013; Monerie et al, 2017). Vellinga et al (2016) examined CMIP5 models and prescribed SSTs using the Met Office's Operational Sea Surface Temperature and Ice Analysis (OSTIA) dataset. The Eastern Pacific and Atlantic SSTs led to an anomalous Walker circulation, resulting in winds becoming westerly from the Atlantic below 850hPa, easterly above 700hPa and a stronger African Easterly Jet (Vellinga et al, 2016). Ultimately, moisture transportation into the Sahel increased, along with precipitation (Vellinga et al, 2016). Their study implies prescribing SSTs improves model representation of Sahel precipitation with a methodology comparable to the AMIP-Hist simulations run in CMIP6. The AMIP-Hist results in this study have an improved representation of Sahel precipitation as seen with the Pearson's *r* correlation coefficients and the spatial distribution of precipitation (Figures 4.2.7 to 4.2.9). Model biases still exist in the AMIP-Hist simulations of precipitation, signifying that SSTs are not the sole uncertainty in CMIP6 models (Figure 4.2.10).

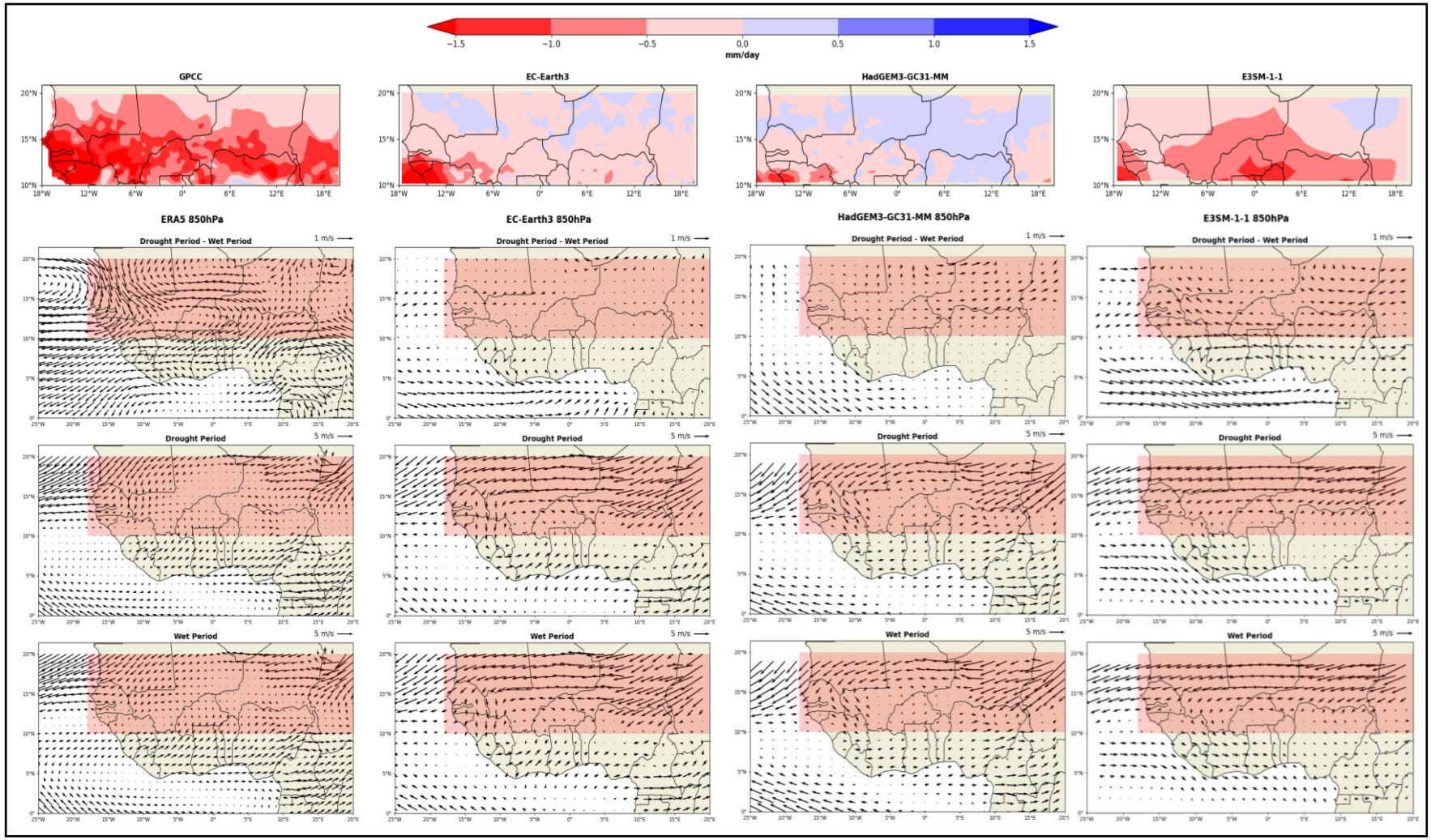

Figure 4.2.18: *A comparison of the differences between the drought (1970-1983) and wet period (1950-1963) for the observations with EC-Earth3 ('best model' according to the time series correlation coefficients), HadGEM3-GC31-MM ('worst model') and E3SM-1-1 (better visual representation) for precipitation (mm/day) and 850hPa circulation (m/s). The anomaly vector plots (top vector one) have an arrow length of 1 m/s whereas the absolute plots are 5 m/s. Positive (negative) numbers represent the drought period being wetter/stronger (drier/weaker) than the wet period.*

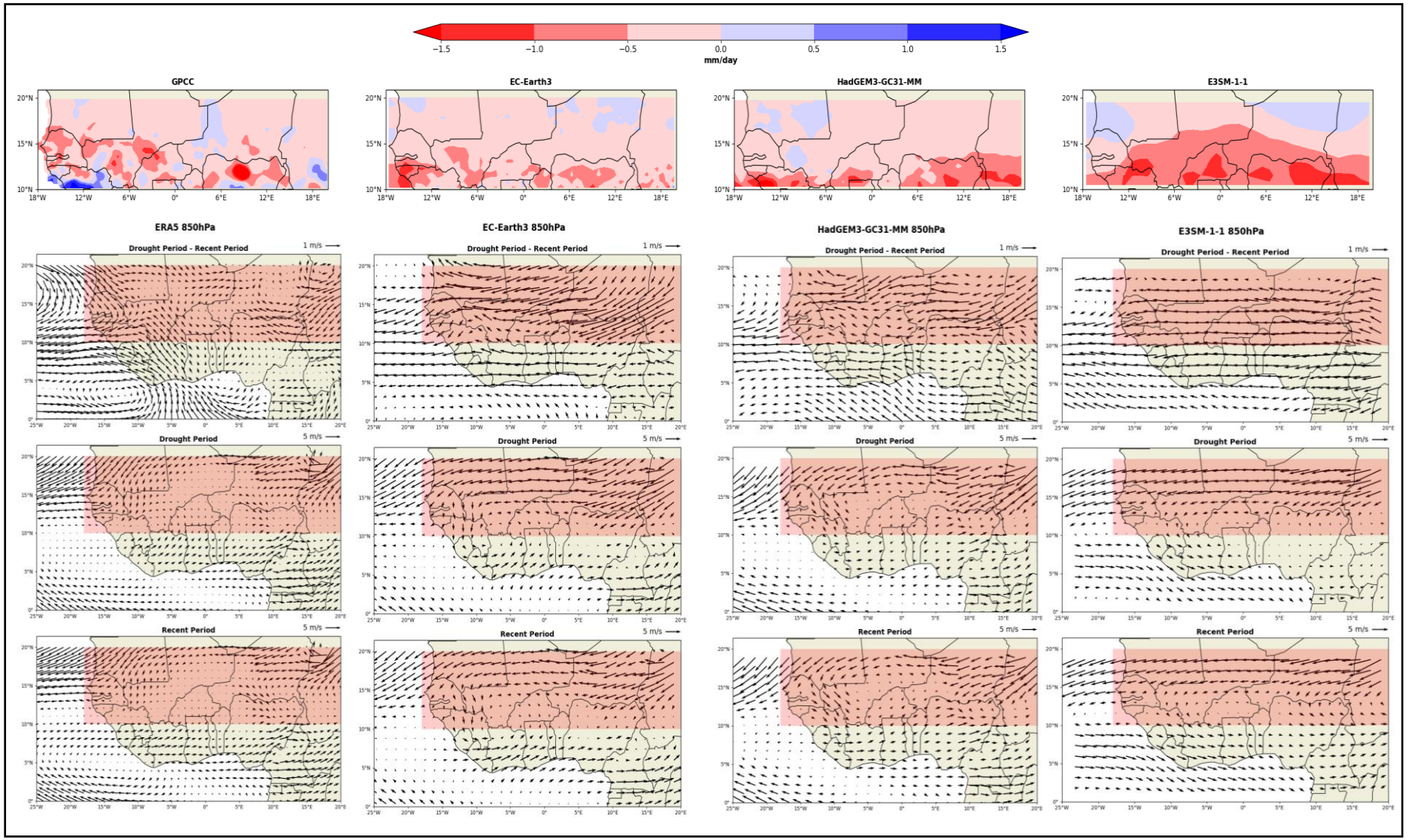

Figure 4.2.19: *As Figure 4.2.18 but for the drought (1970-1983) and recent (2001-2014) periods.*

MIROC6 ranked highly with both CMIP and AMIP-Hist precipitation correlation coefficients so its circulation was analysed. Its spatial representation of the precipitation observations is not the best. In both the coupled and AMIP-Hist plots, the drought and wet period better represents the observations. The coupled drought minus recent plot for precipitation has a larger dry area (Figure 4.2.21), whereas in AMIP-Hist, the Sahel is wetter in the drought than the recent period (Figure 4.2.22).

Precipitation representation is explained by the circulation plots for the coupled model drought minus recent period. The winds are easterly, taking the moisture off the continent (Figure 4.2.21; Parker et al, 2005; Biasutti, 2013; Vellinga et al, 2016). However, the ERA5 data has stronger easterly winds over the Guinea Coast and on the coast around 10ºN. The anomaly plot for the modelled drought and wet periods appears to have little differences in circulation, with any differences being less than 1m/s, contrasting with the observations (Figure 4.2.21).

On the other hand, the drought minus wet plot for the AMIP-Hist simulation shows more resemblance to the observations, although MIROC6 overestimates over eastern Sahel and underestimates the western (Figure 4.2.21). The drought minus recent plot is more dissimilar to the observations and is missing the stronger easterlies over western Sahel that are seen in the observations. This results in the drought period being wetter than the recent period as the model is not capturing anomalies that result in the drought. In addition, MIROC6's AMIP-Hist time series shows the recent period is drier than the drought period, as it does not get the same increase seen in the coupled simulations towards the end of the 20th century (Figure 4.2.20).

On the contrary to the overall conclusions drawn from the other AMIP-Hist models, it seems that prescribing SSTs in MIROC6 has not improved the representation of precipitation for the drought and recent periods. Idealised simulations have suggested the inter-model spread is influenced by the contrasting effects of SSTs and CO_2 within the models and how they have been integrated (Gaetani et al, 2015). For example, warmer SSTs lead to a drier west Sahel, whereas an increase in CO_2 leads to wetting (Gaetani et al, 2015). It also depends on the weighting applied to the various processes and feedbacks in the model set-up (Gaetani et al, 2017). Again, this highlights how working towards resolving the SST uncertainties will not be the only answer to issues with modelling Sahel precipitation.

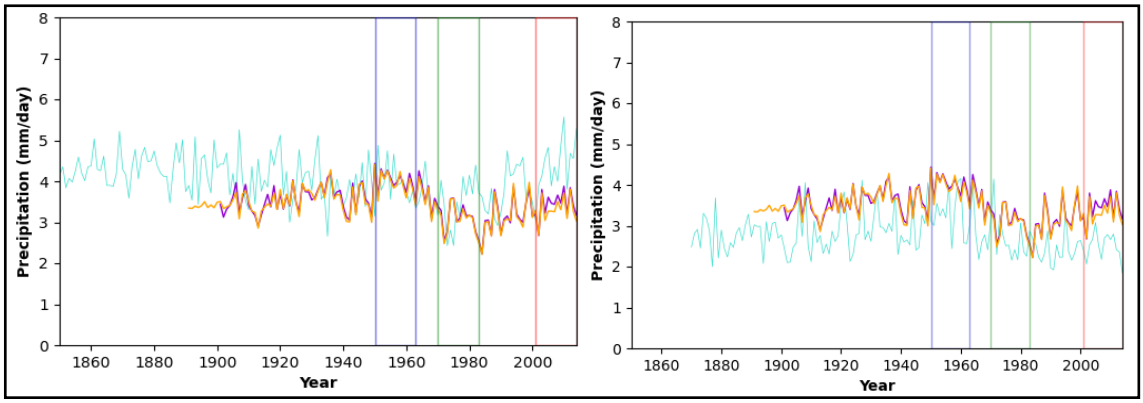

Figure 4.2.20: *Time series of JJAS precipitation (mm/day) over the study region for MIROC6, with CMIP on the left and AMIP-Hist on the right. The blue box represents the wet period, the green the drought and the red the recent period.*

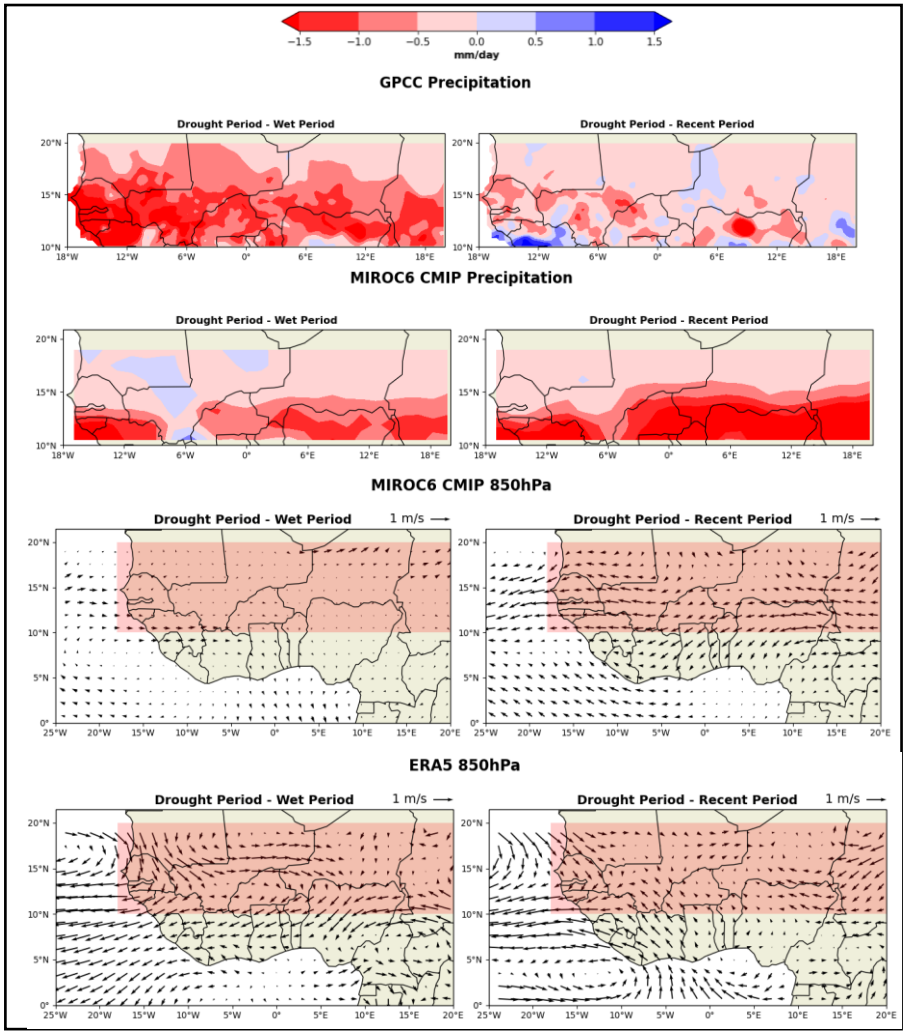

Figure 4.2.21: *Comparison of observations with MIROC6 CMIP precipitation (mm/day) and 850hPa circulation (m/s). Left: anomalies for the drought (1970-1983) and wet (1950-1963) periods. Right: drought and recent (2001-2014) periods. Positive (negative) numbers represent the drought being wetter/stronger (drier/weaker) than the wet period.*

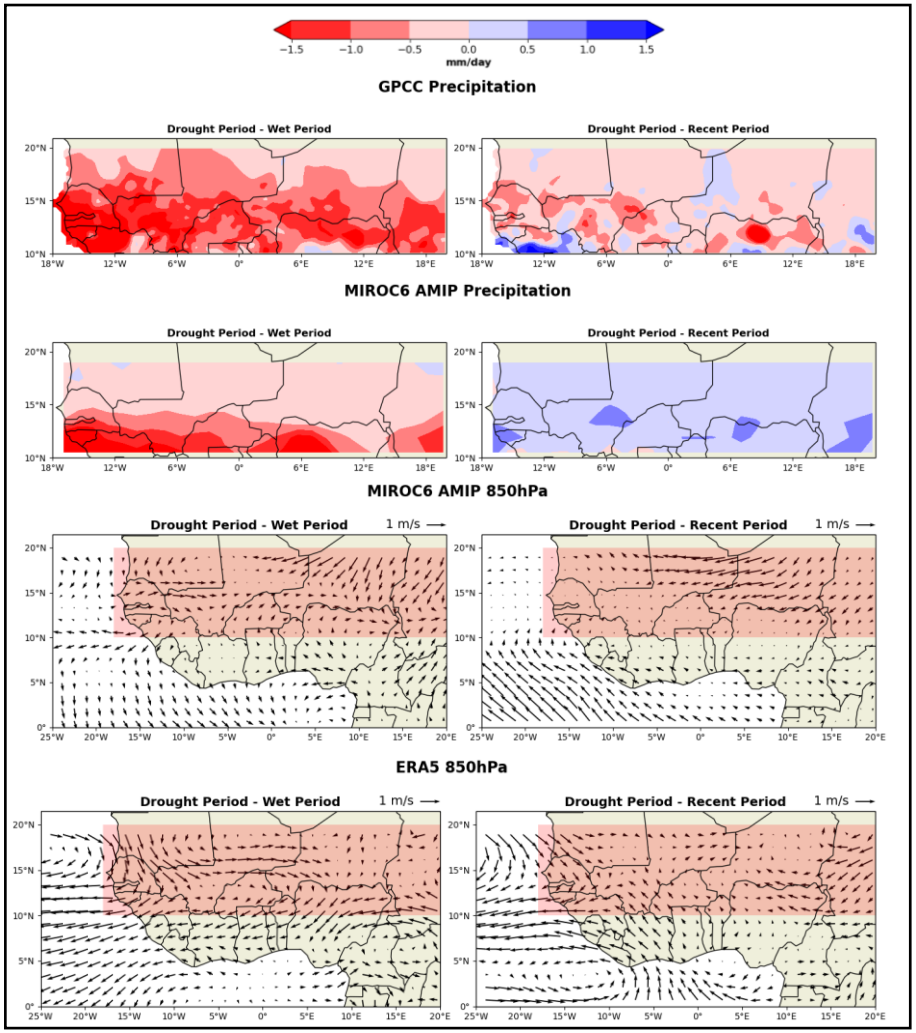

Figure 4.2.22: *As Figure 4.2.21 but for MIROC6 AMIP-Hist (AMIP).*

4.2.6. Summary

Research question 2 asked what factors related to model representation of precipitation variability. A range of factors were explored in response to this: nominal resolution, anthropogenic influence, interactive oceans, sea surface temperatures (SSTs) and circulation.

There is no clear link between the resolution of the coupled models and their representation of observed historical variability in precipitation. Following this, removing the anthropogenic influence in the models increases the differences with the observations, indicating the role of humans on Sahelian precipitation – both modelled and observed. AMIP-Hist models revealed that prescribing the oceans yields stronger correlations and likeness between models and observations, implying that interactive oceans in the coupled models are a source of uncertainty for Sahelian precipitation representation. SSTs influence precipitation through circulation and this was examined in a subset of coupled and atmosphere-only historical models for 850hPa winds. This part of the analysis showed the absolute plots having similarities with the observations but not so much for the anomaly plots, partially linking back to SST representation in the coupled models. The AMIP circulation was slightly better than CMIP in MIROC6 for the drought and wet period comparison, again suggesting how influential interactive oceans are in coupled models.

To summarise these findings in relation to research question 1, which asked whether CMIP6 models could simulate observed interdecadal precipitation variability over the Sahel, histograms were created of the differences between the drought and the wet and recent periods (Figures 4.2.23/24). Most models across all experiments struggle to reproduce the observed magnitude of change between the drought and wet period (Figure 4.2.22). The Historical and Historical-Natural experiments have peaks of over 40% of models in the -0.2-0mm/day bin, whereas AMIP-Hist has two peaks at ~30% of models, one in the same bin and one in the -0.6 to -0.4mm/day bin - 0.5-0.7mm/day lower than the observed differences. On the other hand, the modelled differences between the drought and the recent period for all experiments are weighted between -0.2mm/day and +0.2mm/day (Figure 4.1.32). The coupled historical models peak between the observed values of ~-0.25 and ~-0.35mm/day which suggests ~40% of historical models can capture a similar magnitude of change between the drought and recent periods to the observations. This can be attributed to the anthropogenic influence in the recent period, further emphasising the patterns seen in Figures 4.1.2 and 4.1.3 (Dong and Sutton, 2015).

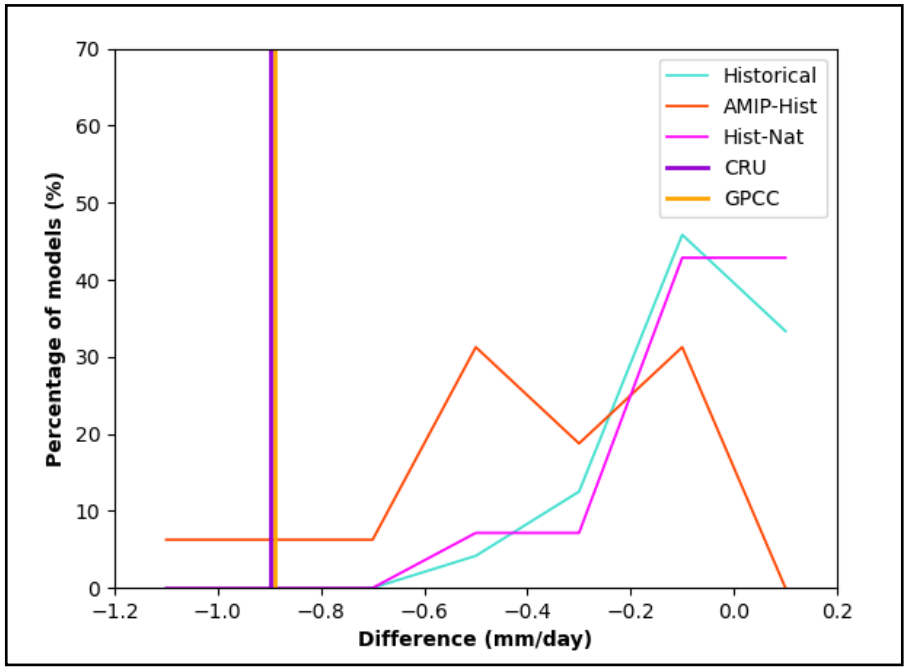

Figure 4.2.23: *Histogram of the difference in JJAS precipitation (mm/day) of the average of the wet period subtracted from the average of the drought period for the different simulations compared to the observational datasets.*

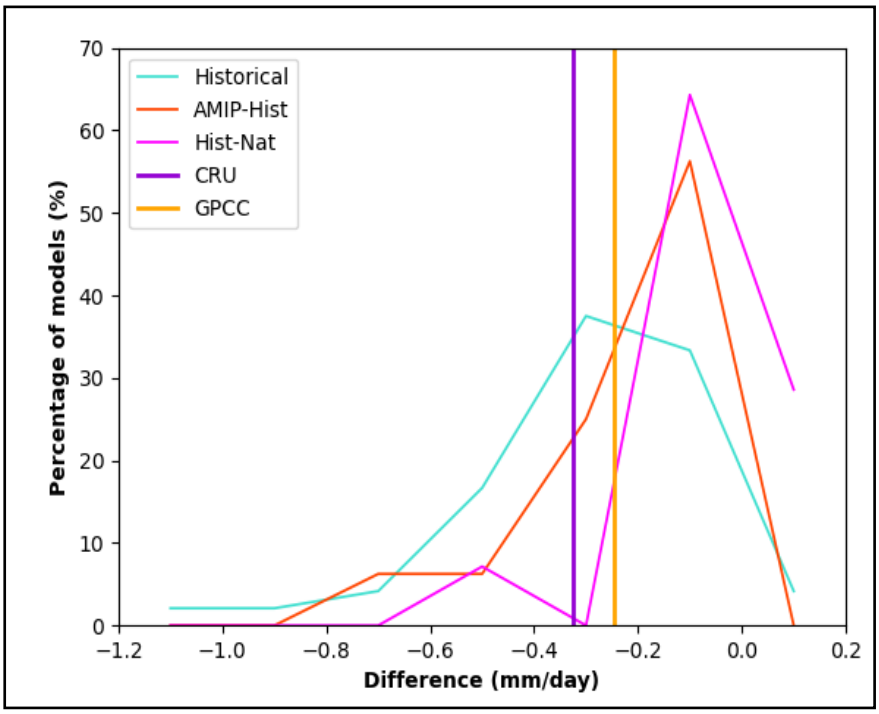

Figure 4.2.24: *As Figure 4.2.23 but for the drought and recent periods.*

4.3. Does evaluation of past variability inform understanding of future change?

Previous research using CMIP3 and CMIP5 models has found that some models have wet projections and some dry (Druyan, 2011; Monerie et al, 2017). In this section, CMIP6 projections will be examined, and it will be explored whether the new understanding gained from the historical simulations can help to interpret future projections.

4.3.1. Temporal Projections

34 out of the 49 models in the historical analysis ran at least one Shared Socioeconomic Pathway (SSP) projection. SSPs 1-2.6, 2-4.5, 3-7.0, 4-6.0 and 5-8.5 are presented here. All models ran SSP5-8.5, with 32 doing SSP1.2-6 and 2-4.5, 29 doing SSP3-7.0 and six on SSP4-6.0. Pearson's *r* correlation coefficients between the historical runs and the observations suggest the models struggle with capturing the long-term variability in the past, thus could affect their projections.

Only the 10-year running mean plots are shown here because the trends are clear. The multi-model mean (MMM) across all SSPs is steady, varying by at most by ~±0.5mm/day in SSP5-8.5 (Figure 4.3.1). In SSPs 4-6.0 and 5-8.5, there appears to be a 20-year period of projected decreased precipitation from 2065 to 2085 (Figure 4.3.1.) This period begins with positive precipitation values just above zero relative to the average of the recent period and ends with negative values just below zero. However, despite this being a clear decreasing period in precipitation, it does begin to increase again after 2085 and the marginal variation in the MMM implies the Sahel might not need to worry about the extremities of climate change.

On the other hand, the higher SSPs tend to have a larger range of projections compared to the lower ones, SSP5-8.5 having a range of +4mm/day to -2mm/day relative to the historical recent period (Figure 4.3.1). Even SSP1-2.6 has a range of +2mm/day to -1mm/day. The models lack agreement in direction of change and either extreme could have profound impacts on the region. CMIP3 (Druyan, 2011) and CMIP5 (Monerie et al, 2017) models also had a wide range of projections, with little consensus on the direction of change. Furthermore, 50% of CMIP5 models had projections of increased Sahelian precipitation, but 25% of models projected reduced precipitation (Biasutti, 2013; Sultan and Gaetani, 2016). So, as well as preparing for droughts, flooding is also a concern for the region (Elagib et al, 2021).

Merging the historical results with the projections exposes the long-term modelled changes over the Sahel (Figure 4.3.2). A step increase in absolute precipitation of ~0.5mm/day is clear in the MMM at the end of the 20th century in all projections, but what follows varies between SSPs. SSP1-2.6 and 2-4.5 appear to have a slight long-term negative trend in precipitation, decreasing to about 0.2-0.3mm/day lower than the peak around 2020 (Figure 4.3.2). SSPs 4-6.0 and 5-8.5 have a steeper step increase compared to the other three SSPs, and despite showing similarities early on to SSP1-2.6 and 4-6.0, SSP3-7.0's long term trends are more consistent with SSP4-6.0 and 5-8.5. Precipitation is projected to increase compared to the beginning of the historical period, even with concerns that the warming projections could result in a drier Sahel (Figures 4.3.2). However, feedbacks could

exist where a drier west Sahel strengthens the monsoon circulation through changes in the vertical structure of circulation, as seen in some CMIP3 and CMIP5 models (James et al, 2015; Monerie et al, 2017). Again, these conclusions relate to the MMM, so the range in models must also be noted. All SSPs have a range of at least 5mm/day, reflecting the lack of agreement across the models in the potential changes in precipitation over the study region.

Figure 4.3.3 further demonstrates the range of projections produced by the models. 11 models have projections that span both positive and negative values compared to the historical recent period. There are 16 models with positive projections and seven have solely negative projections. These proportions are lower than CMIP5, with 47% having positive projections compared to 50%, and 20% compared to 25% for negative projections (Sultan and Gaetani, 2016). Organising the models by resolution on Figure 4.3.3 signifies model resolution has little impact on the projections, for there is no clear trend in projections with decreasing resolution. The six models that ran SSP4-6.0 are medium to lower resolution models with results ranging from ~+1.5mm/day to ~-2mm/day. The models with the largest range are NESM3 and MIROC6. NESM3 has a range of 2.72mm/day of positive projections, whereas MIROC6 has a similar range of 2.22mm/day but is from positive to negative projections. Outside of these two models, the average range is 0.58mm/day.

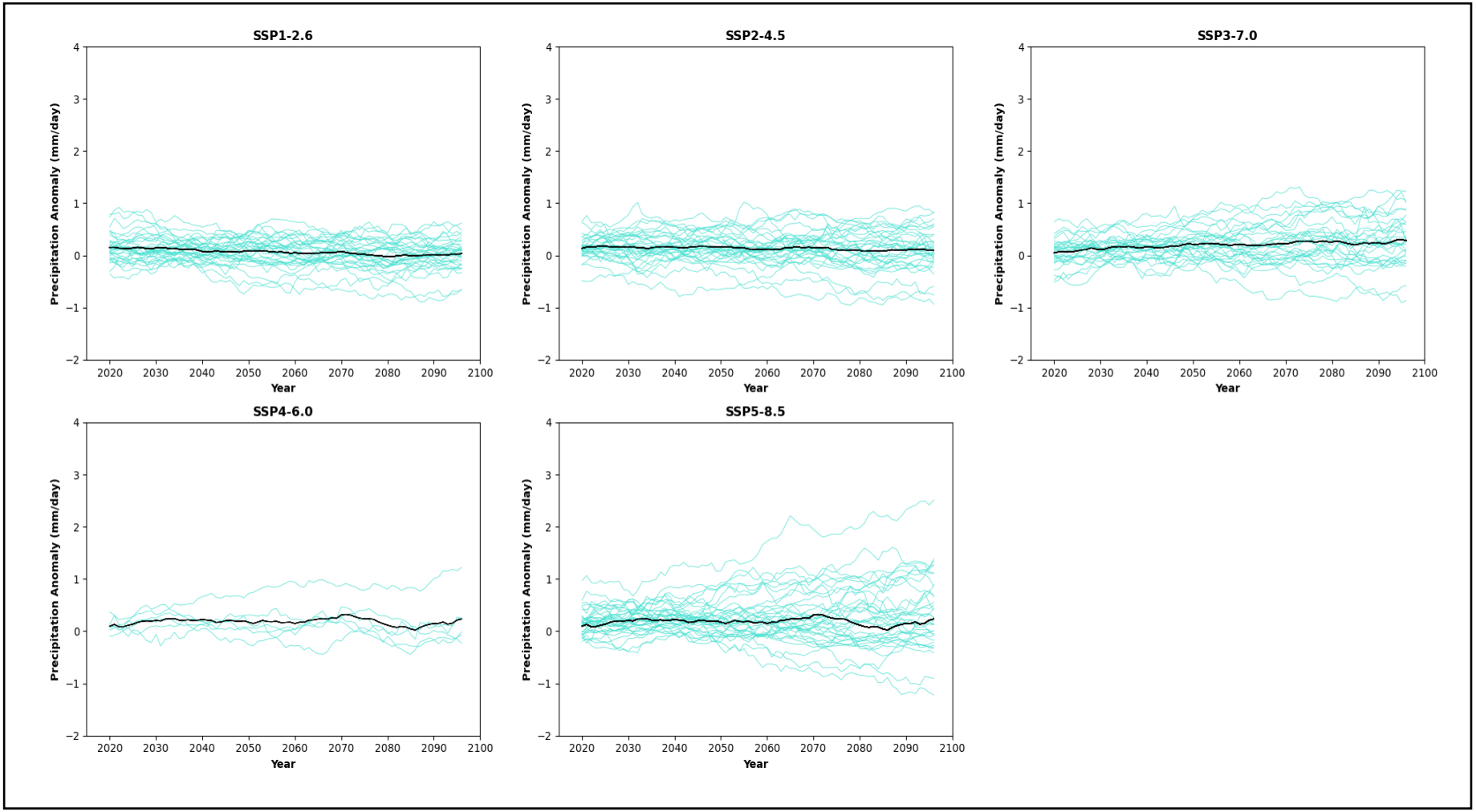

Figure 4.3.1: *Time series of projected JJAS precipitation anomalies (mm/day) from 2015 to 2100 over the study region, calculated relative to the average of the 2001-2014 recent time period, with a 10-year running mean implemented. The black line denotes the multi-model mean.*

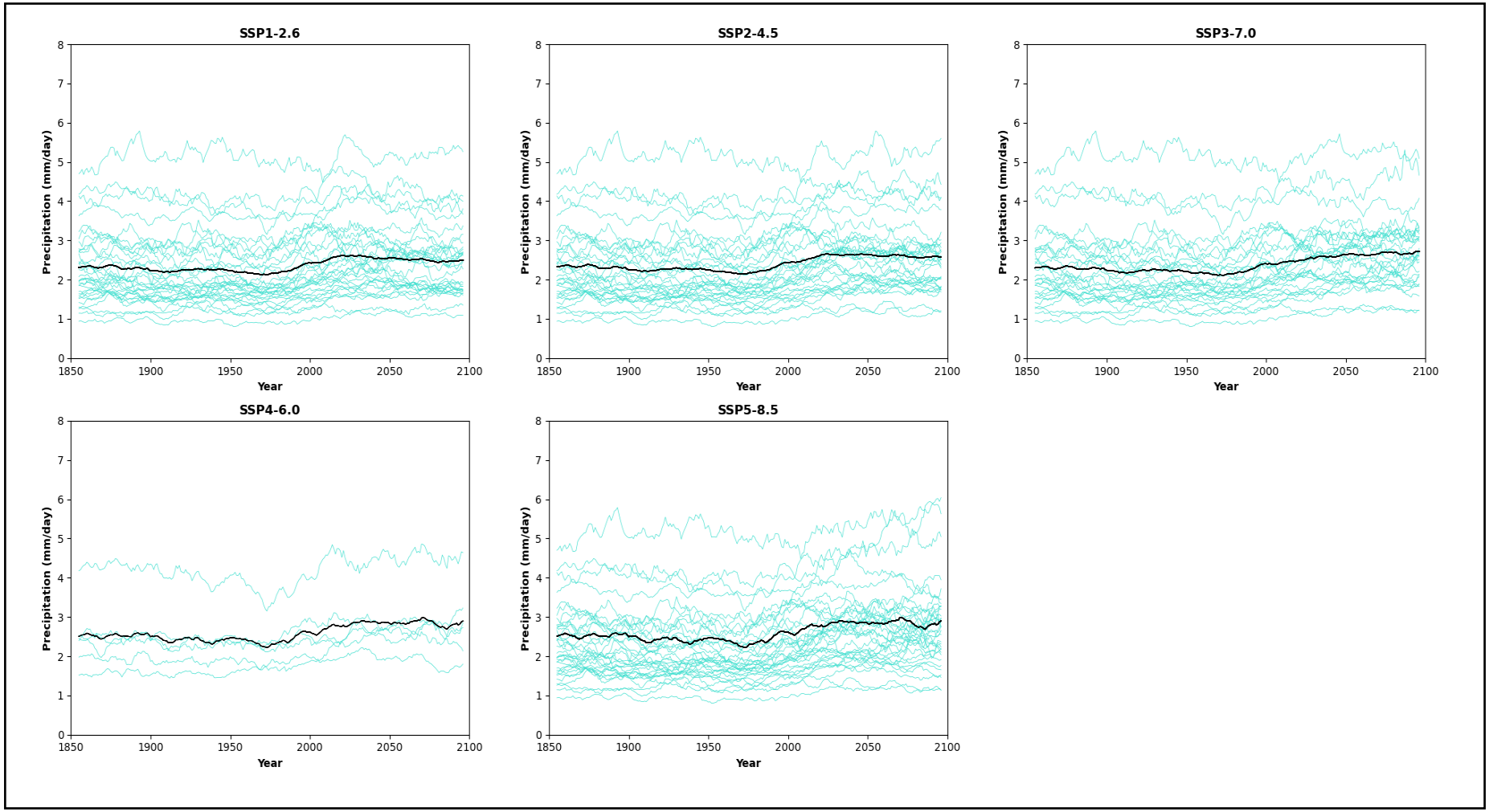

Figure 4.3.2: *Merged time series of JJAS precipitation (mm/day) over the study region from 1850-2100, with a 10-year running mean implemented. The black line denotes the multi-model mean.*

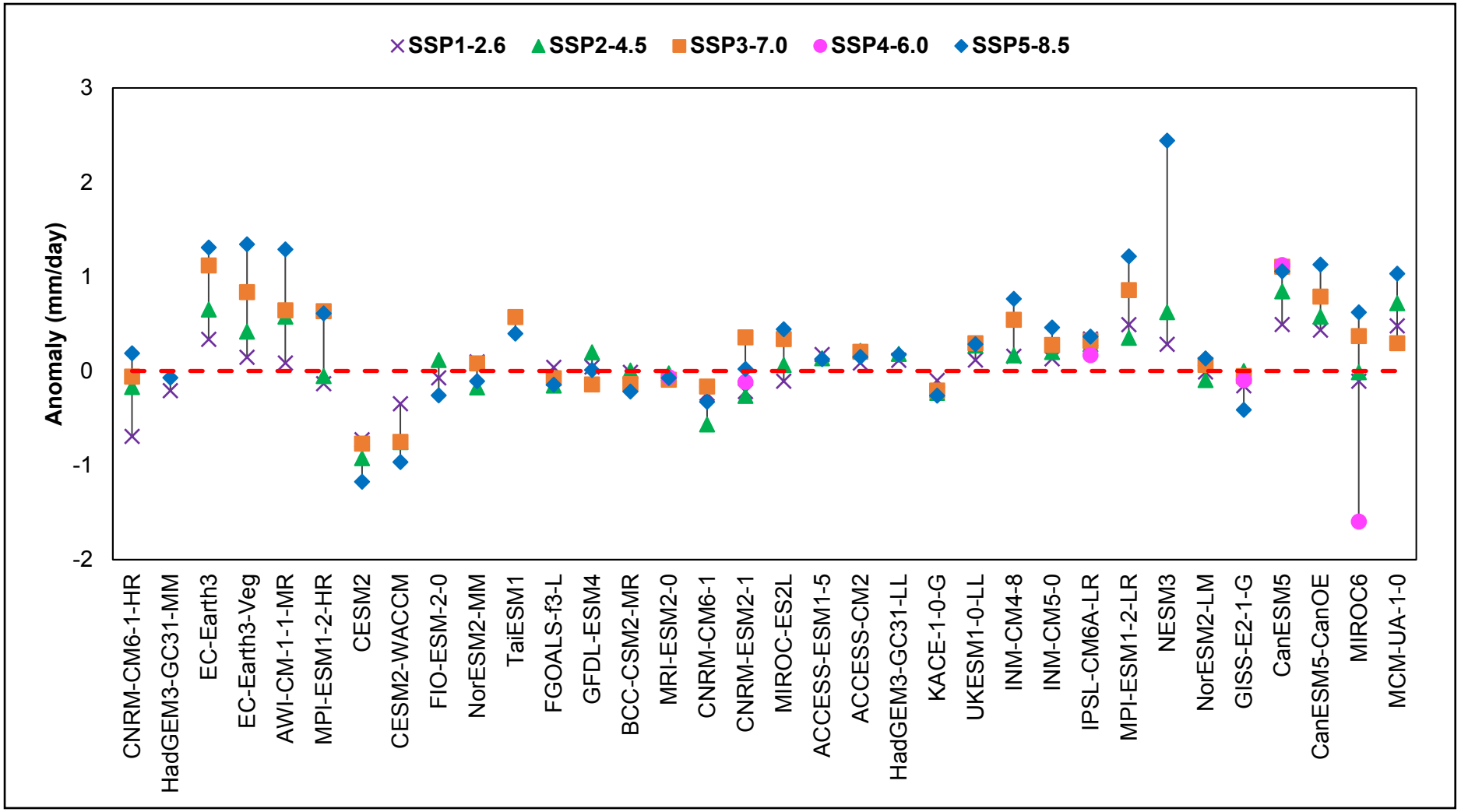

Figure 4.3.3: *The range of anomalies (mm/day) between the different Shared Socioeconomic Pathways (averaged over 2087-2100) and the recent period (2001-2014), organised by nominal resolution.*

4.3.2. Spatial Projections

Across all SSPs and resolution groupings, there is a lack of consensus between the models for the projected direction and magnitude of spatial changes in precipitation relative to the historical recent period (Appendix 1.5). CMIP5 models had projected changes that were not homogenous across the Sahel, as the western Sahel was projected to be drier but central Sahel to be wetter (Monerie et al, 2017).

Increasing model resolution in SSP1-2.6 sees differences become generally smaller, with some exceptions, for example the high-resolution model CESM2 has a large area of drying that is over 1.5mm/day (Appendix 1.5a). These differences tend to be in similar locations in SSP2-4.5 (Appendix 1.5b) and 3-7.0 (Appendix 1.5c), just more enhanced. In some SSP4-6.0 models, the direction of projection changed, such as MIROC6 which becomes predominantly wet rather than dry (Appendix 1.5d). The largest differences tend to be found in SSP5-8.5, indicated by the bold colours of ±1.5mm/day, however this is not consistent across the models (Appendix 1.5e).

None of the models deemed best or worst by the various methods described in section 4.1 ran SSP4-6.0 (Table 4.3.1). Apart from HadGEM3-GC31-MM, which only did SSP1-2.6 and 5-8.5, they all ran the other SSPs. For the medium and higher resolution models, projected changes tend to intensify with increasing SSPs. EC-Earth3's spatial projections are mostly wetter between 0.5 and 1.5mm/day higher than the historical recent period, with a small area of drying up to 1.5mm/day in the south-west that expands with the higher SSP. HadGEM3-GC31-MM has fairly balanced projections between wetting and drying which are between ±1mm/day for SSP1-2.6, increasing to over ±1.5mm/day in SSP5-8.5. ACCESS-CM2 projects small changes across all SSPs. SSP1-2.6 and 2-4.5 have predominantly wet projections reaching up to 1.5mm/day in some places, with some small areas of drying up to 0.5mm/day. There are larger projected dry areas in the west with SSP3-7.0 and 5-8.5 that do reach between 1-1.5mm/day in the south-west, but this is still outweighed by the more dominant wet areas in the east.

However, this pattern of larger changes with increasing SSP does not hold for the lower resolution models (Table 4.3.1). MPI-ESM1-2-LR projects wetting of up to and over 1.5mm/day across the whole of the Sahel in SSP1-2.6, which reduces in intensity in SSP2-4.5, with the south seeing projections between 1-1.5mm/day wetter and the north seeing up to 1mm/day with some marginal drying of 0.5mm/day. SSP3-7.0 is interesting because it has mainly drying between 0.5-1mm/day and a significantly smaller area of wetting up to 1mm/day. For SSP5-8.5, the Sahel is projected to be wetter by up to 1.5mm/day apart from the south-west where there is drying of 1.5mm/day.

Similarly, there is no clear pattern with MCM-UA-1-0 (Table 4.3.1). There are strong projected changes across all SSPs of ±1.5mm/day. In SSP1-2.6, the west Sahel tends to be drier up to 1.5mm/day and the east wet of a comparable magnitude. SSP2-4.5 yields mostly wet projections of up to 1.5mm/day with some drying in central Sahel up to 1.5mm/day. The areas of high magnitude drying and wetting reduce slightly in SSP3-7.0. SSP5-8.5 has mostly wet projections of up to 1.5mm/day with a small dry area of 1.5mm/day in the south-west, comparable to EC-Earth3 and MPI-

ESM1-2-LR.

As well as this, MIROC-E2SL's projections all suggest the Sahel is likely to see drying at the end of the century, apart from SSP3-7.0 which indicates wetting of up to 1.5mm/day (Table 4.3.1). Drying ranges between 0.5 and 1.5mm/day, with higher values in the southern part of the Sahel. Interestingly, SSP2-4.5 has a larger area with higher dry values than SSP5-8.5.

CMIP5 models with increased precipitation projections were the ones with a stronger difference between the SSTs in the hemispheres (Monerie et al, 2017). Park et al (2015) also found the inter-hemisphere SST difference was one of the causes of the differences between models in the direction of Sahel precipitation projections. Examining the anomaly plots for historical SSTs (Figures 4.2.12-4.2.17) reveals some models with wet projections (for example EC-Earth3) do have clear differences between hemispheres across the three historical time periods. HadGEM3-GC31-MM has projected very marginal drying which corresponds with its difference in historical SSTs because there is not a clear inter-hemispheric difference in them. MIROC-E2SL's projections fluctuate around zero for the various SSPs and the historical SST reflects this, as the hemispheres are balanced. It could be likely that these models will carry these broad patterns into the future, supporting the theories proposed by Monerie et al (2017) and Park et al (2015).

Following this, the previously discussed connections between global SSTs and Sahelian precipitation implies projected changes in precipitation are likely to be affected by SSTs (Park et al, 2015; Monerie et al, 2017). Each model is likely to have slightly different variations of the strength and presence of the teleconnections, however, it is hard to measure as the teleconnections vary across time and space (Monerie et al, 2017). In fact, dry projections in CMIP5 were linked to warmer SSTs, heating the troposphere and reducing moisture transport to the Sahel, whereas the wet projections are associated with GHGs increasing net surface radiation, resulting in more evaporation and precipitation (Gateani et al, 2017). Which impact dominates depends on the weight given to each feedback within the climate model (Gaetani et al, 2017). These reasons are likely to still be present in CMIP6 projections and could help explain the broad range of projections by CMIP6 models (Figure 4.3.1).

Model resolution may also influence projections, despite not clearly linking into the projections with the time series. Previous studies have found differences in projections that are associated with the relationship between circulation elements and model resolution (Sultan and Gaetani, 2016). African Easterly Waves are found at ~850hPa, and are linked to precipitation, but this connection was not as clear or present at all in lower resolution models (Vellinga et al, 2016). The higher resolution models projected strong AEWs to increase in frequency by ~12% a decade (Vellinga et al, 2016). Thus, the differences in resolution could feed into precipitation projections through impacting circulation.

However, these discussed influences could be dampened by the aerosol feedback both within the models and reality. Aerosols can increase the albedo, hence more insolation is reflected than absorbed, leading to a smaller difference between land and ocean temperatures, impacting the WAM's circulation dynamics (Zhou et al,

2016). There are other feedbacks which will feed into the relationship between aerosols and monsoons but are not yet fully understood, so the extent of the impact of aerosols on the WAM is yet to be determined for the past, present and future (Zhou et al, 2016). How the feedback is represented within the model could affect their projections, as it may not reflect what is happening within the Sahel climate system (Zhou et al, 2016).

Table 4.3.1: *Comparison of projections by the various Shared Socioeconomic Pathways (SSPs) by the models deemed best and worst according to the methods described in section 4.1. Projections are the difference in anomalies averaged over 2087-2100 and the historical recent period of 2001-2014, in mm/day.*

SSP	**EC-Earth3** Best Temporal Worst Dry Spatial Bias *Higher Resolution*	**HadGEM3-GC31-MM** Worst Temporal *Higher Resolution*	**MPI-ESM1-2-LR** Worst Spatial Representation *Lower Resolution*	**ACCESS-CM2** Worst Dry Temporal Bias *Medium Resolution*	**MCM-1-UA-1-0** Worst Wet Temporal Bias *Lower Resolution*	**MIROC-E2SL** Best Spatial Bias *Lower Resolution*
1-2.6	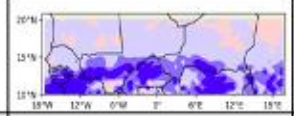	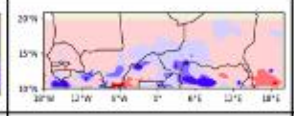	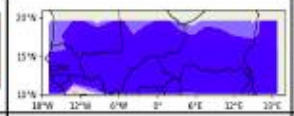	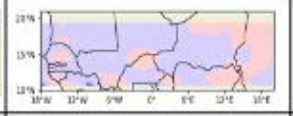	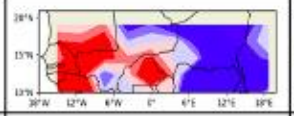	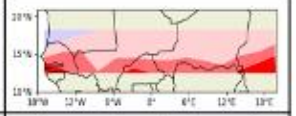
2-4.5	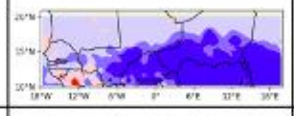		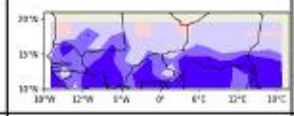	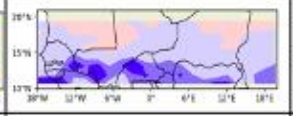	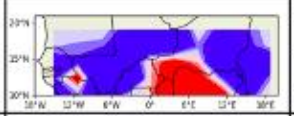	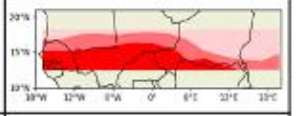
3-7.0	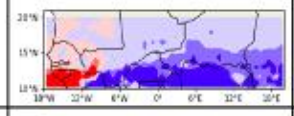		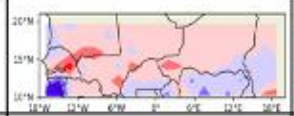	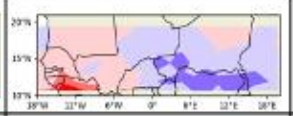	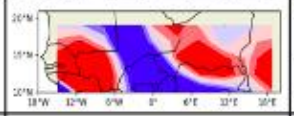	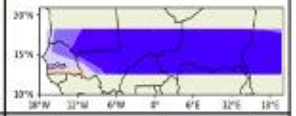
5-8.5	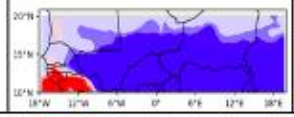	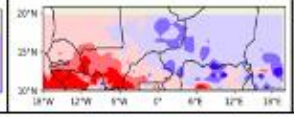	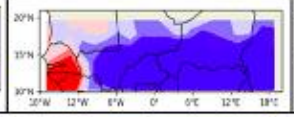	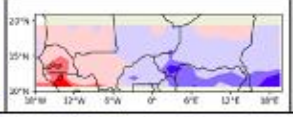	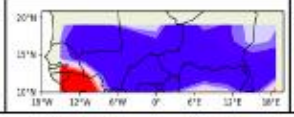	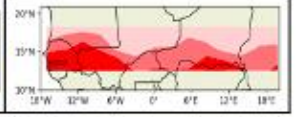

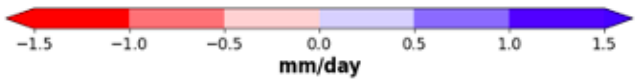

Table 4.3.2 summarises the models deemed best and worst by the different methods in section 4.3.1 and their associated projections. It shows resolution does not seem to have a huge influence on the rankings of the models for the temporal correlation, because both models are in the higher resolution model grouping. However, for the other three methods, the model's resolution is expected to be related to its ranking placement. For the spatial representation method, the higher resolution models are more of a similar resolution to the observations therefore can show a more varying distribution of precipitation than the lower resolution ones. In terms of bias, the higher resolution models are likely to have more uncertainties within each grid box, thus negatively impacting them for spatial bias ranking, but due to the increased resolution, they have a better chance at having values closer to the observations for the temporal bias.

EC-Earth3 appears in the rankings twice – once as the best model from the perspective of the temporal correlations but also as the worst model for the dry spatial bias (Table 4.3.2). The model tends to show wetter projections for both the values and the spatial distribution of precipitation across all four SSPs that it ran. The fact it is one of the worst models for spatial bias may indicate the changes projected by the model could be outweighed by the model bias, affecting the robustness of its results (Ukkola et al, 2020). HadGEM3-GC31-MM projects marginal changes in precipitation over the Sahel, although this could be linked to its inability to capture the variability in historical precipitation.

MPI-ESM1-2-LR's projections are a near match to EC-Earth3's despite being ranked as the worst for spatial representation of precipitation during the drought period. The values increase with the SSP except for SSP2-4.5 which is 0.06mm/day lower than SSP1-2.6, also reflected in the difference maps. However, the categories for the contours on the difference maps are broader compared to the concise values calculated with the time series, hence the values may not always directly transfer to the distributions seen in the spatial representation of precipitation. As well as this, the time series data is a field average over the Sahel which overrides the spatial variation.

Interestingly both models with the worst temporal bias have wetter values for projections over the Sahel. ACCESS-CM2's values are smaller than MCM-UA-1-0's, and the former's highest projection is SSP2-4.5 at +0.21mm/day and the latter's is SSP5-8.5 with +1.03mm/day. Similarly, MCM-UA-1-0 has both wet and dry projections spatially, with the wet projections outweighing the dry ones according to the time series projections. MIROC-E2SL's projections are ~50-75% of those projected by EC-Earth3.

Sea surface temperatures (SSTs) play a role in Sahelian precipitation, and as seen previously, there is a link between the historical distribution of SSTs and model projections. The models with wet projections here – EC-Earth3, MPI-ESM1-2-LR, ACCESS-CM2 and MCM-UA-1-0 (Figures 4.2.12 - 4.2.17) – all have an element of a contrast in SSTs between the hemispheres. The interhemispheric difference in SSTs has been associated with increased Sahelian precipitation (Park et al, 2015; Zhou et al, 2016; Monerie et al, 2017; Monerie et al, 2020). MIROC-E2SL's projections fluctuate around zero, reflecting its SSTs being balanced across the hemispheres (Figures 4.2.16/17). HadGEM3-GC31-MM does not have a clear difference in

historical SSTs between the hemispheres (Figures 4.2.12/13). HadGEM3-GC31-MM's historical 850hPa circulation plots have minimal differences between the drought and the two wetter periods (Figures 4.2.18/19), and the lack of clear Atlantic dipole in the associated historical SST maps helps to explain this. Thus, the variability in Sahelian precipitation in HadGEM3-GC31-MM is limited in the past and hints that this may continue in the future, even with projected GHG emissions.

4.3.3. Summary

Corresponding with previous CMIPs, there is still a lack of consensus in models for the direction, magnitude and location of projected changes in precipitation over the Sahel. On the whole, with the higher SSPs, projected changes tend to be larger, regardless of direction of change.

Evaluating the best and worst models for each method (as discussed in 4.3.1) revealed only a tentative link between historical representation of precipitation and projections. Some model projections can be explained by their historical behaviour, for example, HadGEM3-GC31-MM lacks variability in historical precipitation, which might continue in the future, even with rising GHGs. However, the issue of uniformitarianism arises because the model behaviour might not be the same in their historical simulations as in their projections (Akinsanola and Zhou, 2019). This is also the case for the climate system in reality too (Akinsanola and Zhou, 2019).

Table 4.3.2: *Details of the best and worst performing models according to each method and their projections (mm/day) for the Sahel.*

Method		Model	Resolution group	SSP values (mm/day)	SSP Maps – dominant overall trend
Temporal correlation	Best	EC-Earth3	Higher	1-2.6: +0.34 2-4.5: +0.65 3-7.0: +1.12 5-8.5: +1.31	Between 0-1.5mm/day wetter Larger area of higher wet projections East wet, 1-1.5mm/day, Guinea drier 1.5mm/day Larger area 1.5mm/day wetter, Guinea same
	Worst	HadGEM3-GC31-MM	Higher	1-2.6: -0.21 5-8.5: -0.07	Larger dry area, mainly 0.5mm/day Balanced drying and wetting by ±0.5 to 1mm/day
Spatial representation	Best	E3SM-1-1	Higher	No SSP data available	
	Worst	MPI-ESM1-2-LR	Lower	1-2.6: +0.49 2-4.5: +0.35 3-7.0: +0.86 5-8.5: +1.22	Mainly at least 1.5mm/day wetter Quite even, ±1mm/day drier/wetter 0.5mm/day drier, some wetter areas up to 1mm/day Guinea 1.5mm/day drier, rest 1-1.5mm/day wetter
Temporal bias	Best	E3SM-1-0	Higher	No SSP data available	
	Worst - dry	ACCESS-CM2	Medium	1-2.6: +0.08 2-4.5: +0.21 3-7.0: +0.20 5-8.5: +0.15	Balanced ±0.5mm/day drier/wetter Wetter, mainly 0.5-1mm/day, some 1.5mm/day Quite even, ±1mm/day drier/wetter Quite even, ±1mm/day drier/wetter
	Worst - wet	MCM-UA-1-0	Lower	1-2.6: +0.48 2-4.5: +0.72 3-7.0: +0.29 5-8.5: +1.03	East 1-1.5mm/day wetter, West 1.5mm/day drier Most 1.5mm/day wetter, 1.5mm/day drier over Nigeria East/West 1-1.5mm/day drier, central 1.5mm/day wetter 1.5mm/day wetter apart from 1.5mm/day drier over Liberia
Spatial bias	Best	MIROC-E2SL	Lower	1-2.6: -0.11 2-4.5: +0.06 3-7.0: +0.34 5-8.5: +0.44	Drier – North 0-0.5mm/day, up to 1.5mm/day in South Larger area of 0.5-1.5mm/day drying Nearly whole region 1.5mm/day wetter Mostly 0.5-1mm/day drier
	Worst - dry	EC-Earth3	Higher	1-2.6: +0.34 2-4.5: +0.65 3-7.0: +1.12 5-8.5: +1.31	Between 0-1.5mm/day wetter Larger area of higher wet projections East wet, 1-1.5mm/day, Guinea drier 1.5mm/day Larger area 1.5mm/day wetter, Guinea same as 3-7.0
	Worst - wet	SAM0-UNICON	Higher	No SSP data available	

5. Conclusions

The Sahel region's vulnerability to the impacts of climate change means it is important to understand what possible repercussions could occur in the future. This study examined CMIP6 simulations of Sahel precipitation variability, and whether there is a link between historical CMIP6 model performance and their projections for Sahelian precipitation. The following research questions were considered, arising from the existing literature base.

5.1. Answers to research questions

1. Can CMIP6 models simulate observed interdecadal precipitation variability over the Sahel?

There are various observational datasets available for precipitation over the Sahel. This study predominantly used GPCC and CRU due to their temporal coverage, both having similar fluctuations across time, having a clear wetter period during the 1950s and 1960s, a drought during the 1970s and 1980s and recovery since. CHIRPS, TAMSAT and ERA5-Land begin towards the end of the drought period.

Different methods were used to understand which models could simulate observed interdecadal precipitation variability over the Sahel, with results dependent on the method used. EC-Earth3 was the best model for temporal correlations, with its coefficient being 0.31 at interannual timescales to 0.71 with a 10-year running mean. E3SM-1-1 was the best when examining the spatial representation of the anomaly plots between the drought and wet period. Bias with the drought period was also calculated, with E3SM-1-0 having the smallest temporal bias of -0.06mm/day and MIROC-E2SL having the smallest spatial bias varying around ±1mm/day.

Overall, the models fail to capture the full magnitude of the variability and the differences between the drought and wet/recent periods that is seen in the observations.

2. What factors relate to model representation of precipitation variability?

Model resolution, anthropogenic influence, interactive oceans and sea surface temperatures, and circulation were examined in this study as factors that relate to model representation of precipitation variability.

There is no clear link between model resolution and Sahelian precipitation, in terms of both temporal and spatial variations. Removing the anthropogenic influence weakens correlation coefficients and more muted spatial differences between the observations and both anomaly comparisons. This indicates coupled models do capture the observed variability better when anthropogenic influences are included as seen with the clear increase in precipitation in recent years.

CMIP6 included atmosphere-only simulations as a separate experiment, where the influence of interactive oceans is removed. Compared to the coupled experiments, correlations improved with the time series data, with more models agreeing with the observations and are statistically significant. The multi-model mean (MMM) has similar fluctuations to the observations. Spatial representation improved slightly for both the anomaly and bias plots, but there are still differences that need resolving. AMIP-Hist

correlation coefficients are consistently higher than the CMIP ones. This implies a key uncertainty for representing Sahelian precipitation in coupled models is the portrayal of ocean processes and their coupling to the atmospheric components.

Following the AMIP-Hist results, sea surface temperatures (SSTs) were examined further, as they have been implicated as a driver of the drought. SSTs have feedbacks linked to Sahelian circulation thus could have affected modelled precipitation anomalies. The drought and recent period SST anomaly plots show more resemblance to the observations than the drought and wet period ones. The Atlantic dipole is clearer in the drought and wet period anomaly plots than the drought and recent periods, although the models do not capture the full magnitude of the differences that are seen in the observations. This can help to explain their limited ability in capturing the drought in both the precipitation time series and spatial representation. However, the influence of global warming and the models' recent increase in precipitation can be explained by the recent period SSTs being warmer than the drought period, which is consistent across all models.

Model resolution is thought to impact Sahelian precipitation through atmospheric circulation (Vellinga et al, 2016). HadGEM3-GC31-MM, EC-Earth3 and E3SM-1-1 were analysed for 850hPa winds. Their absolute plots showed similarities to observations however the anomaly plots did not. E3SM-1-1's good representation of drought and wet period precipitation anomalies cannot be explained by its 850hPa circulation. Although, the circulation vector plots can help to explain the drought and recent period precipitation plots. There are weaker westerlies over the Guinea Coast with stronger dry north-easterly winds from the Sahara, signifying a weaker WAM and less precipitation over the Sahel in the drought period. These plots are also affected by SSTs, and a stronger temperature gradient has been found to lead to larger changes in circulation (Monerie et al, 2017). There are smaller differences in SSTs for the drought and wet period hence linking into the smaller differences in circulation. Additionally, the AMIP circulation in MIROC6 is slightly better than CMIP for the drought and wet period plots. However, for the drought and recent period anomalies, CMIP is better than AMIP for circulation, consistent with its precipitation.

Model resolution does not have a clear connection to representation of precipitation variability over the Sahel. The Hist-Nat simulations showed the coupled models better capture the observed variability when anthropogenic influences are included, but this has more of an impact in the recent period. Prescribed SSTs in the AMIP-Hist simulations yielded stronger correlation coefficients and better spatial representation. SSTs are strongly linked to circulation over the Sahel. The drought and recent period SST anomaly plots show a better resemblance to observations than the drought and wet period ones, with this being reflected in the respective precipitation and circulation plots. So, factors associated with ocean representation seem to have the strongest influence on representing Sahelian precipitation variability.

3. <u>Does evaluation of past variability inform understanding of future change?</u>

For the models that ran the Shared Socioeconomic Pathways (SSPs), the inter-model range in anomalies increased with SSPs from +2mm/day to -1mm/day for SSP1-2.6

to +4mm/day to -2mm/day for SSP5-8.5, except for SSP4-6.0 which had a similar range to SSP2-4.5. Based on consistency across scenarios, there were 16 models with solely positive projections, 7 with solely negative and 11 which spanned both positive and negative projections. The lack of agreement between models is consistent with CMIP3 (Druyan, 2011) and CMIP5 conclusions (Monerie et al, 2017). However, the MMM for each SSP are steady around ±0.5mm/day, further signifying why using the MMM can be problematic when not considering the whole range (Daron et al, 2021).

Merging the absolute time series for each SSP with the historical time series revealed a step increase in mean precipitation at the end of the 20th century, potentially linked to anthropogenic greenhouse gases (Dong and Sutton, 2015). This increase stabilises in SSP1-2.6 and 2-4.5 but continues to increase in the other three SSPs. It is unclear why this noticeable rise at the end of the 20th century does not continue in all of the projections. This is based on the MMM, so it must be noted there is wide range in precipitation projections, and the pattern which is clearer with the 10-year running mean. Some models have consistently higher or lower values compared to the MMM, contributing to the wide range.

Spatially analysing the projections compared to the recent period shows the averaging methods result in the time series projections not always directly correlating with the spatial projections. Across all SSPs and resolution groupings there is not a clear consensus over which areas of the Sahel will be drier or wetter in the future. Overall, projected values increase with SSPs. Some models project complete wetting of over 3mm/day over the Sahel and others drying to the same magnitude compared to the recent period.

There does not seem to be a clear connection between the ability of the models to represent the Sahelian droughts when examining the ranked models as a group (Table 4.3.1). For those with available SSP data, all the ‘worst’ models for each method have wet projections apart from HadGEM3-GC31-MM, which projects slight drying. All the ‘best’ models have projections of wetting too. SSP5-8.5 has the strongest change for all models, apart from HadGEM3-GC31-MM. When looking at all the models with SSP data, there are some with larger wet/dry projections, which suggests the models that are deemed the ‘best’ and ‘worst’ per each method do not reflect the potential range of projections for the Sahel.

Nevertheless, there are hints from historical model behaviour about future projections, as seen with HadGEM3-GC31-MM. This model struggles with capturing historical precipitation variability. As discussed, the interhemispheric difference in SSTs is a key influence on Sahelian precipitation. HadGEM3-GC31-MM does not have a clear Atlantic dipole in the drought and wet period anomaly SST plots, which then feeds into the corresponding circulation plots for 850hPa winds. There are minimal differences between the drought and wet period 850hPa winds, linking into the spatial distribution of precipitation for the same comparison. The future changes could be marginal because HadGEM3-GC31-MM does not have strong variability in the 20th century so might not change much with future GHG emissions. It could also potentially be linked to the band of precipitation being displaced too south, as seen

with other Hadley Centre models (e.g. HadGEM3-RA, Diallo et al, 2014), hence a drier Sahel region. It may be that models in which the Sahel is too dry struggle to generate large precipitation variability, because there is very little rain there in any time period.

5.2. Limitations and Future Work

There is no perfect method for examining models: time series data averages out the spatial variation across the region, and maps average out interannual variability in precipitation. As well as this, classing the reliability of model projections according to present day bias is not overly accurate due to a lack of association between the present bias and projected precipitation (Monerie et al, 2017). Furthermore, Lee and Wang (2014) compared model performance in past to observations and similarly showed there are complications with using bias to classify model performance.

E3SM-1-1 had a good representation of the observations for the anomaly plot between the drought and wet periods, despite its circulation plots lacking similarities to the observations. This alludes to the idea that this model in particular is getting the precipitation right for the wrong reason. Addressing this could be achieved through examining different pressure levels for the circulation or examining different variables in more detail to explore the drivers of the drought.

There are circulation elements which are not examined in this study but play a role in Sahelian precipitation. One such example is the Tropical Easterly Jet (TEJ) which is usually found at 200hPa, and feedbacks are linked with the African Easterly Jet (AEJ) but are not fully understood (Monerie et al, 2017). There is a strong correlation between reduced Sahelian precipitation and the AEJ migrating southward with a weakened TEJ, with a more northern AEJ being associated with anomalous wet years over the Sahel (Grist and Nicholson, 2001). The AEJ can also take moisture away from the Sahel, reducing precipitation (Patricola and Cook, 2008). Examining these elements further would aid understanding of the behaviour of precipitation over the Sahel in CMIP6 models.

To investigate further the impact of resolution on the representation of precipitation over the Sahel, future work could analyse individual models at different resolution. Vellinga et al (2016) did this for the Met Office UM, where they examined three different resolutions and compared their decadal variability in Sahel precipitation. There were definite differences between the higher and lower resolution models (Vellinga et al, 2016). Similarly, it has been suggested models which do not capture the drought may be too dry all year round (Birch et al, 2014; James et al, 2018). Sometimes the monsoon circulation is displaced too far south which means even with the associated climatic feedbacks initiating a drought, no drought is seen over the Sahel because the precipitation was not there in the first place (James et al, 2018). Following this, higher resolution models have been found to simulate the monsoon circulation further into the continent than lower resolution ones, resulting in precipitation over the Sahel (Birch et al, 2014). The models are more likely to capture a drought over the Sahel with changes in associated feedbacks because of the improved monsoon circulation location. Keeping within the CMIP framework, models

from HighResMIP could be used to examine these differences alongside the coupled ones (Eyring et al, 2016).

The Sahel is a unique region in terms of its geographical location and relationship with various climatic feedbacks that link the atmosphere, ocean, and land (Zhou et al, 2016). For this reason, the insight gained from this study cannot be directly applied elsewhere. However, this study revealed CMIP6 models do still struggle with modelling precipitation when compared to observations, particularly with the large scale interdecadal variability linked to SSTs. There have been some improvements following CMIP5, predominantly linked to model developments, but representation still varies between models. Examining AMIP-Historical simulations implied the interactive oceans in coupled models play a large role in this discrepancy. Similarly, exploring the Historical-Natural simulations over the Sahel in the recent wetter period hinted that the fully coupled models may capture the recent anthropogenic influence on precipitation, which could be an interesting avenue for future work. Evaluating other regions will aid understanding whether these findings are unique to the Sahel, or whether they consistent across the globe.

There are a lack of studies analysing CMIP6 historical simulations for specific droughts elsewhere, but studies that have examined general drought patterns across the globe (e.g. Papalexiou et al, 2021) have found biases exist with low precipitation values and that uncertainties are larger in the tropics than other latitudes. Papalexiou et al (2021) compared CMIP6 historical drought representation to several observational datasets using the Standardised Precipitation Index. They found CMIP6 models did not reproduce the spatial patterns of precipitation that well across the globe, with a maximum agreement of 36% of grid cells for average drought duration and 40% for variation in precipitation (Papalexiou et al, 2021). This suggests the signal to noise ratio seen in modelled Sahelian precipitation is consistent with the global patterns.

5.3. Concluding remarks

CMIP6 models have improved on CMIP5 in terms of model set-up and parameterisations. However, their representation of Sahelian precipitation, both during the 1970/80s drought period and the preceding and following wet periods, still needs improving, as they fail to simulate the magnitude of the difference between the dry and wet periods. There are uncertainties that are not yet fully understood. For example, removing the interactive oceans in AMIP does improve representation slightly but does not fully resolve the differences between models and observations. Undertaking the future work suggested will contribute to closing this research gap.

Projections for the Sahel by CMIP6 models still do not agree on the direction of potential change by the end of the century, consistent with previous studies of CMIP3 and CMIP5 models. There is not a clear link between historical model performance and resolution. Although, some projections can be partly explained by historical model behaviour, such as SSTs. This suggests improving historical performance could increase confidence in model projections for the Sahel.

REFERENCES

1. Akinsanola, A. & Zhou, W. (2019). Ensemble-based CMIP5 simulations of West African summer monsoon rainfall: current climate and future changes. *Theoretical and Applied Climatology*, 136, pp.1021-1031.
2. Akinsanola, A., Ogunjobi, K., Ajayi, V., Adefisan, E., Omotosho, J. & Sanogo, S. (2017) Comparison of five gridded precipitation products at climatological scales over West Africa. *Meteorology and Atmospheric Physics,* 129, pp.669-689.
3. Andrews, M., Ridley, J., Wood, R., Andrews, T., Blockley, E., Booth, B., Burke, E., Dittus, A., Florek, P., Gray, L., Haddad, S., Hardiman, S., Hermanson, L., Hodson, D., Hogan, E., Jones, G., Knight, J., Kuhlbrodt, T., Misios, S., Mizielinski, M., Ringer, M., Robson, J. & Sutton, R. (2020) Historical Simulations With HadGEM3-GC3.1 for CMIP6. *Journal of Advances in Modeling Earth Systems*, 12 (e2019MS001995), pp.1-34.
4. Bader, J. & Latif, M. (2003). The impact of decadal-scale Indian Ocean sea surface temperature anomalies on Sahelian rainfall and the North Atlantic Oscillation. *Geophysical Research Letters*, *30*(22).
5. Badr, H., Dezfuli, A., Zaitchik, B. & Peters-Lidard, C. (2016). Regionalizing Africa: patterns of precipitation variability in observations and global climate models. *Journal of Climate*, 29(24), pp.9027-9043.
6. Bamba Sylla, M., Elguindi, N., Giorgi, F. & Wisser, D. (2016). Projected robust shift of climate zones over West Africa in response to anthropogenic climate change for the late 21st century. *Climatic Change*, 134, pp.241-253.
7. Barry, A., Caesar, J., Klein Tank, A., Aguilar, E., McSweeney, C., Cyrille, A., Nikiema, M., Narcisse, K., Sima, F., Stafford, G., Touray, L., Ayilari-Naa, J., Mendes, C., Tounkara, M., Gar-Glahn, E., Coulibaly, M., Dieh, M., Mouhaimouni, M., Oyegade, J., Sambou, E. & Laogbessi, E. (2018). West Africa climate extremes and climate change. *International Journal of Climatology*, 38 (Suppl. 1), pp.e-921-e938.
8. Becker, A., Finger, P., Meyer-Christoffer, A., Rudolf, B. Schamm, K., Schneider, U. & Ziese, M. (2013) A description of the global land-surface precipitation data products of the Global Precipitation Climatology Centre with sample applications including centennial (trend) analysis from 1901–present**.** *Earth System Science Data*, 5, pp.71-99.
9. Bercos-Hickey, E., Nathan, T. & Chen, S. (2020). On the relationship between the African Easterly Jet, Saharan mineral dust aerosols, and West African precipitation. *Journal of Climate*, *33*(9), pp.3533-3546.
10. Biasutti, M. (2013). Forced Sahel rainfall trends in the CMIP5 archive. *Journal of Geophysical Research: Atmospheres,* 118, pp.1613-1623.
11. Biasutti, M. & Giannini, A. (2006). Robust Sahel drying in response to late 20th century forcings. *Geophysical Research Letters*, *33*(11).
12. Binns, T. (1990) Is Desertification a Myth? *Geography*, 75 (2), pp.106-113.
13. Birch, C., Parker, D., Marsham, J., Copsey, D. & Garcia-Carreras, L. (2014). A seamless assessment of the role of convection in the water cycle of the West

African monsoon. *Journal of Geophysical Research: Atmospheres*, *119*(6), pp.2890-2912.
14. Brannan, A. & Martin, E. (2018). Future characteristics of African Easterly Wave tracks. *Climate Dynamics*, 2019 (52), pp.5567-5584.
15. Brooks, N. (2004). Drought in the African Sahel: variability, change and agency. *Tyndall Centre Working Paper No.61*, 2004.
16. Caminade, C. & Terray, L. (2010). Twentieth century Sahel rainfall variability as simulated by the ARPEGE AGCM, and future changes. *Climate Dynamics*, 35, pp.75-94.
17. Chen, Z., Zhou, T., Zhang, L., Chen, X., Zhang, W. & Jiang, J. (2020). Global Land Monsoon Precipitation Changes in CMIP6 Projections. *Geophysical Research Letters*, 47, e2019GL086902. https://doi.org/10.1029/2019GL086902
18. Couvreux, F., Guichard, F., Bock, O., Campistron, B., Lafore, J. & Redelsperger, J. (2010). Synoptic variability of the monsoon flux over West Africa prior to the onset. *Quarterly Journal of the Royal Meteorological Society*, *136*(S1), pp.159-173.
19. Dai, A., Lamb, P., Trenberth, K., Hulme, M., Jones, P. & Xie, P. (2004) The Recent Sahel Drought is Real. *International Journal of Climatology,* 24, pp.1323-1331.
20. Daron, J., Lorenz, S., Taylor, A. and Dessai, S., 2021. Communicating future climate projections of precipitation change. *Climatic Change*, *166*(1), pp.1-20.
21. Dembélé, M. & Zwart, S. (2016) Evaluation and comparison of satellite-based rainfall products in Burkina Faso, West Africa. *International Journal of Remote Sensing*, 37(17), pp.3995-4014.
22. Deser, C., Tomas, R. & Sun, L. (2015). The role of ocean–atmosphere coupling in the zonal-mean atmospheric response to Arctic sea ice loss. *Journal of Climate*, *28*(6), pp.2168-2186.
23. Diallo, I., Bain, C., Gaye, A., Moufouma-Okia, W., Niang, C., Dieng, M. & Graham, R. (2014). Simulation of the West African monsoon onset using the HadGEM3-RA regional climate model. *Climate dynamics*, 43(3-4), pp.575-594.
24. Dong, B. & Sutton, R. (2015). Dominant role of greenhouse-gas forcing in the recovery of Sahel rainfall. *Nat. Clim. Change* 5, 757–760. doi: 10.1038/nclimate2664
25. Druyan, L. (2011). Studies of 21st-century precipitation trends over West Africa. *International Journal of Climatology*, *31*(10), pp.1415-1424.
26. Elagib, N., Al Zayed, I., Saad, S., Mahmood, M., Basheer, M. & Fink, A. (2021). Debilitating floods in the Sahel are becoming frequent. *Journal of Hydrology*, *599*, p.126362.
27. Eyring, V., Bony, S., Meehl, G., Senior, C., Stevens, B., Stouffer, R. & Taylor, K. (2016). Overview of the Coupled Model Intercomparison Project Phase 6 (CMIP6) experimental design and organization. *Geoscientific Model Development, European Geosciences Union*, 2016, 9 (5), pp.1937- 1958. 10.5194/gmd-9-1937-2016. hal-01339069

28. Flaounas, E., Janicot, S., Bastin, S. & Roca, R. (2012). The West African monsoon onset in 2006: sensitivity to surface albedo, orography, SST and synoptic scale dry-air intrusions using WRF. *Climate dynamics*, *38*(3), pp.685-708.
29. Folland, C.K., Palmer, T. & Parker, D. (1986). Sahel rainfall and worldwide sea temperatures, 1901–85. *Nature*, *320*(6063), pp.602-607.
30. Funk, C., Harrison, L., Alexander, L., Peterson, P., Behrangi, A. & Husak, G. (2019). Exploring trends in wet-season precipitation and drought indices in wet, humid and dry regions. *Environmental Research Letters*, *14*(11), p.115002.
31. Funk, C., Peterson, P., Landsfeld, M., Pedreros, D., Verdin, J., Shukla, S., Husak, G., Rowland, J., Harrison, L., Hoell, A. & Michaelsen, J. (2015). The climate hazards infrared precipitation with stations—a new environmental record for monitoring extremes, *Scientific data*, 2(1), pp.1-21.
32. Gaetani, M., Flamant, C., Bastin, S., Janicot, S., Lavaysse, C., Hourdin, F., Braconnot, P. & Bony, S. (2017). West African monsoon dynamics and precipitation: the competition between global SST warming and CO_2 increase in CMIP5 idealized simulations. *Climate Dynamics*, 48(3-4), pp.1353-1373.
33. Gaetani, M., Flamant, C., Hourdin, F., Bastin, S., Braconnot, P. & Bony, S. (2015) The competitive impacts of global SST warming and CO_2 increase on Sahelian rainfall: results from CMIP5 idealized simulations. In *Our Common Future Under Climate Change, International Scientific Conference* (pp. P-3330).
34. Giannini, A. (2010). Mechanisms of climate change in the semiarid African Sahel: The local view. *Journal of Climate*, *23*(3), pp.743-756.
35. Giannini, A. & Kaplan, A. (2019). The role of aerosols and greenhouse gases in Sahel drought and recovery. *Climatic Change*, *152*(3), pp.449-466.
36. Giannini, A., Biasutti, M. & Verstraete, M. (2008). A climate model-based review of drought in the Sahel: Desertification, the re-greening and climate change. *Global and Planetary Change*, 64, pp.119-128.
37. Giannini, A., Saravanan, R. & Chang, P. (2003). Oceanic forcing of Sahel rainfall on interannual to interdecadal time scales. *Science*, *302*(5647), pp.1027-1030.
38. Gleixner, S., Demissie, T. & Diro, G. (2020). Did ERA5 Improve Temperature and Precipitation Reanalysis over East Africa? *Atmosphere*, 11(996), p.1-19.
39. Global Precipitation Climatology Centre (2020) Visualize and Download GPCC Products. [WWW] https://opendata.dwd.de/climate_environment/GPCC/html/download_gate.html (25/01/2021)
40. Greene, A., Giannini, A. & Zebiak, S. (2009). Drought return times in the Sahel: a question of attribution. *Geophysical Research Letters*, *36*(12), L12701.
41. Grist, J. & Nicholson, S. (2001). A study of the dynamic factors influencing the rainfall variability in the West African Sahel. *Journal of climate*, *14*(7), pp.1337-1359.
42. Haarsma, R., Selten, F., Weber, S. & Kliphuis, M. (2005). Sahel rainfall variability and response to greenhouse warming. *Geophysical Research Letters*, *32*(17).

43. Harris, I., Osborn, T.J., Jones, P. & Lister, D. (2020). Version 4 of the CRU TS monthly high-resolution gridded multivariate climate dataset. *Scientific data*, *7*(1), pp.1-18.
44. Hersbach, H., Bell, B., Berrisford, P., Hirahara, S., Horányi, A., Muñoz-Sabater, J., Nicolas, J., Peubey, C., Radu, R., Schepers, D. & Simmons, A. (2020). The ERA5 global reanalysis. *Quarterly Journal of the Royal Meteorological Society*, 146(730), pp.1999-2049.
45. Hwang, Y. & Frierson, D. (2013). Link between the double-Intertropical Convergence Zone problem and cloud biases over the Southern Ocean. *Proceedings of the National Academy of Sciences*, *110*(13), pp.4935-4940.
46. IPCC. (2021) Summary for Policymakers. *Climate Change 2021: The Physical Science Basis. Contribution of Working Group I to the Sixth Assessment Report of the Intergovernmental Panel on Climate Change* [Masson-Delmotte, V., P. Zhai, A. Pirani, S.L. Connors, C. Péan, S. Berger, N. Caud, Y. Chen, L. Goldfarb, M.I. Gomis, M. Huang, K. Leitzell, E. Lonnoy, J.B.R. Matthews, T.K. Maycock, T. Waterfield, O. Yelekçi, R. Yu, and B. Zhou (eds.)]. In Press.
47. James, R., Washington, R. & Jones, R. (2015). Process-based assessment of an ensemble of climate projections for West Africa. *Journal of Geophysical Research: Atmospheres*, 120, pp.1221-1238.
48. James, R., Washington, R., Abiodun, B., Kay, G., Mutemi, J., Pokam, W., Hart, N., Artan, G. & Senior, C. (2018). Evaluating climate models with an African lens. *Bulletin of the American Meteorological Society*, *99*(2), pp.313-336.
49. Kennedy, J., Dunn, R., McCarthy, M., Titchner, H. & Morice, C. (2017). Global and regional climate in 2016. *Weather* 72, pp.219–225. https://doi.org/10.1002/wea.3042.
50. Kucharski, F., Zeng, N. & Kalnay, E. (2013). A further assessment of vegetation feedback on decadal Sahel rainfall variability. *Climate Dynamics,* 40, pp.1453–1466. doi:10.1007/s00382-012-1397-x
51. Lau, K., Shen, S., Kim, K. & Wang, H. (2006). A multimodel study of the twentieth-century simulations of Sahel drought from the 1970s to 1990s. *Journal of Geophysical Research: Atmospheres*, 111 (D07111), pp.1-9.
52. Lavaysse, C., Flamant, C., Evan, A., Janicot, S. & Gaetani, M. (2016). Recent climatological trend of the Saharan heat low and its impact on the West African climate. *Climate Dynamics*, *47*(11), pp.3479-3498.
53. Lavaysse, C., Flamant, C., Janicot, S. & Knippertz, P. (2010). Links between African easterly waves, midlatitude circulation and intraseasonal pulsations of the West African heat low. *Quarterly Journal of the Royal Meteorological Society,* 136(s1), pp.141-158.
54. Lee, J. & Wang, B. (2014). Future change of global monsoon in the CMIP5. *Climate Dynamics*, *42*(1-2), pp.101-119.
55. Maidment, R., Grimes, D., Allan, R., Tarnavsky, E., Stringer, M., Hewison, T., Roebeling, R. & Black, E. (2014). The 30 year TAMSAT African Rainfall

Climatology And Time series (TARCAT) data set. *Journal of Geophysical Research* DOI: 10.1002/2014JD021927.
56. Martin, E. & Thorncroft, C. (2014). Sahel rainfall in multimodel CMIP5 decadal hindcasts. *Geophysical Research Letters,* 41 (6), pp.2169-2175.
57. Mishra, A. & Singh, V. (2010). A review of drought concepts. *Journal of hydrology*, 391(1-2), pp.202-216.
58. Mohino, E., S. Janicot, S., & Bader, J. (2011). Sahel rainfall and decadal to multi-decadal sea surface temperature variability, *Climate Dynamics*, 37, pp.419–440, doi:10.1007/s00382-010-0867-2.
59. Monerie, P-A., Wainwright, C., Sidibe, M. & Akinsanola, A. (2020). Model uncertainties in climate change impacts on Sahel precipitation in ensembles of CMIP5 and CMIP6 simulations. *Climate Dynamics*, 55, pp.1385-1401.
60. Monerie, P., Fontaine, B. & Roucou, P. (2012). Expected future changes in the African monsoon between 2030 and 2070 using some CMIP3 and CMIP5 models under a medium-low RCP scenario. *Journal of Geophysical Research: Atmospheres*, *117*(D16).
61. Monerie, P.A., Sanchez-Gomez, E. & Boé, J. (2017). On the range of future Sahel precipitation projections and the selection of a sub-sample of CMIP5 models for impact studies. *Climate Dynamics*, *48*(7-8), pp.2751-2770.
62. Muñoz-Sabater, J. (2019) ERA5-Land monthly averaged data from 1981 to present. Copernicus Climate Change Service (C3S) Climate Data Store (CDS). (Throughout 2021) 10.24381/cds.68d2bb30
63. Muñoz-Sabater, J., Dutra, E., Agustí-Panareda, A., Albergel, C., Arduini, G., Balsamo, G., Boussetta, S., Choulga, M., Harrigan, S., Hersbach, H., Martens, B., Miralles, D., Piles, M., Rodríguez Fernández, N. & Zsoter, E. (2019) ERA5-Land: A state-of-the-art global reanalysis dataset for land applications. *In preparation for ESSD.*
64. N'Datchoh, E., Diallo, I., Konaré, A., Silué, S., Ogunjobi, K., Diedhiou, A. & Doumbia, M. (2018). Dust induced changes on the West African summer monsoon features. *International Journal of Climatology*, *38*(1), pp.452-466.
65. National Center for Atmospheric Research Staff (2020) The Climate Data Guide: GPCC: Global Precipitation Climatology Center. [WWW] https://climatedataguide.ucar.edu/climate-data/gpcc-global-precipitation-climatology-centre. (25/01/2021).
66. Niang, I., Ruppel, O., Abdrabo, M., Essel, A., Lennard, C., Padgham, J. & Urquhart, P. (2014). Africa. In: Climate Change 2014: Impacts, Adaptation, and Vulnerability. Part B: Regional Aspects. Contribution of Working Group II to the Fifth Assessment Report of the Intergovernmental Panel on Climate Change [Barros, V.R., C.B. Field, D.J. Dokken, M.D. Mastrandrea, K.J. Mach, T.E. Bilir, M. Chatterjee, K.L. Ebi, Y.O. Estrada, R.C. Genova, B. Girma, E.S. Kissel, A.N. Levy, S. MacCracken, P.R. Mastrandrea, and L.L. White (eds.)]. Cambridge University Press, Cambridge, United Kingdom and New York, NY, USA, pp. 1199-1265.
67. Nicholson, S. (2009). A revised picture of the structure of the “monsoon” and land ITCZ over West Africa. *Climate Dynamics*, *32*(7), pp.1155-1171.

68. Nicholson, S. (2013) The West African Sahel: A Review of Recent Studies on the Rainfall Regime and Its Interannual Variability. *ISRN Meteorology*, 2013 (453521), pp.1-32.
69. Nicholson, S. & Klotter, D. (2021). The Tropical Easterly Jet over Africa, its representation in six reanalysis products, and its association with Sahel rainfall. *International Journal of Climatology*, 41(1), pp.328-347.
70. Orlowsky, B. & Seneviratne, S.I. (2013). Elusive drought: uncertainty in observed trends and short-and long-term CMIP5 projections. *Hydrology and Earth System Sciences*, *17*(5), pp.1765-1781.
71. Papalexiou, S., Rajulapati, C., Andreadis, K., Foufoula-Georgiou, E., Clark, M. & Trenberth, K. (2021). Probabilistic evaluation of drought in CMIP6 simulations. *Earth's future*, *9*(10), p.e2021EF002150.
72. Park, J. Y., Bader, J., and Matei, D. (2015). Northern-hemispheric differential warming is the key to understanding the discrepancies in the projected Sahel rainfall. *Nature Commununications.* 6, 5985. doi: 10.1038/ncomms6985
73. Parker, D., Burton, R., Diongue-Niang, A., Ellis, R., Felton, M., Taylor, C., Thorncroft, C., Bessemoulin, P. & Tompkins, A. (2005). The diurnal cycle of the West African monsoon circulation. *Quarterly Journals of the Royal Meteorological Society,* 131, pp.2839-2860.
74. Patricola, C. & Cook, K. (2008). Atmosphere/vegetation feedbacks: A mechanism for abrupt climate change over northern Africa. *Journal of Geophysical Research: Atmospheres*, *113*(D18).
75. Paxian, A., Sein, D., Panitz, H., Warscher, M., Briel, M., Engel, T., Tödter, J., Krause, A., Cabos Narvaez, W., Fink, A., Ahrens, B., Knutsmann, H., Jacob, D. & Paeth, H. (2016). Bias reduction in decadal predictions of West African monsoon rainfall using regional climate models. *Journal of Geophysical Research: Atmospheres*, 121, pp.1715-1735.
76. Polo, I., Ullmann, A., Roucou, P. & Fontaine, B. (2011). Weather regimes in the Euro-Atlantic and Mediterranean sector, and relationship with West African rainfall over the 1989–2008 period from a self-organizing maps approach. *Journal of Climate*, *24*(13), pp.3423-3432.
77. Quagraine, K. A., Nkrumah, F., Klein, C., Browne Klutse, N. & Quagraine, K. T. (2020) West African Summer Monsoon Precipitation Variability as Represented by Reanalysis Datasets. *Climate*, 8 (11), pp.1-18.
78. Rayner, N., Parker, D., Horton, E., Folland, C., Alexander, L., Rowell, D., Kent, E. & Kaplan, A. (2003). Global analyses of sea surface temperature, sea ice, and night marine air temperature since the late nineteenth century. *Journal of Geophysical Research: Atmospheres*, 108(D14).
79. Sacré Regis M, Mouhamed, L., Kouakou, K., Adeline, B., Arona, D., Koffi Claude A, Talnan Jean H, Obahoundje, S. & Issiaka, S. (2020). Using the CHIRPS Dataset to Investigate Historical Changes in Precipitation Extremes in West Africa. *Climate*, 8(7), p.1-28.
80. Santer, B., Taylor, K., Gleckler, P., Bonfils, C., Barnett, T., Pierce, D., Wigley, T., Mears, C., Wentz, F., Brüggemann, W. & Gillett, N. (2009). Incorporating model

quality information in climate change detection and attribution studies. *Proceedings of the National Academy of Sciences*, *106*(35), pp.14778-14783.

81. Scannell, C., Booth, B., Dunstone, N., Rowell, D., Bernie, D., Kasoar, M., Voulgarakis, A., Wilcox, L., Acosta Navarro, J., Seland, Ø. & Paynter, D. (2019). The influence of remote aerosol forcing from industrialized economies on the future evolution of East and West African rainfall. *Journal of Climate*, 32(23), pp.8335-8354.
82. Sheen, K., Smith, D., Dunstone, N., Eade, R., Powell, D. & Vellinga, M. (2017). Skilful prediction of Sahel summer rainfall on inter annual and multi-year timescales. *Nature Communications,* 8, pp.1-12.
83. Sheffield, J. & Wood, E. (2008) Projected changes in drought occurrence under future global warming from multi-model, multi-scenario, IPCC AR4 simulations. *Climate Dynamics*, 31, pp.79-105.
84. Sow, M., Guichard, F., Dixon, R., Diakhate, M., Lou, S. & Gaye, A. (2021). The added value in CMIP6 models for simulating west African rainfall and its related extreme indices. *Earth and Space Science Open Archive ESSOAr*.
85. Sultan, B. & Gaetani, M. (2016). Agriculture in West Africa in the Twenty-First Century: Climate Change and Impacts Scenarios, and Potential for Adaptation. *Frontiers in Plant Science*, 7 (1262), pp.1-20.
86. Swart, N., Cole, J., Kharin, V., Lazare, M., Scinocca, J., Gillett, N., Anstey, J., Arora, V., Christian, J., Hanna, S. & Jiao, Y. (2019) The canadian earth system model version 5 (CanESM5. 0.3). *Geoscientific Model Development*, 12(11), pp.4823-4873.
87. Tarnavsky, E., Grimes, D., Maidment, R., Black, E., Allan, R., Stringer, M., Chadwick, R. & Kayitakire, F. (2014). Extension of the TAMSAT Satellite-based Rainfall Monitoring over Africa and from 1983 to present. *Journal of Applied Meteorology and Climate* DOI 10.1175/JAMC-D-14-0016.1
88. Taylor, K., Stouffer, R. & Meehl, G. (2012). An overview of CMIP5 and the experiment design. *Bulletin of the American Meteorological Society*, 93(4), pp.485-498.
89. Tebaldi, C., Debeire, K., Eyring, V., Fischer, E., Fyfe, J., Friedlingstein, P., Knutti, R., Lowe, J., O'Neill, B., Sanderson, B. & Van Vuuren, D. (2021). Climate model projections from the scenario model intercomparison project (ScenarioMIP) of CMIP6. *Earth System Dynamics*, *12*(1), pp.253-293.
90. Ukkola, A., De Kauwe, M., Roderick, M., Abramowitz, G. & Pitman, A. (2020). Robust Future Changes in Meteorological Drought in CMIP6 Projections Despite Uncertainty in Precipitation. *Geophysical Research Letters,* 46, e2020GL087820. https://doi.org/10.1029/2020GL087820
91. University of East Anglia Climatic Research Unit; Harris, I., Jones, P. & Osborn, T. (2020): CRU TS4.04: Climatic Research Unit (CRU) Time-Series (TS) version 4.04 of high-resolution gridded data of month-by-month variation in climate (Jan. 1901-Dec. 2019). Centre for Environmental Data

Analysis. https://catalogue.ceda.ac.uk/uuid/89e1e34ec3554dc98594a5732622bce9 (01/12/2021).
92. Vellinga, M., Roberts, M., Vidale, P. L., Mizielinski, M. S., Demory, M.-E., Schiemann, R., Strachan, J., & Bain, C. (2016). Sahel decadal rainfall variability and the role of model horizontal resolution, *Geophysical Research Letters*, 43, pp.326– 333, doi:10.1002/2015GL066690.
93. Vigaud, N. & Giannini, A. (2019). West African convection regimes and their predictability from submonthly forecasts. *Climate Dynamics*, *52*(11), pp.7029-7048.
94. Vizy, E. K., K. H. Cook, J. Crétat, & N. Neupane (2013). Projections of a wetter Sahel in the twenty-first century from global and regional models, J. Clim., 26(13), 4664–4687, doi:10.1175/JCLI-D-12-00533.1.
95. Vogel, M., Hauser, M. & Seneviratne, S. (2020). Projected changes in hot, dry and wet extreme events' clusters in CMIP6 multi-model ensemble. *Environmental Research Letters*, 15 (094021), pp.1-11.
96. Zebaze, S., Jain, S., Salunke, P., Shafiq, S. & Mishra, S. (2019) Assessment of CMIP5 multimodel mean for the historical climate of Africa. *Atmospheric Science Letters,* 20 (e926), pp.1-12.
97. Zhou, T., Turner, A., Kinter, J., Wang, B., Qian, Y., Chen, X., Wang, B., Liu, B., Wu, B. & Zou, L. (2016). Overview of the global monsoons model inter-comparison project (GMMIP). *Geoscientific Model Development Discuss*, *2016*, pp.1-25.

APPENDIX 1: SUPPLEMENTARY INFORMATION

1a. Prolonged dry periods

Table 1a: *All dry years in the observations during the drought alongside years in prolonged dry periods – three or more years with a dry anomaly that is more than one times the standard deviation – for the coupled models. Green highlight represents the years falling within the defined drought period of 1970-1983. All years in the observations that fall in the drought period are included to signify the extent of the drying.*

GPCC	1972	1973		1976	1977		1982	1983	1984	1985	1986	1987									
CRU	1972	1973		1976			1982	1983	1984	1985	1986	1987									
ACCESS-CM2	1907	1908	1909																		
ACCESS-ESM1-5	1970	1971	1972	1973																	
AWI-ESM-1-1-LR	1905	1906	1907		1992	1993	1994														
BCC-ESM1	1951	1952	1953	1954																	
CESM2-FV2	1910	1911	1912		1968	1969	1970														
CNRM-CM6-1	1936	1937	1938	1939																	
CNRM-ESM2-1	1948	1949	1950																		
E3SM-1-0	1915	1916	1917																		
E3SM-1-1	1965	1966	1967		1971	1972	1973		1975	1976	1977	1978	1987	1988	1989	1991	1991	1992	1993		
E3SM-1-1-ECA	1970	1971	1972																		
EC-Earth3	1902	1903	1904		1912	1913	1914														
FIO-ESM-2-0	1901	1902	1903																		
GISS-E2-1-G	1968	1969	1970																		
HadGEM3-GC31-LL	1977	1978	1979	1980	1981	1982															
IITM-ESM	1970	1971	1972																		
INM-CM5-0	1875	1876	1877		1981	1982	1983														
IPSL-CM6A-LR	1876	1877	1878																		
KACE-1-0-G	1938	1939	1940																		
MIROC6	1972	1973	1974	1975		1988	1989	1990													
MPI-ESM-1-2-HAM	1955	1956	1957																		
MPI-ESM1-2-HR	1902	1903	1904	1905	1906		1908	1909	1910	1911	1912	1913									
MPI-ESM1-2-LR	1919	1920	1921	1922	1923																
MRI-ESM2-0	1973	1974	1975																		
NESM3	1924	1925	1926		1964	1965	1966		1974	1975	1976										
SAM0-UNICON	1907	1908	1909	1910																	
TaiESM1	1978	1979	1980																		

No prolonged dry period: AWI-CM-1-1-MR, BCC-CSM2-MR, CAMS-CSM1-0, CanESM5, CanESM5-CanOE, CAS-ESM2-0, CESM2, CESM2-WACCM, CESM2-WACCM-FV2, CNRM-CM6-1-HR, EC-Earth3-Veg, FGOALS-f3-L, GFDL-ESM4, GISS-E2-1-G-CC, GISS-E2-1-H, HadGEM3-GC31-MM, INM-CM4-8, MCM-UA-1-0, MIROC-ES2L, MPI-ESM-1-2-HAM, NorESM2-LM, NorESM2-MM, UKESM1-0-LL

1b. Prolonged wet periods

Table 1b: *Years in prolonged wet periods – three or more years with a wet anomaly that is more than one times the standard deviation – for both the observations and coupled models. Yellow highlight represents the years falling within the defined wet period of 1950-1963 and blue highlight is the recent wet period of 2001-2014. All years in the observations that fall in the wet period are included.*

GPCC	1952	1953	1954	1955		1957	1958	1959		1961					
CRU	1952	1953	1954	1955		1957	1958	1959		1961					
AWI-CM-1-1-MR	1850	1851	1852	1853	1854										
AWI-ESM-1-1-LR	1861	1862	1863	1864		1870	1871	1872							
BCC-CSM2-MR	1918	1919	1920												
CanESM5	2003	2004	2005		2011	2012	2013								
CanESM5-CanOE	2002	2003	2004	2005		2009	2010	2011	2012	2013	2014				
CESM2	1998	1999	2000		2011	2012	2013								
CNRM-CM6-1	2004	2005	2006												
CNRM-CM6-1-HR	1996	1997	1998												
CNRM-ESM2-1	1997	1998	1999		2011	2012	2013								
E3SM-1-1	1855	1856	1857	1858	1859	1860	1861		1894	1895	1896				
EC-Earth3-Veg	1991	1992	1993	1994	1995		2006	2007	2008		2011	2012	2013	2014	
HadGEM3-GC31-LL	1860	1861	1862	1863											
IITM-ESM	1958	1959	1960												
IPSL-CM6A-LR	1995	1996	1997												
KACE-1-0-G	1864	1865	1866												
MCM-UA-1-0	1888	1889	1890	1891		1959	1960	1961	1962		1989	1990	1991		
MIROC-ES2L	1933	1934	1935												
MPI-ESM-1-2-HAM	2012	2013	2014												
MPI-ESM1-2-HR	2005	2006	2007												
MPI-ESM1-2-LR	1997	1998	1999	2000		2012	2013	2014							
MRI-ESM2-0	1857	1858	1859												
NESM3	2006	2007	2008												
SAM0-UNICON	1863	1864	1865		1870	1871	1872								
TaiESM1	1859	1860	1861	1862											

No prolonged wet periods: ACCESS-CM2, ACCESS-ESM1-5, BCC-ESM1, CAMS-CSM1-0, CAS-ESM2-0, CESM2-FV2, CESM2-WACCM, CESM2-WACCM-FV2, E3SM-1-0, E3SM-1-1-ECA, EC-Earth3, FGOALS-f3-L, FIO-ESM-2-0, GFDL-ESM4, GISS-E2-1-G, GISS-E2-1-G-CC, GISS-E2-1-H, HadGEM3-GC31-MM, IITM-ESM, INM-CM4-8, INM-CM5-0, KACE-1-0-G, MIROC6, NorESM2-LM, NorESM2-MM, UKESM1-0-LL

2. Coupled correlation coefficients
2a. Interannual

Table 2a: *Table of correlation coefficients between the models and GPCC/CRU for the coupled historical runs on the interannual timescale. Light green highlight signifies a strong positive correlation (r>=0.26) and orange a strong negative correlation (r<=-0.26), according to Lau et al 2006's criteria. The pale blue highlight represents the correlation being significant at the 95% confidence interval. Higher resolution models are blue, medium resolution are green and lower resolution are yellow.*

Model	GPCC		CRU		Model	GPCC		CRU	
	Pearson's R	P-Value	Pearson's R	P-Value		Pearson's R	P-Value	Pearson's R	P-Value
ACCESS-CM2	-0.0680	0.474	-0.0655	0.491	GFDL-ESM4	0.0604	0.525	0.0496	0.602
ACCESS-ESM1-5	0.155	0.102	0.155	0.102	GISS-E2-1-G	-0.0195	0.837	-0.00140	0.988
AWI-CM-1-1-MR	-0.100	0.290	-0.115	0.227	GISS-E2-1-G-CC	-0.0378	0.691	-0.0598	0.529
AWI-ESM-1-1-LR	-0.155	0.102	-0.171	0.0709	GISS-E2-1-H	0.0187	0.844	0.0118	0.901
BCC-CSM2-MR	-0.0243	0.798	-0.0241	0.800	HadGEM3-GC31-LL	0.0601	0.527	0.0418	0.661
BCC-ESM1	-0.0477	0.616	-0.0435	0.647	HadGEM3-GC31-MM	-0.0589	0.535	-0.0666	0.483
CAMS-CSM1-0	0.0663	0.485	0.0604	0.525	IITM-ESM	0.123	0.195	0.113	0.233
CanESM5	-0.146	0.123	-0.0985	0.300	INM-CM4-8	-0.00991	0.917	-0.0509	0.593
CanESM5-CanOE	-0.0671	0.480	-0.0414	0.663	INM-CM5-0	0.0441	0.642	0.0452	0.635
CAS-ESM2-0	0.0959	0.312	0.0898	0.344	IPSL-CM6A-LR	0.0241	0.800	0.0531	0.576
CESM2	0.0211	0.824	0.0217	0.819	KACE-1-0-G	0.0230	0.809	0.0489	0.607
CESM2-FV2	-0.0133	0.889	-0.0288	0.762	MCM-UA-1-0	0.0271	0.776	0.0320	0.737
CESM2-WACCM	-0.00439	0.963	0.00612	0.949	MIROC6	0.0366	0.701	0.0561	0.555
CESM2-WACCM-FV2	-0.0380	0.690	-0.0267	0.779	MIROC-ES2L	-0.0590	0.535	-0.0619	0.515
CNRM-CM6-1	-0.215	0.0224	-0.186	0.0486	MPI-ESM-1-2-HAM	0.0232	0.808	0.0100	0.917
CNRM-CM6-1-HR	-0.172	0.0684	-0.162	0.0870	MPI-ESM1-2-HR	0.0945	0.320	0.124	0.192
CNRM-ESM2-1	-0.211	0.0247	-0.201	0.0327	MPI-ESM1-2-LR	-0.132	0.162	-0.106	0.266
E3SM-1-0	0.0776	0.414	0.0525	0.581	MRI-ESM2-0	0.125	0.187	0.123	0.195
E3SM-1-1	0.0176	0.853	0.00498	0.958	NESM3	-0.0509	0.592	-0.0165	0.862
E3SM-1-1-ECA	0.233	0.0131	0.212	0.0243	NorESM2-LM	-0.0198	0.835	-0.0388	0.684
EC-Earth3	0.313	0.000724	0.350	0.000144	NorESM2-MM	-0.0657	0.489	-0.0549	0.564
EC-Earth3-Veg	-0.0957	0.313	-0.0567	0.551	SAM0-UNICON	0.0950	0.317	0.104	0.273
FGOALS-f3-L	-0.00143	0.988	-0.0110	0.908	TaiESM1	0.0679	0.475	0.0456	0.631
FIO-ESM-2-0	-0.0349	0.714	0.00670	0.944	UKESM1-0-LL	0.0436	0.646	0.0666	0.483

2b. Five year running mean

Table 2b: *As Table 2a, but for the five-year running mean coefficients.*

Model	GPCC		CRU		Model	GPCC		CRU	
	Pearson's R	P-Value	Pearson's R	P-Value		Pearson's R	P-Value	Pearson's R	P-Value
ACCESS-CM2	-0.149	0.123	-0.122	0.206	GFDL-ESM4	0.0357	0.713	-0.00431	0.964
ACCESS-ESM1-5	0.245	0.0104	0.259	0.00659	GISS-E2-1-G	0.0327	0.736	0.0369	0.703
AWI-CM-1-1-MR	-0.259	0.00660	-0.279	0.00329	GISS-E2-1-G-CC	0.0312	0.747	-0.000445	0.996
AWI-ESM-1-1-LR	-0.156	0.105	-0.177	0.0655	GISS-E2-1-H	-0.0259	0.789	-0.00328	0.973
BCC-CSM2-MR	-0.232	0.0151	-0.217	0.0233	HadGEM3-GC31-LL	0.186	0.0532	0.168	0.0809
BCC-ESM1	-0.133	0.168	-0.128	0.183	HadGEM3-GC31-MM	0.0668	0.490	0.0670	0.4886
CAMS-CSM1-0	0.234	0.0145	0.267	0.0050	IITM-ESM	0.224	0.0190	0.230	0.0161
CanESM5	-0.241	0.0116	-0.177	0.0659	INM-CM4-8	0.102	0.292	0.0568	0.55775
CanESM5-CanOE	-0.247	0.00959	-0.198	0.0385	INM-CM5-0	0.290	0.00226	0.301	0.0015
CAS-ESM2-0	0.219	0.0219	0.250	0.00868	IPSL-CM6A-LR	0.112	0.244	0.122	0.20489
CESM2	0.0716	0.460	0.0896	0.354	KACE-1-0-G	0.241	0.0116	0.293	0.00201
CESM2-FV2	-0.129	0.181	-0.116	0.228	MCM-UA-1-0	0.339	0.000312	0.314	0.000884
CESM2-WACCM	-0.0278	0.774	0.00866	0.929	MIROC6	0.298	0.00167	0.316	0.000804
CESM2-WACCM-FV2	-0.0291	0.764	-0.00681	0.944	MIROC-ES2L	0.102	0.291	0.0902	0.351
CNRM-CM6-1	-0.429	3.18E-06	-0.395	2.10E-05	MPI-ESM-1-2-HAM	-0.0959	0.321	-0.0827	0.392
CNRM-CM6-1-HR	-0.410	9.72E-06	-0.379	4.79E-05	MPI-ESM1-2-HR	0.117	0.227	0.171	0.0759
CNRM-ESM2-1	-0.445	1.25E-06	-0.422	4.78E-06	MPI-ESM1-2-LR	-0.406	1.21E-05	-0.378	5.05E-05
E3SM-1-0	0.0573	0.554	0.0574	0.553	MRI-ESM2-0	0.403	1.40E-05	0.395	2.18E-05
E3SM-1-1	-0.0763	0.430	-0.0508	0.600	NESM3	-0.136	0.157	-0.0831	3.90E-01
E3SM-1-1-ECA	0.488	7.10E-08	0.485	8.81E-08	NorESM2-LM	0.0555	0.566	0.0694	0.474
EC-Earth3	0.623	4.80E-13	0.641	5.89E-14	NorESM2-MM	-0.0410	0.672	-0.0470	0.627
EC-Earth3-Veg	-0.309	0.00109	-0.252	0.00824	SAM0-UNICON	0.392	2.53E-05	0.390	2.81E-05
FGOALS-f3-L	-0.211	0.0275	-0.225	0.0189	TaiESM1	0.209	0.0295	0.168	0.0816
FIO-ESM-2-0	-0.0954	0.324	-0.0803	0.406	UKESM1-0-LL	0.0609	0.529	0.118	2.23E-01

2c. 10 year running mean

Table 2c: *As Table 2a, but for the 10-year running mean coefficients.*

Model	GPCC		CRU		Model	GPCC		CRU	
	Pearson's R	P-Value	Pearson's R	P-Value		Pearson's R	P-Value	Pearson's R	P-Value
ACCESS-CM2	-0.137	0.1640	-0.117	0.239	GFDL-ESM4	-0.0565	0.569	-0.0917	0.355
ACCESS-ESM1-5	0.267	0.00607	0.260	0.00762	GISS-E2-1-G	-0.0299	0.764	-0.0579	0.559
AWI-CM-1-1-MR	-0.295	0.00233	-0.297	0.00221	GISS-E2-1-G-CC	-0.0131	0.895	-0.0384	0.699
AWI-ESM-1-1-LR	-0.175	0.0751	-0.206	0.0363	GISS-E2-1-H	-0.0728	0.463	-0.0736	0.458
BCC-CSM2-MR	-0.290	0.00282	-0.279	0.00412	HadGEM3-GC31-LL	0.246	0.0117	0.218	0.0264
BCC-ESM1	-0.149	0.131	-0.154	0.119	HadGEM3-GC31-MM	0.120	0.227	0.112	0.258
CAMS-CSM1-0	0.277	0.00447	0.308	0.00145	IITM-ESM	0.307	0.00151	0.290	0.00279
CanESM5	-0.277	0.00443	-0.229	0.0193	INM-CM4-8	0.105	0.291	0.0508	0.609
CanESM5-CanOE	-0.361	0.000168	-0.314	0.00118	INM-CM5-0	0.333	0.000542	0.331	0.0005890
CAS-ESM2-0	0.279	0.00407	0.289	0.00294	IPSL-CM6A-LR	0.0741	0.454	0.0671	0.499
CESM2	0.0618	0.533	0.0658	0.507	KACE-1-0-G	0.326	0.000730	0.384	5.84E-05
CESM2-FV2	-0.183	0.0625	-0.1688	0.0868	MCM-UA-1-0	0.520	1.53E-08	0.488	1.52E-07
CESM2-WACCM	-0.101	0.308	-0.071	0.477	MIROC6	0.398	2.84E-05	0.393	3.65E-05
CESM2-WACCM-FV2	0.0241	0.808	0.042	0.672	MIROC-ES2L	0.118	0.233	0.0994	0.315
CNRM-CM6-1	-0.506	4.21E-08	-0.483	2.13E-07	MPI-ESM-1-2-HAM	-0.232	0.0177	-0.228	0.0199
CNRM-CM6-1-HR	-0.538	3.85E-09	-0.516	2.12E-08	MPI-ESM1-2-HR	0.106	0.286	0.151	0.126
CNRM-ESM2-1	-0.530	7.19E-09	-0.502	5.50E-08	MPI-ESM1-2-LR	-0.619	2.51E-12	-0.595	2.74E-11
E3SM-1-0	-0.0076	0.939	-0.00357	0.971	MRI-ESM2-0	0.547	1.89E-09	0.513	2.53E-08
E3SM-1-1	-0.0965	0.330	-0.0676	0.495	NESM3	-0.160	0.105	-0.118	0.233
E3SM-1-1-ECA	0.627	1.13E-12	0.625	1.39E-12	NorESM2-LM	-0.0261	0.793	-0.024	0.809
EC-Earth3	0.716	1.36E-17	0.718	9.34E-18	NorESM2-MM	-0.0614	0.536	-0.078	0.431
EC-Earth3-Veg	-0.416	1.13E-05	-0.381	6.46E-05	SAM0-UNICON	0.606	9.25E-12	0.601	1.50E-11
FGOALS-f3-L	-0.142	0.151	-0.165	0.0943	TaiESM1	0.257	0.00834	0.217	0.0271
FIO-ESM-2-0	-0.0775	0.434	-0.0869	0.381	UKESM1-0-LL	0.0408	0.681	0.104	0.292

3. Historical-Natural correlation coefficients

Table 3a: *Table of correlation coefficients between the models and GPCC/CRU for the Historical-Natural runs on the interannual timescale. Green highlight signifies a strong positive correlation (r>=0.26) and orange a strong negative correlation (r<=-0.26) according to Lau et al 2006's criteria. The blue highlight represents the correlation being significant at the 95% confidence interval.*

Model	GPCC		CRU	
	Pearson's R	P-Value	Pearson's R	P-Value
ACCESS-CM2	0.228	0.0153	0.241	0.010
ACCESS-ESM1-5	0.0898	0.344	0.108	0.257
BCC-CSM2-MR	0.0638	0.502	0.0977	0.303
CanESM5	0.0184	0.846	0.022	0.817
CESM2	0.129	0.172	0.118	0.211
CNRM-CM6-1	-0.0409	0.667	-0.045	0.637
FGOALS-g3	-0.0951	0.316	-0.104	0.274
GFDL-CM4	0.093	0.326	0.078	0.411
GISS-E2-1-G	0.0037	0.969	0.019	0.840
HadGEM3-GC31-LL	0.0876	0.356	0.069	0.471
IPSL-CM6A-LR	0.00636	0.947	0.0108	0.910
MIROC6	0.0488	0.607	0.0354	0.710
MRI-ESM2-0	0.104	0.273	0.088	0.353
NorESM2-LM	-0.016	0.863	-0.001	0.994

Table 3b: *As Table 3a, but for the five-year running mean.*

Model	GPCC		CRU	
	Pearson's R	P-Value	Pearson's R	P-Value
ACCESS-CM2	0.382	4.13E-05	0.404	4.13E-05
ACCESS-ESM1-5	0.130	0.177	0.161	0.0951
BCC-CSM2-MR	0.00602	0.950	0.0789	0.415
CanESM5	0.0375	0.699	0.0464	0.632
CESM2	0.471	2.41E-07	0.470	2.41E-07
CNRM-CM6-1	-0.0766	0.429	-0.0814	0.400
FGOALS-g3	-0.0614	0.526	-0.0396	0.682
GFDL-CM4	0.123	0.203	0.145	0.133
GISS-E2-1-G	-0.0422	0.663	-0.0238	0.806
HadGEM3-GC31-LL	0.192	0.0455	0.162	0.0932
IPSL-CM6A-LR	0.145	0.133	0.127	0.187
MIROC6	-0.0403	0.678	-0.062	0.523
MRI-ESM2-0	0.185	0.0543	0.170	0.0765
NorESM2-LM	0.127	0.188	0.111	0.252

Table 3c: *As Table 3a, but for the 10-year running mean.*

Model	GPCC		CRU	
	Pearson's R	P-Value	Pearson's R	P-Value
ACCESS-CM2	0.447	1.98E-06	0.460	9.00E-07
ACCESS-ESM1-5	0.241	0.0138	0.269	0.00568
BCC-CSM2-MR	-0.0763	0.441	-0.00430	0.965
CanESM5	0.0522	0.598	0.0659	0.506
CESM2	0.719	7.79E-18	0.714	1.66E-17
CNRM-CM6-1	-0.251	0.0101	-0.270	0.00551
FGOALS-g3	-0.155	0.117	-0.128	0.194
GFDL-CM4	0.140	0.156	0.169	0.0869
GISS-E2-1-G	-0.121	0.222	-0.103	0.299
HadGEM3-GC31-LL	0.266	0.00642	0.217	0.0271
IPSL-CM6A-LR	0.246	0.0117	0.220	0.0249
MIROC6	-0.0435	0.661	-0.0857	0.387
MRI-ESM2-0	0.191	0.0522	0.199	0.0430
NorESM2-LM	0.178	0.0699	0.173	0.0791

4. AMIP-Historical correlation coefficients

Table 4: *Table of correlation coefficients between the models and GPCC/CRU for the AMIP historical runs on the interannual timescale. Green highlight signifies a strong positive correlation (r>=0.26), according to Lau et al 2006's criteria. The blue highlight represents the correlation being significant at the 95% confidence interval.*

Model	GPCC		CRU	
	Pearson's R	P-Value	Pearson's R	P-Value
BCC-CSM2-MR	0.275	0.00321	0.311	0.000796
CAMS-CSM1-0	0.187	0.0468	0.197	0.0362
CanESM5	0.138	0.144	0.205	0.0296
CESM2	0.487	4.42E-08	0.518	4.14E-09
CNRM-CM6-1	0.195	0.0380	0.190	0.0436
CNRM-CM6-1-HR	0.146	0.122	0.178	0.0592
CNRM-ESM2-1	0.0418	0.660	0.0625	0.511
FGOALS-f3-L	0.358	0.000101	0.361	8.51E-05
FGOALS-g3	0.252	0.00714	0.288	0.00201
FIO-ESM-2-0	0.351	0.000137	0.379	3.46E-05
GFDL-CM4	0.368	5.94E-05	0.425	2.69E-06
IITM-ESM	0.250	0.00746	0.267	0.00422
IPSL-CM6A-LR	0.390	1.99E-05	0.419	3.78E-06
MIROC6	0.320	0.000552	0.342	0.000211
MRI-ESM2-0	0.382	2.97E-05	0.417	4.23E-06
TaiESM1	0.391	1.90E-05	0.449	5.99E-07

5. Spatial Projections

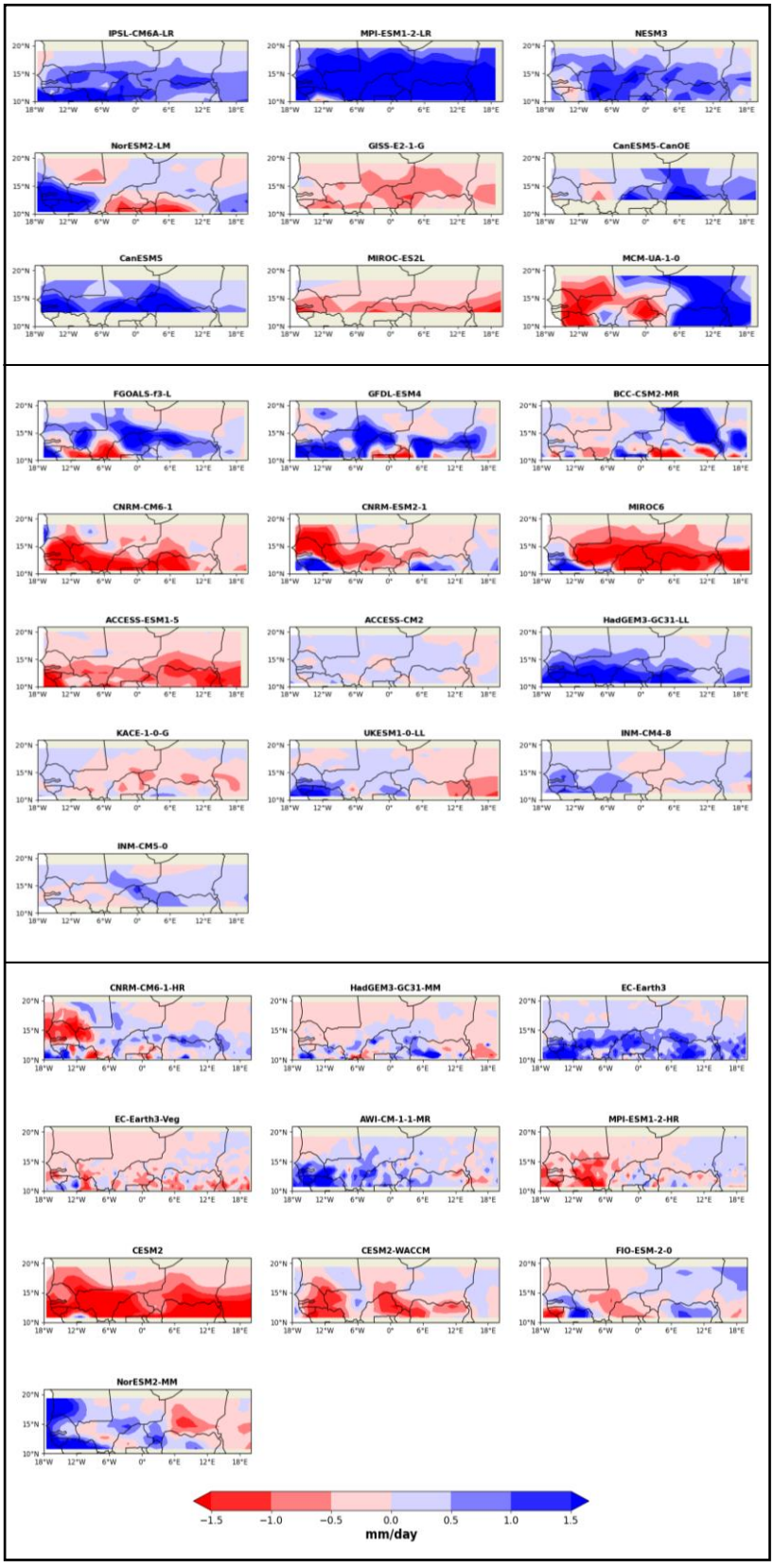

Figure 5a: *Difference maps of the modelled 2087-2100 average minus the recent period average (2001-2014) monsoon season precipitation (mm/day) for SSP1-2.6, ordered by nominal resolution smallest to largest. From top to bottom: lower, medium and higher resolution models.*

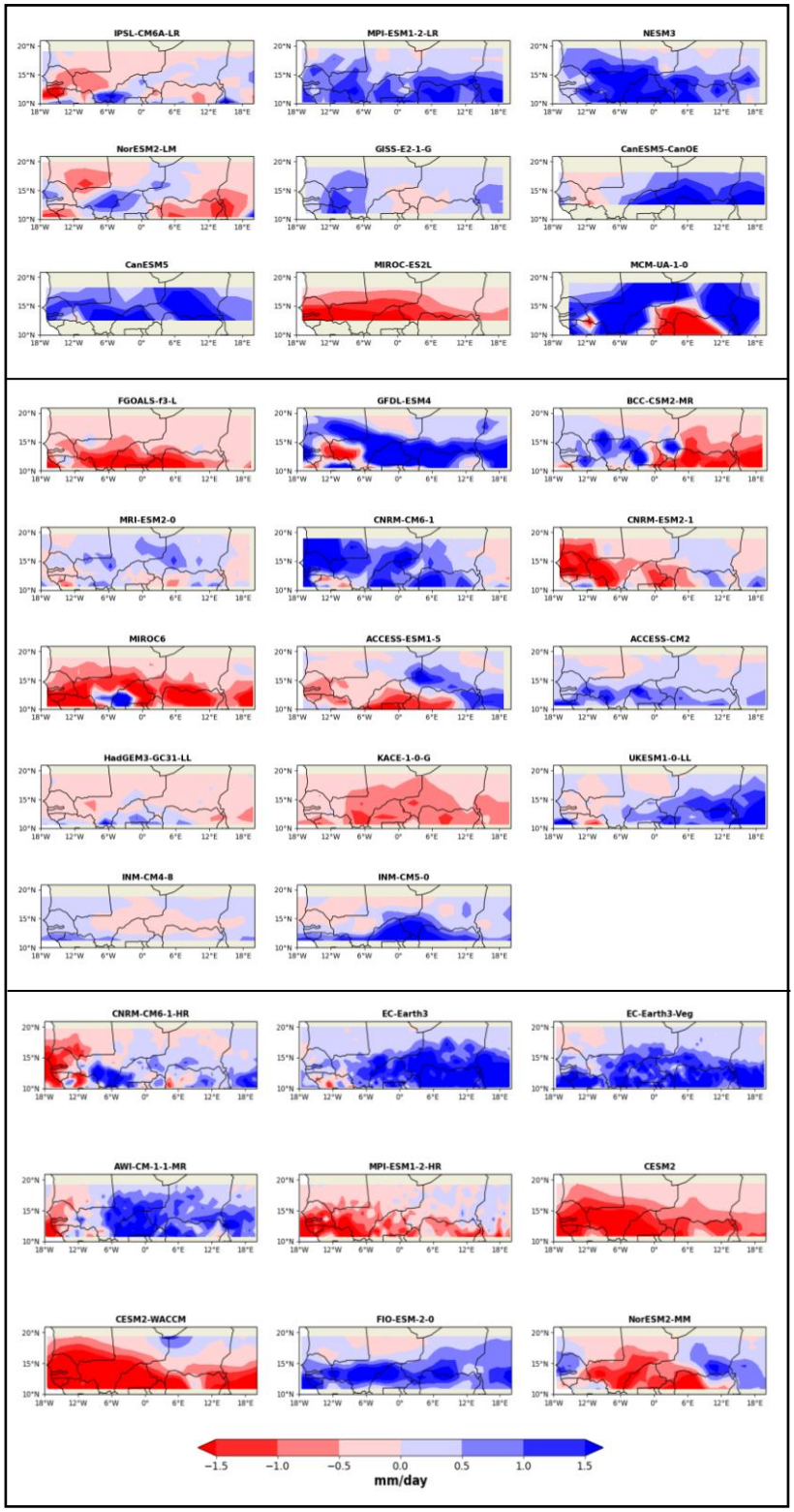

Figure 5b: *As Figure 5a but for SSP2-4.5.*

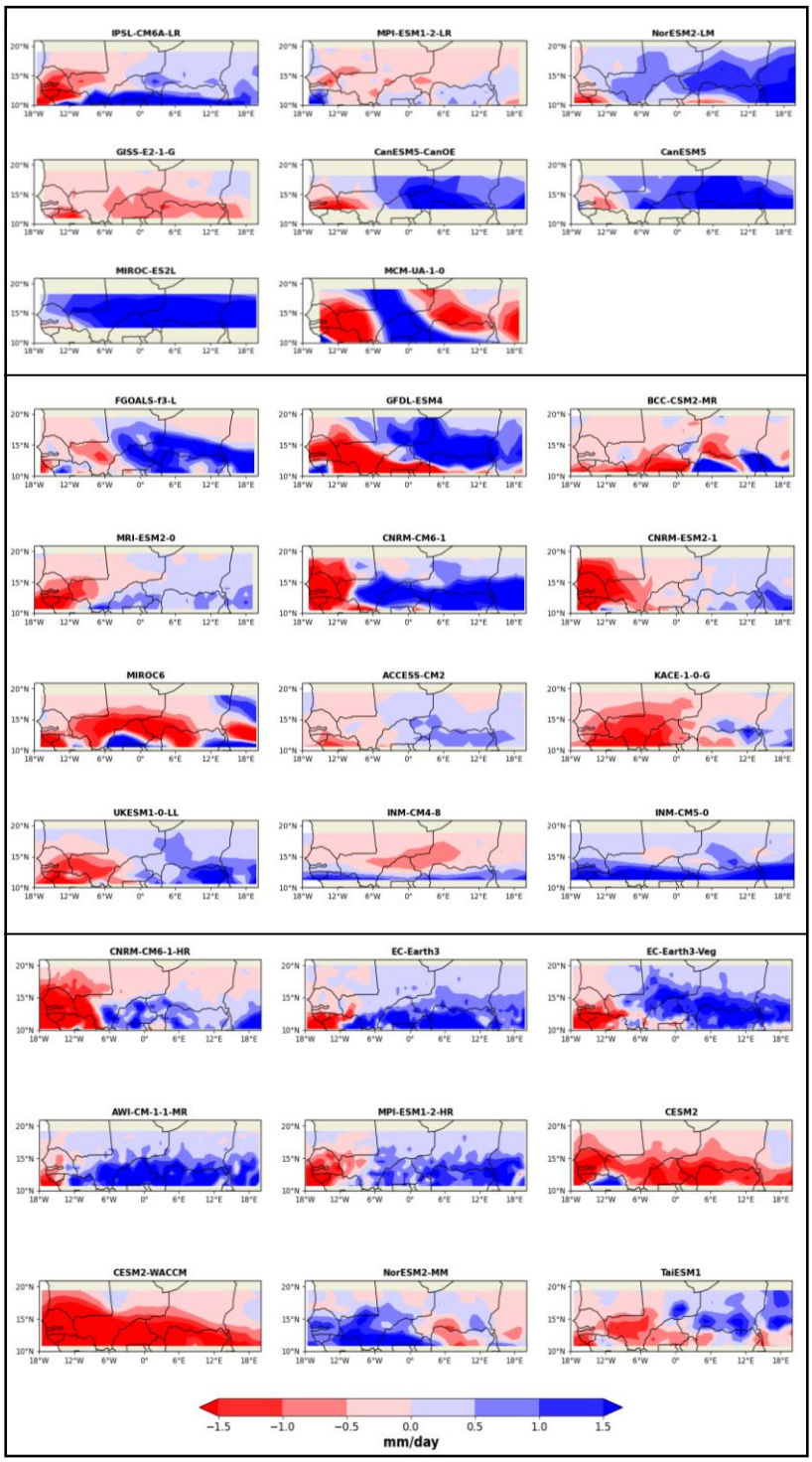

Figure 5c: *As Figure 5a but for SSP3-7.0.*

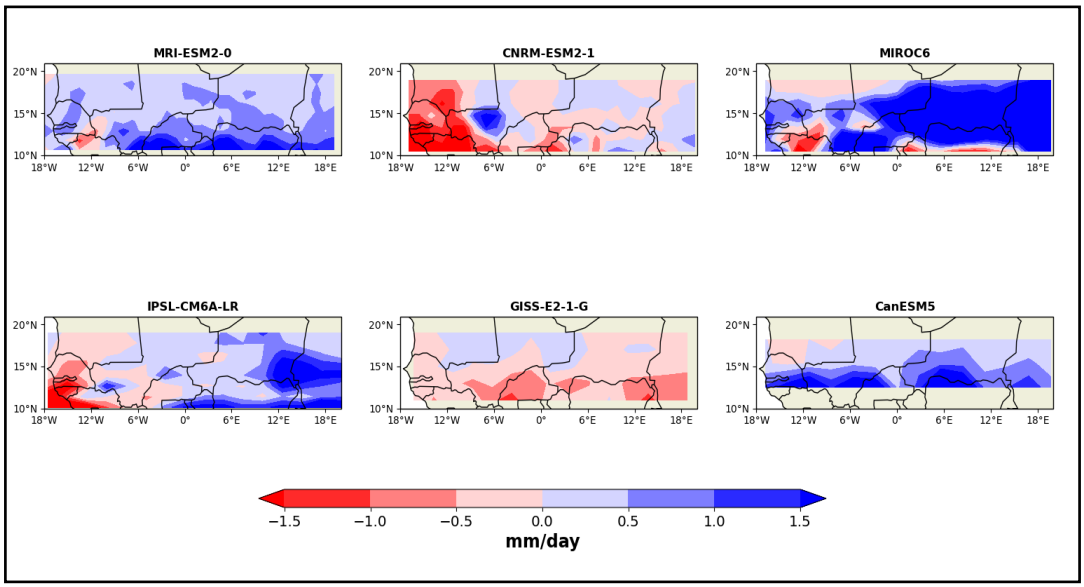

Figure 5d: *As Figure 5a, but for SSP4-6.0 and the top row are medium resolution models, with the bottom row lower resolution models.*

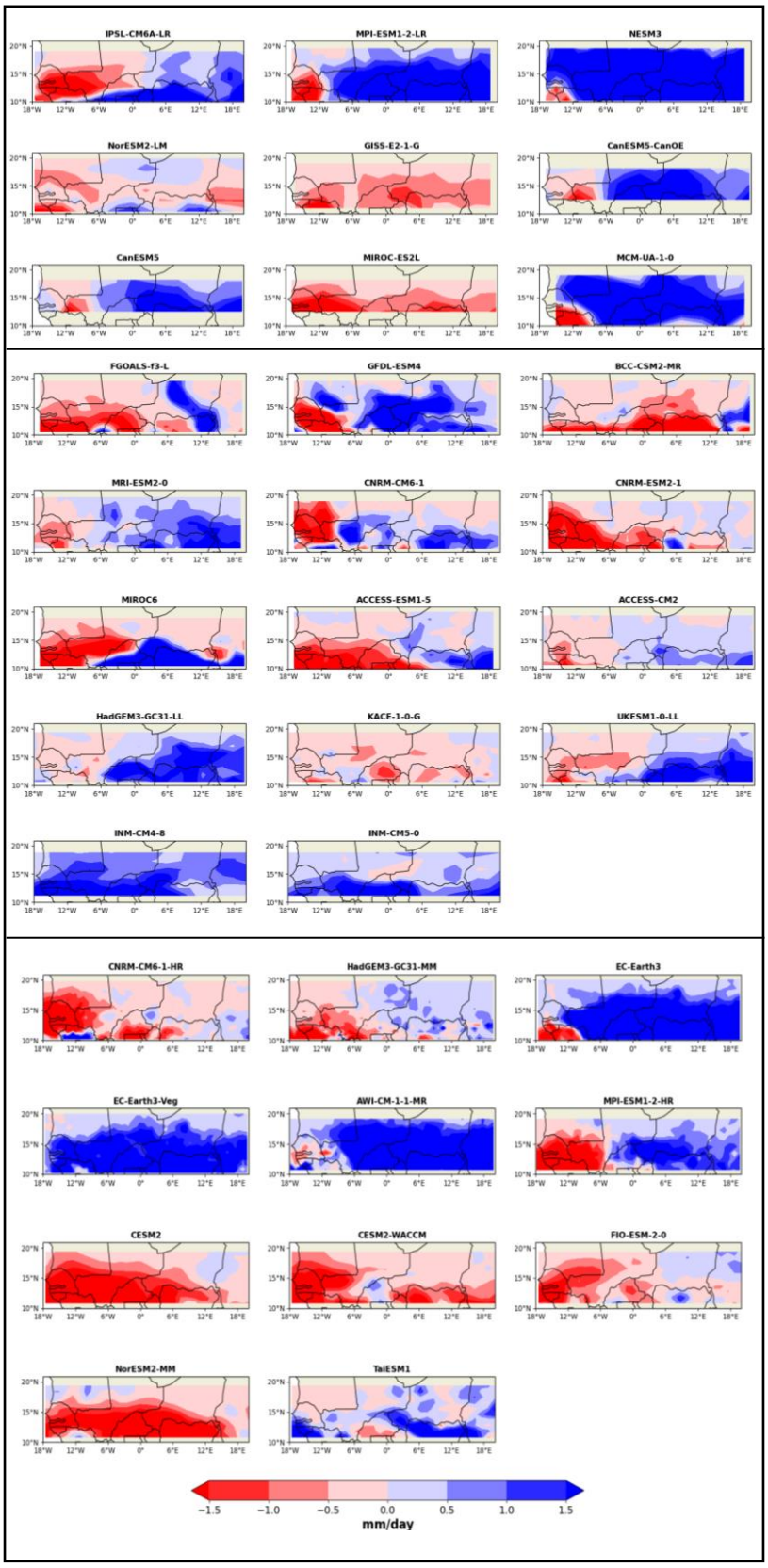

Figure 5e: *As Figure 5a but for SSP5-8.5.*

APPENDIX 2: TABLE OF CMIP6 MODELS

Table 1: *Summary of models used in this study. The variant label is made up of four indices, r<k>i<l>p<m>f<n>, where k is realisation index, l is initialisation index, m is physics index and n is forcing index. The historical period is 1850-2014, as per the CMIP6 requirements.*

Model	Modelling Group	Atmospheric Resolution (longitude/latitude unless specified)	Oceanic Resolution (longitude/latitude unless specified)	Variant Label	Aerosol and Land components	References (experiment and model description)
ACCESS-CM2	Commonwealth Scientific and Industrial Research Organisation, (CSIRO) Australia, Australian Research Council Centre of Excellence for Climate System Science (ARCCSS)	MetUM-HadGEM3-GA7.1 (N96; 192 x 144 longitude/latitude; 85 levels; top level 85 km)	ACCESS-OM2 (GFDL-MOM5, tripolar primarily 1º; 360 x 300 longitude/latitude; 50 levels; top grid cell 0-10 m)	r1i1p1f1	Aerosol = UKCA-GLOMAP-mode, dust included as a separate simulation to the other aerosols. Land = CABLE2.5, vegetation distribution is kept at the year 1850 distribution	Dix et al (2019) Bi et al (2020)
ACCESS-ESM1-5	Commonwealth Scientific and Industrial Research Organisation, Aspendale, Victoria 3195, Australia	HadGAM2 (r1.1, N96; 192 x 145 longitude/latitude; 38 levels; top level 39255 m)	ACCESS-OM2 (MOM5, tripolar primarily 1º; 360 x 300 longitude/latitude; 50 levels; top grid cell 0-10 m)	r10i1p1f1	Aerosol= CLASSIC (v1.0), no dust Land = CABLE2.4, vegetation distribution is kept at the year 1850 distribution	Ziehn et al (2019) Ziehn et al (2020)
AWI-ESM-1-1-LR	Alfred Wegener Institute, Helmholtz Centre for Polar and Marine Research, Germany	ECHAM6.3.04p1 (T63L47 native atmosphere T63 gaussian grid; 192 x 96 longitude/latitude; 47 levels; top level 80 km	FESOM 1.4 (unstructured grid in the horizontal with 126859 wet nodes; 46 levels; top grid cell 0-5 m	r1i1p1f1	Aerosol = Interactive within ECHAM6.3.04p1 Land = JSBACH, dynamic vegetation	Danek et al (2020) Stevens et al (2013)
BCC-CSM2-MR	Beijing Climate Center, Beijing, China	BCC-AGCM3-MR (T106; 320 x 160	MOM4 (1/3º 10ºS-10ºN, 1/3-1º 10º-30º N/S, and 1º in high	r1i1p1f1	Aerosols = Prescribed, both	Wu et al (2019) Wu et al (2018)

		longitude/latitude; 46 levels; top level 1.46 hPa)	latitudes; 360 x 232 longitude/latitude; 40 levels; top grid cell 0-10 m)		direct and indirect effects included Land = BCC-AVIM2, dynamic vegetation	
BCC-ESM1	Beijing Climate Center, Beijing, China	BCC-AGCM3-LR (T42; 128 x 64 longitude/latitude; 26 levels; top level 2.19 hPa)	MOM4 (1/3° 10°S-10°N, 1/3-1° 10°-30° N/S, and 1° in high latitudes; 360 x 232 longitude/latitude; 40 levels; top grid cell 0-10 m)	r1i1p1f1	Aerosols = Prognostic, both direct and indirect effects included Land = BCC-AVIM2, dynamic vegetation	Zhang et al (2018) Wu et al (2018)
CAMS-CSM1-0	Chinese Academy of Meteorological Sciences, Beijing, China	ECHAM5_CAMS (T106; 320 x 160 longitude/latitude; 31 levels; top level 10 mb)	MOM4 (tripolar; 360 x 200 longitude/latitude, primarily 1° latitude/longitude, down to 1/3° within 30° of the equatorial tropics; 50 levels; top grid cell 0-10 m)	r1i1p1f1	Aerosols = uses historical values and includes the effects on radiation Land = ECHAM5 coupled with Common Land Model, fixed land-use forcing,	Rong (2019) Rong et al (2021) Xin et al (2019)
CanESM5	Canadian Centre for Climate Modelling and Analysis, Environment and Climate Change Canada	CanAM5 (T63L49 native atmosphere, T63 Linear Gaussian Grid; 128 x 64 longitude/latitude; 49 levels; top level 1 hPa)	NEMO3.4.1 (ORCA1 tripolar grid, 1° with refinement to 1/3° within 20° of the equator; 361 x 290 longitude/latitude; 45 vertical levels; top grid cell 0-6.19 m) with Canadian Model of Ocean Carbon	r10i1p1f1	Aerosols = Interactive Land = Canadian Land Surface Scheme (CLASS) and the Canadian Terrestrial Ecosystem Model (CTEM), dynamic vegetation	Swart et al (2019a) Swart et al (2019b)
CanESM5-CanOE	Canadian Centre for Climate Modelling and Analysis, Environment and Climate Change Canada	CanAM5 (T63L49 native atmosphere, T63 Linear Gaussian Grid; 128 x 64 longitude/latitude; 49 levels; top level 1 hPa)	NEMO3.4.1 (ORCA1 tripolar grid, 1° with refinement to 1/3° within 20° of the equator; 361 x 290	r1i1p2f1	Aerosols = Interactive Land = Canadian Land Surface	Swart et al (2019a) Swart et al (2019b)

			longitude/latitude; 45 vertical levels; top grid cell 0-6.19 m) with Canadian Ocean Ecosystem model		Scheme (CLASS) and the Canadian Terrestrial Ecosystem Model (CTEM), dynamic vegetation	
CAS-ESM2-0	Chinese Academy of Sciences, Beijing, China	IAP AGCM 5.0 (Finite difference dynamical core; 256 x 128 longitude/latitude; 35 levels; top level 2.2 hPa)	LICOM2.0 (LICOM2.0, primarily 1°; 362 x 196 longitude/latitude; 30 levels; top grid cell 0-10 m)	r1i1p1f1	Aerosol = IAP AACM	Chai (2020)
CESM2	National Center for Atmospheric Research	CAM6 (0.9x1.25 finite volume grid; 288 x 192 longitude/latitude; 32 levels; top level 2.25 mb)	POP2 (320x384 longitude/latitude; 60 levels; top grid cell 0-10 m)	r1i1p1f1	Aerosol = MAM4 (0.9° x 1.25° finite volume grid; 288 x 192 longitude/ latitude; 32 levels; top level 2.25 mb) Land = interactive (CLM5)	Danabasoglu (2019a) Danabasoglu et al (2020)
CESM2-FV2	National Center for Atmospheric Research	CAM6 (1.9x2.5 finite volume grid; 144 x 96 longitude/latitude; 32 levels; top level 2.25 mb)	POP2 (320x384 longitude/latitude; 60 levels; top grid cell 0-10 m)	r1i1p1f1	Aerosol = MAM4 (1.9° x 2.5° finite volume grid; 144 x 96 longitude/latitude; 32 levels; top level 2.25 mb) Land = interactive, CLM5 at 1.9° latitude x 2.5° longitude	Danabasoglu (2019b) Danabasoglu et al (2020)
CESM2-WACCM	National Center for Atmospheric Research	CAM6 (0.9x1.25 finite volume grid; 288 x 192 longitude/latitude; 70 levels; top level 4.5e-6 mb)	POP2 (320x384 longitude/latitude; 60 levels; top grid cell 0-10 m)	r1i1p1f1	Aerosol = MAM4 (0.9° x 1.25° finite volume grid; 288 x 192 longitude/ latitude; 70 levels; top level 4.5e-6 mb)	Danabasoglu (2019c) Danabasoglu et al (2020)

					Land = interactive (CLM5)	
CESM2-WACCM-FV2	National Center for Atmospheric Research	CAM6 (1.9x2.5 finite volume grid; 144 x 96 longitude/latitude; 70 levels; top level 4.5e-6 mb)	POP2 (320x384 longitude/latitude; 60 levels; top grid cell 0-10 m)	r1i1p1f1	Aerosol = MAM4 (1.9^{o} x 2.5^{o} finite volume grid; 144 x 96 longitude/latitude; 70 levels; top level 4.5e-6 mb) Land = interactive (CLM5, 1.9^{o} x 2.5^{o})	Danabasoglu (2019d) Danabasoglu et al (2020)
CNRM-CM6-1	CNRM (Centre National de Recherches Meteorologiques, France), CERFACS (Centre Europeen de Recherche et de Formation Avancee en Calcul Scientifique, France)	Arpege 6.3 (T127; Gaussian Reduced with 24572 grid points in total distributed over 128 latitude circles (with 256 grid points per latitude circle between 30^{o}N and 30^{o}S reducing to 20 grid points per latitude circle at 88.9^{o}N and 88.9^{o}S); 91 levels; top level 78.4 km)	Nemo 3.6 (eORCA1, tripolar primarily 1^{o}; 362 x 294 longitude/latitude; 75 levels; top grid cell 0-1 m)	r10i1p1f2	Aerosol = Prescribed monthly fields computed by TACTIC_v2 scheme. Land = Fixed, using ECOCLIMAP-II.	Voldoire (2018) Voldoire et al (2019)
CNRM-CM6-1-HR	CNRM (Centre National de Recherches Meteorologiques, France), CERFACS (Centre Europeen de Recherche et de Formation Avancee en Calcul Scientifique, France)	Arpege 6.3 (T359; Gaussian Reduced with 181724 grid points in total distributed over 360 latitude circles (with 720 grid points per latitude circle between 32.2^{o}N and 32.2^{o}S reducing to 18 grid points per latitude circle at 89.6^{o}N and 89.6^{o}S)); 91 levels; top level 78.4 km)	Nemo 3.6 (eORCA025, tripolar primarily 1/4^{o}; 1442 x 1050 longitude/latitude; 75 levels; top grid cell 0-1 m)	r1i1p1f2	Aerosol = Prescribed monthly fields computed by TACTIC_v2 scheme. Land = Fixed vegetation, using ECOCLIMAP-II.	Voldoire (2018) Voldoire et al (2019)
CNRM-ESM2-1	CNRM (Centre National de Recherches Meteorologiques, France), CERFACS	Arpege 6.3 (T127; Gaussian Reduced with 24572 grid points in total distributed over 128 latitude circles (with 256	Nemo 3.6 (eORCA1, tripolar primarily 1^{o}; 362 x 294 longitude/latitude; 75	r10i1p1f2	Aerosol = Interactive, using TACTIC_V2. Land = SURFEXv8.0,	Séférian et al (2019) Séférian (2018)

	(Centre Europeen de Recherche et de Formation Avancee en Calcul Scientifique, France)	grid points per latitude circle between 30°N and 30°S reducing to 20 grid points per latitude circle at 88.9°N and 88.9°S); 91 levels; top level 78.4 km	levels; top grid cell 0-1 m)		interactive, includes feedbacks between dust and vegetation,	
E3SM-1-0	LLNL (Lawrence Livermore National Laboratory, USA); ANL (Argonne National Laboratory, USA); BNL (Brookhaven National Laboratory, USA); LANL (Los Alamos National Laboratory, USA); LBNL (Lawrence Berkeley National Laboratory, USA); ORNL (Oak Ridge National Laboratory, USA); PNNL (Pacific Northwest National Laboratory, USA); SNL (Sandia National Laboratories, USA).	EAM (v1.0, cubed sphere spectral-element grid; 1° average grid spacing; 90 x 90 x 6 longitude/latitude/cube face; 72 levels; top level 0.1 hPa)	MPAS-Ocean (v6.0, variable resolution 60 km to 30 km; 60 levels; top grid cell 0-10 m)	r1i1p1f1	Aerosol = MAM4, interactive aerosols, same grid as atmosphere Land = ELMv1.0, fixed vegetation.	Bader et al (2019a) Golaz et al (2019)
E3SM-1-1	LLNL (Lawrence Livermore National Laboratory, USA); ANL (Argonne National Laboratory, USA); BNL (Brookhaven National Laboratory, USA); LANL (Los Alamos National Laboratory, USA); LBNL (Lawrence Berkeley National Laboratory, USA); ORNL (Oak	EAM (v1.1, cubed sphere spectral-element grid; 1° average grid spacing; 90 x 90 x 6 longitude/latitude/ cubeface; 72 levels; top level 0.1 hPa)	MPAS-Ocean (v6.0, variable resolution 60 km to 30 km; 60 levels; top grid cell 0-10 m)	r1i1p1f1	Aerosol = MAM4, interactive aerosols, same grid as atmosphere Land: ELM v1.1, same grid as atmosphere, interactive vegetation. MOSART (v1.1, 0.5° latitude/longitude grid)	Bader et al (2019b) Burrows et al (2020)

	Ridge National Laboratory, USA); PNNL (Pacific Northwest National Laboratory, USA); SNL (Sandia National Laboratories, USA).					
E3SM-1-1-ECA	LLNL (Lawrence Livermore National Laboratory, USA); ANL (Argonne National Laboratory, USA); BNL (Brookhaven National Laboratory, USA); LANL (Los Alamos National Laboratory, USA); LBNL (Lawrence Berkeley National Laboratory, USA); ORNL (Oak Ridge National Laboratory, USA); PNNL (Pacific Northwest National Laboratory, USA); SNL (Sandia National Laboratories, USA).	EAM (v1.1, cubed sphere spectral-element grid; 1º average grid spacing; 90 x 90 x 6 longitude/latitude/cube face; 72 levels; top level 0.1 hPa)	MPAS-Ocean (v6.0, variable resolution 60 km to 30 km; 60 levels; top grid cell 0-10 m)	r1i1p1f1	Aerosol = MAM4, interactive aerosols, same grid as atmosphere Land = ELM v1.1, same grid as atmosphere, interactive vegetation, includes active biogeochemistry associated with plant and soil carbon, as well as mechanisms with nutrients. MOSART (v1.1, 0.5º latitude/ longitude grid)	Burrows et al (2020) Bader et al (2020)
EC-Earth3	Earth Consortium, Europe	IFS cy36r4 (TL255, linearly reduced Gaussian grid equivalent to 512 x 256 longitude/latitude; 91 levels; top level 0.01 hPa)	NEMO3.6 (ORCA1 tripolar primarily 1º with meridional refinement down to 1/3º in the tropics; 362 x 292 longitude/latitude; 75 levels; top grid cell 0-1 m)	r10i1p1f1	Aerosols = Forcings taken from the CMIP6 dataset including stratospheric aerosols (optical properties). Tropospheric aerosols derived from modelled pre-industrial values combined with a	EC-Earth Consortium (EC-Earth) (2019a). Döscher et al (2021)

					model of anthropogenic aerosols. Land = HTESSEL, dynamic vegetation	
EC-Earth3-Veg	Earth Consortium, Europe	80km horizontal, 0.35º x 0.35º, 91 vertical levels IFS cy36r4 (TL255, linearly reduced Gaussian grid equivalent to 512 x 256 longitude/latitude; 91 levels; top level 0.01 hPa)	75 layers, 1º resolution, equator has mesh refinement NEMO3.6 (ORCA1 tripolar primarily 1º with meridional refinement down to 1/3º in the tropics; 362 x 292 longitude/latitude; 75 levels; top grid cell 0-1 m)	r1i1p1f1	Aerosols = Forcings taken from the CMIP6 dataset including stratospheric aerosols (optical properties). Tropospheric aerosols derived from modelled pre-industrial values combined with a model of anthropogenic aerosols. Land = HTESSEL, dynamic vegetation, also includes the reciprocal effects of soil water on evapotranspiration, surface albedo and roughness length, which feeds into the defined effective vegetation cover.	Rivera and Arnould (2020) Wyser et al (2020) EC-Earth Consortium (EC-Earth) (2019b) Döscher et al (2021)
FGOALS-f3-L	Chinese Academy of Sciences, Beijing, China	FAMIL2.2 (Cubed-sphere, 360 x 180 longitude/ latitude; 32 levels; top level 2.16 hPa)	LICOM3.0 (LICOM3.0, tripolar primarily 1deg; 360 x 218 longitude/ latitude; 30 levels; top grid cell 0-10 m)	r1i1p1f1	Aerosols = Prescribed, as per CMIP6 requirements. Land = CLM4.0, prescribed with	Yu (2019) He et al (2019) Guo et al (2020)

					monthly mean observed values	
FIO-ESM-2-0	FIO (First Institute of Oceanography, State Oceanic Administration, China), QNLM (Qingdao National Laboratory for Marine Science and Technology, China)	CAM4 (0.9x1.25 finite volume grid; 192 x 288 longitude/latitude; 26 levels; top level ~2 hPa)	POP2-W (POP2 coupled with MASNUM surface wave model, Displaced Pole; 320 x 384 longitude/latitude; 60 levels; top grid cell 0-10 m)	r1i1p1f1	Aerosol = Prescribed monthly fields Land = CLM4.0 (same grid as atmosphere)	Song et al (2019)
GFDL-ESM4	National Oceanic and Atmospheric Administration, Geophysical Fluid Dynamics Laboratory, USA	GFDL-AM4.1 (Cubed-sphere - 1º nominal horizontal resolution; 360 x 180 longitude/latitude; 49 levels; top level 1 Pa)	GFDL-OM4p5 (GFDL-MOM6, tripolar - nominal 0.5º; 720 x 576 longitude/latitude; 75 levels; top grid cell 0-2 m)	r1i1p1f1	Aerosol = Interactive, including dust emissions Land = GFDL-LM4.1, dynamic to a certain extent as the nitrogen cycle is not interactive but the six carbon pools are live.	Krasting et al (2018) Dunne et al (2020)
GISS-E2-1-G	Goddard Institute for Space Studies, USA	GISS-E2.1 (2.5º x 2º, 144 x 90 longitude/latitude; 40 levels; top level 0.1 hPa)	GISS Ocean (1.25º x 1º; 288 x 180 longitude/latitude; 32 levels; top grid cell 0-10 m)	r101i1p1f1	Aerosol = Prescribed Land = GISS LSM, prescribed vegetation	NASA Goddard Institute for Space Studies (2018) Kelley et al (2020) Miller et al (2021)
GISS-E2-1-G-CC	Goddard Institute for Space Studies, USA	GISS-E2.1 (2.5º x 2º; 144 x 90 longitude/latitude; 40 levels; top level 0.1 hPa)	GISS Ocean (1.25º x 1º; 288 x 180 longitude/latitude; 32 levels; top grid cell 0-10 m)	r1i1p1f1	Aerosol = Prescribed Land = GISS LSM, prescribed vegetation, interactive carbon cycle	NASA Goddard Institute for Space Studies (2019a) Kelley et al (2020) Miller et al (2021)
GISS-E2-1-H	Goddard Institute for Space Studies, New York, USA	GISS-E2.1 (2.5º x 2º; 144 x 90 longitude/latitude; 40 levels; top level 0.1 hPa)	HYCOM Ocean (~1º tripolar grid; 360 x 180 longitude/latitude; 26 levels; top grid cell 0-10 m)	r10i1p1f1	Aerosol = Prescribed Land = GISS LSM, prescribed vegetation	NASA Goddard Institute for Space Studies (2019b) Kelley et al (2020)

HadGEM3-GC31-LL	Met Office Hadley Centre, UK	192 x 144, 85 levels, 135km MetUM-HadGEM3-GA7.1 (N96; 192 x 144 longitude/latitude; 85 levels; top level 85 km)	360 x 330, 75 levels (mainly 1º resolution, 1/3 degree in tropics) NEMO-HadGEM3-GO6.0 (eORCA1 tripolar primarily 1º with meridional refinement down to 1/3º in the tropics; 360 x 330 longitude/latitude; 75 levels; top grid cell 0-1 m)	r1i1p1f3	Aerosol = UKCA-GLOMAP-mode, dust included as a separate simulation to the other aerosols using CLASSIC scheme Land = dynamic vegetation in JULES-HadGEM3-GL7.1, different tile groupings.	Williams et al (2017) Ridley et al (2019a) Walters et al (2019)
HadGEM3-GC31-MM	Met Office Hadley Centre, UK	MetUM-HadGEM3-GA7.1 (N216; 432 x 324 longitude/latitude; 85 levels; top level 85 km)	NEMO-HadGEM3-GO6.0 (eORCA025 tripolar primarily 0.25º; 1440 x 1205 longitude/latitude; 75 levels; top grid cell 0-1 m)	r1i1p1f3	Aerosol = UKCA-GLOMAP-mode, dust included as a separate simulation to the other aerosols using CLASSIC scheme Land = dynamic vegetation in JULES-HadGEM3-GL7.1, different tile groupings.	Williams et al (2017) Ridley et al (2019b) Walters et al (2019)
IITM-ESM	Centre for Climate Change Research, Indian Institute of Tropical Meteorology Pune, India	IITM-GFSv1 (T62L64, Linearly Reduced Gaussian Grid; 192 x 94 longitude/latitude; 64 levels; top level 0.2 mb)	MOM4p1 (tripolar, primarily 1º; 360 x 200 longitude/latitude; 50 levels; top grid cell 0-10 m)	r1i1p1f1	Aerosol = prescribed using MAC-v2 Land = NOAH LSMv2.7.1	Swapna et al (2015) Raghavan & Panickal (2019)
INM-CM4-8	Institute for Numerical Mathematics, Russian Academy of Science, Russia	INM-AM4-8 (2x1.5º; 180 x 120 longitude/latitude; 21 levels; top level sigma = 0.01)	INM-OM5 (North Pole shifted to 60ºN, 90ºE; 360 x 318 longitude/latitude; 40 levels; sigma vertical coordinate)	r1i1p1f1	Aerosol = interactive using INM-AER1 Land = prescribed INM-LND1	Volodin et al (2019a) Volodin et al (2018)

INM-CM5-0	Institute for Numerical Mathematics, Russian Academy of Science, Russia	INM-AM5-0 (2x1.5º; 180 x 120 longitude/latitude; 73 levels; top level sigma = 0.0002)	INM-OM5 (North Pole shifted to 60ºN, 90ºE. 0.5x0.25º; 720 x 720 longitude/latitude; 40 levels; vertical sigma coordinate)	r10i1p1f1	Aerosol = interactive using INM-AER1 Land = prescribed using INM-LND1	Volodin et al (2019b) Volodin et al (2017)
IPSL-CM6A-LR	Institut Pierre Simon Laplace, France	LMDZ (NPv6, N96; 144 x 143 longitude/latitude; 79 levels; top level 40000 m)	NEMO-OPA (eORCA1.3, tripolar primarily 1º; 362 x 332 longitude/latitude; 75 levels; top grid cell 0-2 m)	r10i1p1f1	Aerosol = climatologies prescribed, the interactive option is not activated. Land = prescribed using ORCHIDEE (v2.0, Water/ Carbon/Energy mode)	Boucher et al (2018) Boucher et al (2020)
KACE-1-0-G	National Institute of Meteorological Sciences/Korea Meteorological Administration, Climate Research Division, Republic of Korea	MetUM-HadGEM3-GA7.1 (N96; 192 x 144 longitude/latitude; 85 levels; top level 85 km)	MOM4p1 (tripolar primarily 1º; 360 x 200 longitude/latitude; 50 levels; top grid cell 0-10 m)	r1i1p1f1	Aerosol = calculated using UKCA-GLOMAP-mode Land = prescribed vegetation within JULES-HadGEM3-GL7.1, with nine different categories using Land Use Harmonization data version 2 or data from the Max Planck Institute for Meteorology	Byun et al (2019) Lee et al (2020)
MCM-UA-1-0	Department of Geosciences, University of Arizona, USA	R30L14 (3.75 x 2.5º (long-lat) configuration; 96 x 80 longitude/latitude; 14 levels; top level 0.015 sigma, 15 mb)	MOM1.0 (MOM1, 1.875 x 2.5º; 192 x 80 longitude/latitude; 18 levels; top grid cell 0-40 m)	r1i1p1f1	Aerosol = Modifies surface albedos Land = simplified processes	Delworth et al (2002) Stouffer (2019)

MIROC-ES2L	JAMSTEC (Japan Agency for Marine-Earth Science and Technology, Japan), AORI (Atmosphere and Ocean Research Institute, The University of Tokyo, Japan), NIES (National Institute for Environmental Studies, Japan), and R-CCS (RIKEN Center for Computational Science, Japan)	CCSR AGCM (T42; 128 x 64 longitude/latitude; 40 levels; top level 3 hPa)	COCO4.9 (tripolar primarily 1°; 360 x 256 longitude/ latitude; 63 levels; top grid cell 0-2 m)	r10i1p1f2	Aerosol = dynamic elements within SPRINTARS6.0 Land = prescribed using MATSIRO6.0 + VISIT-e ver.1.0	Hajima et al (2019) Hajima et al (2020)
MIROC6	JAMSTEC (Japan Agency for Marine-Earth Science and Technology, Japan), AORI (Atmosphere and Ocean Research Institute, The University of Tokyo, Japan), NIES (National Institute for Environmental Studies, Japan), and R-CCS (RIKEN Center for Computational Science, Japan)	CCSR AGCM (T85; 256 x 128 longitude/latitude; 81 levels; top level 0.004 hPa)	COCO4.9 (tripolar primarily 1°; 360 x 256 longitude/ latitude; 63 levels; top grid cell 0-2 m)	r10i1p1f1	Aerosol = dynamic using SPRINTARS6.0 Land = prescribed in MATSIRO6.0	Tatebe & Watanabe (2018) Tatebe et al (2019)
MPI-ESM-1-2-HAM	ETH Zurich, Switzerland; Max Planck Institut fur Meteorologie, Germany; Forschungszentrum Julich, Germany; University of Oxford, UK; Finnish	ECHAM6.3 (spectral T63; 192 x 96 longitude/latitude; 47 levels; top level 0.01 hPa)	MPIOM1.63 (bipolar GR1.5, approximately 1.5°; 256 x 220 longitude/latitude; 40 levels; top grid cell 0-12 m)	r1i1p1f1	Aerosol = prescribed using HAM2.3 Land = Simulated using JSBACH 3.20	No experiment citation available. Mauritsen et al (2019)

	Meteorological Institute, Finland; Leibniz Institute for Tropospheric Research, Germany; Center for Climate Systems Modeling (C2SM) at ETH Zurich, Switzerland					
MPI-ESM1-2-HR	Max Planck Institute for Meteorology	ECHAM6.3 (spectral T127; 384 x 192 longitude/latitude; 95 levels; top level 0.01 hPa)	MPIOM1.63 (tripolar TP04, approximately 0.4°; 802 x 404 longitude/latitude; 40 levels; top grid cell 0-12 m)	r10i1p1f1	Aerosol = prescribed using MACv2-SP Land = prescribed within JSBACH3.20	Jungclaus et al (2019) Mauritsen et al (2019)
MPI-ESM1-2-LR	Max Planck Institute for Meteorology	ECHAM6.3 (spectral T63; 192 x 96 longitude/latitude; 47 levels; top level 0.01 hPa)	MPIOM1.63 (bipolar GR1.5, approximately 1.5°; 256 x 220 longitude/latitude; 40 levels; top grid cell 0-12 m)	r10i1p1f1	Aerosol = prescribed using MACv2-SP Land = Simlated using JSBACH3.20	Weiners et al (2019) Mauritsen et al (2019)
MRI-ESM2-0	Meteorological Research Institute, Japan	MRI-AGCM3.5 (TL159; 320 x 160 longitude/latitude; 80 levels; top level 0.01 hPa)	MRI.COM4.4 (tripolar primarily 0.5° latitude/ 1° longitude with meridional refinement down to 0.3 deg within 10 degrees north and south of the equator; 360 x 364 longitude/latitude; 61 levels; top grid cell 0-2 m)	r1i1000p1f1	Aerosol = prescribed using MASINGAR mk2r4 (TL95; 192 x 96 longitude/latitude; 80 levels; top level 0.01 hPa) Land = Prescribed using HAL 1.0	Yukimoto et al (2019a) Yukimoto et al (2019b)
NESM3	Nanjing University of Information Science and Technology, China	ECHAM v6.3 (T63; 192 x 96 longitude/latitude; 47 levels; top level 1 Pa)	NEMO v3.4 (NEMO v3.4, tripolar primarily 1°; 384 x 362 longitude/latitude; 46 levels; top grid cell 0-6 m)	r1i1p1f1	Aerosol = prescribed Land = dynamic vegetation within JSBACH v3.1	Cao and Wang (2019) Cao et al (2018)

NorESM2-LM	NorESM Climate modeling Consortium consisting of CICERO (Center for International Climate and Environmental Research, Oslo), MET-Norway (Norwegian Meteorological Institute, Oslo), NERSC (Nansen Environmental and Remote Sensing Center, Bergen), NILU (Norwegian Institute for Air Research, Kjeller), UiB (University of Bergen, Bergen), UiO (University of Oslo) and UNI (Uni Research, Bergen)	CAM-OSLO (2º resolution; 144 x 96; 32 levels; top level 3 mb)	MICOM (1º resolution; 360 x 384; 70 levels; top grid cell minimum 0-2.5 m [native model uses hybrid density and generic upper-layer coordinate interpolated to z-level for contributed data])	r1i1p1f1	Aerosol = natural emissions are interactive using OsloAero Land = prescribed within CLM	Seland et al (2019) Seland et al (2020)
NorESM2-MM	NorESM Climate modeling Consortium consisting of CICERO (Center for International Climate and Environmental Research, Oslo), MET-Norway (Norwegian Meteorological Institute, Oslo), NERSC (Nansen Environmental and Remote Sensing Center, Bergen), NILU (Norwegian Institute for Air Research, Kjeller), UiB	CAM-OSLO (1º resolution; 288 x 192; 32 levels; top level 3 mb)	MICOM (1 º resolution; 360 x 384; 70 levels; top grid cell minimum 0-2.5 m [native model uses hybrid density and generic upper-layer coordinate interpolated to z-level for contributed data])	r1i1p1f1	Aerosol = natural emissions are interactive using OsloAero Land = prescribed, CLM	Bentsen et al (2019) Seland et al (2020)

	(University of Bergen), UiO (University of Oslo) and UNI (Uni Research, Bergen)					
SAM0-UNICON	Seoul National University, Republic of Korea	CAM5.3 with UNICON (1°; 288 x 192 longitude/ latitude; 30 levels; top level ~2 hPa)	POP2 (Displaced Pole; 320 x 384 longitude/latitude; 60 levels; top grid cell 0-10 m)	r1i1p1f1	Aerosol = prescribed within MAM3 Land = prescribed within CLM4.0	Park and Shin (2019) Park et al (2019)
TaiESM1	Research Centre for Environmental Change, Taiwan	TaiAM1 (0.9° x 1.25°; 288 x 192 longitude/latitude; 30 levels; top level ~2 hPa)	POP2 (320 x 384 longitude/latitude; 60 levels; top grid cell 0-10 m)	r1i1p1f1	Aerosol = SNAP – parameterises in bulk. Land = CLM4.0 – prescribed vegetation but includes consideration of dust deposition and vegetation impacts on albedo.	Lee and Liang (2020) Lee et al (2020)
UKESM1-0-LL	Met Office Hadley Centre, UK and National Institute of Meteorological Sciences/Korea Meteorological Administration, Climate Research Division, Republic of Korea	MetUM-HadGEM3-GA7.1 (N96; 192 x 144 longitude/latitude; 85 levels; top level 85 km)	NEMO-HadGEM3-GO6.0 (eORCA1 tripolar primarily 1° with meridional refinement down to 1/3° in the tropics; 360 x 330 longitude/latitude; 75 levels; top grid cell 0-1 m)	r13i1p1f2	Aerosol = Dynamic using UKCA-GLOMAP-mode Land = Dynamic using JULES-ES-1.0	Byun (2020) Sellar et al (2019)

REFERENCES

1. Bader, D., Leung, R., Taylor, M. & McCoy, R. (2019b). E3SM-Project E3SM1.1 model output prepared for CMIP6 CMIP historical. Latest version. Earth System Grid Federation. https://doi.org/10.22033/ESGF/CMIP6.11485
2. Bader, D., Leung, R., Taylor, M. & McCoy, R. (2020). E3SM-Project E3SM1.1ECA model output prepared for CMIP6 CMIP historical. Latest version. Earth System Grid Federation. https://doi.org/10.22033/ESGF/CMIP6.11486
3. Bader, D., Leung, R., Taylor, M.& McCoy, R. (2019a). E3SM-Project E3SM1.0 model output prepared for CMIP6 CMIP historical. Latest version. Earth System Grid Federation. https://doi.org/10.22033/ESGF/CMIP6.4497
4. Bentsen, M., Oliviè, D., Seland, Ø., Toniazzo, T., Gjermundsen, A., Graff, L., Debernard, J., Gupta, A., He, Y., Kirkevåg, A., Schwinger, J., Tjiputra, J., Aas, K., Bethke, I., Fan, Y., Griesfeller, J., Grini, A., Guo, C., Ilicak, M., Karset, I., Landgren, O., Liakka, J., Moseid, K., Nummelin, A., Spensberger, C., Tang, H., Zhang, Z., Heinze, C., Iversen, T. & Schulz, M. (2019). *NCC NorESM2-MM model output prepared for CMIP6 CMIP historical*. Latest version. Earth System Grid Federation. https://doi.org/10.22033/ESGF/CMIP6.8040
5. Bi, D., Dix, M., Marsland, S., O'Farrell, S., Sullivan, A., Bodman, R., Law, R., Harman, I., Srbinovsky, J., Rashid, H.A. & Dobrohotoff, P. (2020) Configuration and spin-up of ACCESS-CM2, the new generation Australian Community Climate and Earth System Simulator Coupled Model. *Journal of Southern Hemisphere Earth Systems Science*, 70(1), pp.225-251.
6. Boucher, O., Denvil, S., Levavasseur, G., Cozic, A., Caubel, A., Foujols, M-A., Meurdesoif, Y., Cadule, P., Devilliers, M., Ghattas, J., Lebas, N., Lurton, T., Mellul, L., Musat, I., Mignot, J. & Cheruy, F. (2018). IPSL IPSL-CM6A-LR model output prepared for CMIP6 CMIP historical. Latest version. Earth System Grid Federation. https://doi.org/10.22033/ESGF/CMIP6.5195
7. Boucher, O., Servonnat, J., Albright, A., Aumont, O., Balkanski, Y., Bastrikov, V., Bekki, S., Bonnet, R., Bony, S., Bopp, L. & Braconnot, P. (2020). Presentation and evaluation of the IPSL-CM6A-LR climate model. *Journal of Advances in Modeling Earth Systems*, *12*(7), p.e2019MS002010.
8. Burrows, S., Maltrud, M., Yang, X., Zhu, W., Jeffrey, N., Shi, X., Ricciuto, D., Wang, S., Bisht, G., Tang, J., Wolfe, J., Harrop, B., Singh, B., Brent, L., Baldwin, S., Zhoul, T., Cameron-Smith, P., Keen, N., Collier, N., Xu., Hunke, E., Elliot, S., Turner, A., Li, H., Wang, H., Golaz, J., Bond-Lamberty, B., Hoffman, F., Riley, W., Thornton, P., Calvin, K. & Leung, L. (2020) The DOE E3SM v1.1biogeochemistry configuration: Description and simulated ecosystem-climate responses to historical changes in forcing. *Journal of Advances in Modeling Earth Systems*, 12, e2019MS001766. https://doi.org/10.1029/2019MS001766

9. Byun, Y-H. (2020). *NIMS-KMA UKESM1.0-LL model output prepared for CMIP6 CMIP historical*. Latest version. Earth System Grid Federation. https://doi.org/10.22033/ESGF/CMIP6.8379
10. Byun, Y-H., Lim, Y-J., Sung, H.M, Kim, J., Sun, M., Kim, B-H. (2019). NIMS-KMA KACE1.0-G model output prepared for CMIP6 CMIP historical. Latest version. Earth System Grid Federation. https://doi.org/10.22033/ESGF/CMIP6.8378
11. Cao, J. & Wang, B. (2019). *NUIST NESMv3 model output prepared for CMIP6 CMIP historical*. Latest version. Earth System Grid Federation. https://doi.org/10.22033/ESGF/CMIP6.8769
12. Cao, J., Wang, B., Yang, Y.M., Ma, L., Li, J., Sun, B., Bao, Y., He, J., Zhou, X. & Wu, L., (2018). The NUIST Earth System Model (NESM) version 3: description and preliminary evaluation. *Geoscientific Model Development*, *11*(7), pp.2975-2993.
13. Chai, Z. (2020) CAS CAS-ESM1.0 model output prepared for CMIP6 CMIP historical. Latest version. Earth System Grid Federation. https://doi.org/10.22033/ESGF/CMIP6.3353
14. Danabasoglu, G. (2019a) NCAR CESM2 model output prepared for CMIP6 CMIP historical. Latest version. Earth System Grid Federation. https://doi.org/10.22033/ESGF/CMIP6.7627
15. Danabasoglu, G. (2019b) NCAR CESM2-FV2 model output prepared for CMIP6 CMIP historical. Latest version. Earth System Grid Federation. https://doi.org/10.22033/ESGF/CMIP6.11297
16. Danabasoglu, G. (2019c) NCAR CESM2-WACCM model output prepared for CMIP6 CMIP historical. Latest version. Earth System Grid Federation. https://doi.org/10.22033/ESGF/CMIP6.10071
17. Danabasoglu, G. (2019d) NCAR CESM2-WACCM-FV2 model output prepared for CMIP6 CMIP historical. Latest version. Earth System Grid Federation. https://doi.org/10.22033/ESGF/CMIP6.11298
18. Danabasoglu, G., Lamarque, J.F., Bacmeister, J., Bailey, D.A., DuVivier, A.K., Edwards, J., Emmons, L.K., Fasullo, J., Garcia, R., Gettelman, A. & Hannay, C. (2020). The community earth system model version 2 (CESM2) *Journal of Advances in Modeling Earth Systems*, *12*(2).
19. Danek, C., Shi, X., Stepanek, C., Yang, H., Barbi, D., Hegewald, J. & Lohmann, G. (2020) AWI AWI-ESM1.1LR model output prepared for CMIP6 CMIP historical. Latest version. Earth System Grid Federation. https://doi.org/10.22033/ESGF/CMIP6.9328
20. Delworth, T., Stouffer, R., Dixon, K., Spelman, M., Knutson, T., Broccoli, A., Kushner, P. & Wetherald, R. (2002). Review of simulations of climate variability and change with the GFDL R30 coupled climate model. *Climate Dynamics*, *19*(7), pp.555-574.
21. Dix, M., Bi, D., Dobrohotoff, P., Fiedler, R., Harman, I., Law, R., Mackallah, C., Marsland, S., O'Farrell, S., Rashid, H., Srbinovsky, J., Sullivan, A., Trenham, C., Vohralik, P., Watterson, I., Williams, G., Woodhouse, M., Bodman, R., Dias,

F.B., Domingues, C., Hannah, N., Heerdegen, A., Savita, A., Wales, S., Allen, C., Druken, K., Evans, B., Richards, C., Ridzwan, S.M., Roberts, D., Smillie, J., Snow, K., Ward, M. & Yang, R (2019) CSIRO-ARCCSS ACCESS-CM2 model output prepared for CMIP6 CMIP historical. Latest vversion. Earth System Grid Federation. https://doi.org/10.22033/ESGF/CMIP6.4271

22. Döscher, R., Acosta, M., Alessandri, A., Anthoni, P., Arneth, A., Arsouze, T., Bergmann, T., Bernadello, R., Bousetta, S., Caron, L. & Carver, G. (2021). The EC-Earth3 earth system model for the climate model intercomparison project 6. Geoscientific Model Development Discussions, pp.1-90.
23. Dunne, J., Horowitz, L., Adcroft, A., Ginoux, P., Held, I., John, J., Krasting, J., Malyshev, S., Naik, V., Paulot, F. & Shevliakova, E. (2020). The GFDL Earth System Model version 4.1 (GFDL-ESM 4.1): Overall coupled model description and simulation characteristics. *Journal of Advances in Modeling Earth Systems*, 12(11), p.e2019MS002015.
24. EC-Earth Consortium (EC-Earth) (2019a). EC-Earth-Consortium EC-Earth3 model output prepared for CMIP6 CMIP historical. Latest version. Earth System Grid Federation. https://doi.org/10.22033/ESGF/CMIP6.4700
25. EC-Earth Consortium (EC-Earth) (2019b). EC-Earth-Consortium EC-Earth3-Veg model output prepared for CMIP6 CMIP historical. Latest version. Earth System Grid Federation. https://doi.org/10.22033/ESGF/CMIP6.4706
26. Golaz, J., Caldwell, P., Van Roekel, L., Petersen, M., Tang, Q., Wolfe, J., Abeshu, G., Anantharaj, V., Asay-Davis, X., Bader, D. & Baldwin, S. (2019) The DOE E3SM coupled model version 1: Overview and evaluation at standard resolution. *Journal of Advances in Modeling Earth Systems*, 11(7), pp.2089-2129.
27. Guangqing, Z., Yunquan, Z., Jinrong, J., He, Z., Baodong, W., Hang, C., Tianyi, W., Huiqun, H., Jiawen, Z., Liang, Y. & Minghua, Z. (2020) Earth system model: CAS-ESM. *Frontiers of Data and Computing*, 2(1), pp.38-54.
28. Guo, Y., Yu, Y., Lin, P., Liu, H., He, B., Bao, Q., Zhao, S. & Wang, X. (2020). Overview of the CMIP6 historical experiment datasets with the climate system model CAS FGOALS-f3-L. *Advances in Atmospheric Sciences*, 37(10), pp.1057-1066.
29. Hajima, T., Abe, M., Arakawa, O., Suzuki, T., Komuro, Y., Ogura, T., Ogochi, K., Watanabe, M., Yamamoto, A., Tatebe, H., Noguchi, M.A., Ohgaito, R., Ito, A., Yamazaki, D., Ito, A., Takata, K., Watanabe, S., Kawamiya, M. & Tachiiri, K. (2019). MIROC MIROC-ES2L model output prepared for CMIP6 CMIP historical. Latest version. Earth System Grid Federation. https://doi.org/10.22033/ESGF/CMIP6.5602
30. Hajima, T., Watanabe, M., Yamamoto, A., Tatebe, H., Noguchi, M.A., Abe, M., Ohgaito, R., Ito, A., Yamazaki, D., Okajima, H. & Ito, A. (2020). Development of the MIROC-ES2L Earth system model and the evaluation of biogeochemical processes and feedbacks. *Geoscientific Model Development*, *13*(5), pp.2197-2244.

31. He, B., Bao, Q., Wang, X., Zhou, L., Wu, X., Liu, Y., Wu, G., Chen, K., He, S., Hu, W. & Li, J. (2019). CAS FGOALS-f3-L model datasets for CMIP6 historical atmospheric model Intercomparison project simulation. *Advances in Atmospheric Sciences*, 36(8), pp.771-778.
32. Jungclaus, J., Bittner, M., Wieners, K-H., Wachsmann, F., Schupfner, M., Legutke, S., Giorgetta, M., Reick, C., Gayler, V., Haak, H., de Vrese, P., Raddatz, T., Esch, M., Mauritsen, T., von Storch, J-S., Behrens, J., Brovkin, V., Claussen, M., Crueger, T., Fast, I., Fiedler, S., Hagemann, S., Hohenegger, C., Jahns, T., Kloster, S., Kinne, S., Lasslop, G., Kornblueh, L., Marotzke, J., Matei, D., Meraner, K., Mikolajewicz, U., Modali, K., Müller, W., Nabel, J., Notz, D., Peters, K., Pincus, R., Pohlmann, H., Pongratz, J., Rast, S., Schmidt, H., Schnur, R., Schulzweida, U., Six, K., Stevens, B., Voigt, A. & Roeckner, E. (2019). *MPI-M MPI-ESM1.2-HR model output prepared for CMIP6 CMIP historical*. Latest version. Earth System Grid Federation. https://doi.org/10.22033/ESGF/CMIP6.6594
33. Kelley, M., Schmidt, G., Nazarenko, L., Bauer, S., Ruedy, R., Russell, G., Ackerman, A., Aleinov, I., Bauer, M., Bleck, R. & Canuto, V. (2020). GISS-E2. 1: Configurations and climatology. *Journal of Advances in Modeling Earth Systems*, *12*(8), p.e2019MS002025.
34. Krasting, J., John, J., Blanton, C., McHugh, C., Nikonov, S., Radhakrishnan, A., Rand, K., Zadeh, N., Balaji, V., Durachta, J., Dupuis, C., Menzel, R., Robinson, T., Underwood, S., Vahlenkamp, H., Dunne, K., Gauthier, P., Ginoux, P., Griffies, S., Hallberg, R., Harrison, M., Hurlin, W., Malyshev, S., Naik, V., Paulot, F., Paynter, D., Ploshay, J., Reichl, B., Schwarzkopf, D., Seman, C., Silvers, L., Wyman, B., Zeng, Y., Adcroft, A., Dunne, J., Dussin, R., Guo, H., He, J., Held, I., Horowitz, L., Lin, P., Milly, P., Shevliakova, E., Stock, C., Winton, M., Wittenberg, A., Xie, Y. & Zhao, M. (2018). NOAA-GFDL GFDL-ESM4 model output prepared for CMIP6 CMIP historical. Latest version. Earth System Grid Federation. https://doi.org/10.22033/ESGF/CMIP6.8597
35. Lee, J., Kim, J., Sun, M., Kim, B., Moon, H., Sung, H.M, Kim, J. & Byun, Y-H. (2020). Evaluation of the Korea meteorological administration advanced community earth-system model (K-ACE). *Asia-Pacific Journal of Atmospheric Sciences*, *56*(3), pp.381-395.
36. Lee, W-L. & Liang, H-C (2020). *AS-RCEC TaiESM1.0 model output prepared for CMIP6 CMIP historical*. Latest version. System Grid Federation. https://doi.org/10.22033/ESGF/CMIP6.9755
37. Lee, W-L., Wang, Y-C., Shiu, C-J., Tsai, I-c., Tu, C-Y., Lan, Y-Y., Chen, J-P., Pan, H-L. & Huang-Hsiung, H. (2020) Taiwan Earth System Model Version 1: description and evaluation of mean state. *Geoscientific Model Development*. 13, pp.3887-3904.
38. Mauritsen, T., Bader, J., Becker, T., Behrens, J., Bittner, M., Brokopf, R., Brovkin, V., Claussen, M., Crueger, T., Esch, M. & Fast, I. (2019). Developments in the MPI-M Earth System Model version 1.2 (MPI-ESM1. 2)

and its response to increasing CO2. *Journal of Advances in Modeling Earth Systems*, *11*(4), pp.998-1038.
39. Miller, R., Schmidt, G., Nazarenko, L., Bauer, S., Kelley, M., Ruedy, R., Russell, G., Ackerman, A., Aleinov, I., Bauer, M. & Bleck, R. (2021). CMIP6 Historical Simulations (1850–2014) With GISS-E2. 1. *Journal of Advances in Modeling Earth Systems*, *13*(1), p.e2019MS002034.
40. NASA Goddard Institute for Space Studies (NASA/GISS) (2018). NASA-GISS GISS-E2.1G model output prepared for CMIP6 CMIP historical. Latest version. Earth System Grid Federation. https://doi.org/10.22033/ESGF/CMIP6.7127
41. NASA Goddard Institute for Space Studies (NASA/GISS) (2019a). NASA-GISS GISS-E2-1-G-CC model output prepared for CMIP6 CMIP historical. Latest version. Earth System Grid Federation. https://doi.org/10.22033/ESGF/CMIP6.11762
42. NASA Goddard Institute for Space Studies (NASA/GISS) (2019b). NASA-GISS GISS-E2.1H model output prepared for CMIP6 CMIP historical. Latest version. Earth System Grid Federation. https://doi.org/10.22033/ESGF/CMIP6.7128
43. Park, S. & Shin, J. (2019). *SNU SAM0-UNICON model output prepared for CMIP6 CMIP historical*. Latest version. Earth System Grid Federation. https://doi.org/10.22033/ESGF/CMIP6.7789
44. Park, S., Shin, J., Kim, S., Oh, E. & Kim, Y. (2019). Global climate simulated by the Seoul National University atmosphere model version 0 with a unified convection scheme (SAM0-UNICON). *Journal of Climate*, *32*(10), pp.2917-2949.
45. Raghavan, K. & Panickal, S. (2019). CCCR-IITM IITM-ESM model output prepared for CMIP6 CMIP historical. Latest version. Earth System Grid Federation. https://doi.org/10.22033/ESGF/CMIP6.3708
46. Ridley, J., Menary, M., Kuhlbrodt, T., Andrews, M. & Andrews, T. (2019a). MOHC HadGEM3-GC31-LL model output prepared for CMIP6 CMIP historical. Latest version. Earth System Grid Federation. https://doi.org/10.22033/ESGF/CMIP6.6109
47. Ridley, J., Menary, M., Kuhlbrodt, T., Andrews, M. & Andrews, T. (2019b). MOHC HadGEM3-GC31-MM model output prepared for CMIP6 CMIP historical. Latest version. Earth System Grid Federation. https://doi.org/10.22033/ESGF/CMIP6.6112
48. Rong, X. (2019) CAMS CAMS_CSM1.0 model output prepared for CMIP6 CMIP historical. Latest version. Earth System Grid Federation. https://doi.org/10.22033/ESGF/CMIP6.9754
49. Rong, X., Li, J., Chen, H., Su, J., Hua, L., Zhang, Z. & Xin, Y. (2021) The CMIP6 historical simulation datasets produced by the climate system model CAMS-CSM. *Advances in Atmospheric Sciences*, 38(2), pp.285-295.
50. Seferian, R, (2018). CNRM-CERFACS CNRM-ESM2-1 model output prepared for CMIP6 CMIP historical. Latest version. Earth System Grid Federation. https://doi.org/10.22033/ESGF/CMIP6.4068

51. Séférian, R., Nabat, P., Michou, M., Saint-Martin, D., Voldoire, A., Colin, J., Decharme, B., Delire, C., Berthet, S., Chevallier, M. & Sénési, S. (2019) Evaluation of CNRM Earth System Model, CNRM-ESM2-1: Role of Earth System Processes in Present-Day and Future Climate. *Journal of Advances in Modeling Earth Systems*, 11(12), pp.4182-4227.
52. Seland, Ø., Bentsen, M., Olivié, D., Toniazzo, T., Gjermundsen, A., Graff, L.S., Debernard, J.B., Gupta, A.K., He, Y.C., Kirkevåg, A. & Schwinger, J. (2020). Overview of the Norwegian Earth System Model (NorESM2) and key climate response of CMIP6 DECK, historical, and scenario simulations. *Geoscientific Model Development*, *13*(12), pp.6165-6200.
53. Seland, Ø., Bentsen, M., Oliviè, D., Toniazzo, T., Gjermundsen, A., Graff, Lise S., Debernard, J., Gupta, A., He, Y., Kirkevåg, A., Schwinger, J., Tjiputra, J., Aas, K., Bethke, I., Fan, Y., Griesfeller, J., Grini, A., Guo, C., Ilicak, M., Karset, I., Landgren, O., Andreas; L., Johan; M., Kine O., Nummelin, A., Spensberger, C., Tang, H., Zhang, Z., Heinze, C., Iversen, T. & Schulz, M. (2019). *NCC NorESM2-LM model output prepared for CMIP6 CMIP historical*. Latest version. Earth System Grid Federation. https://doi.org/10.22033/ESGF/CMIP6.8036
54. Sellar, A., Jones, C., Mulcahy, J., Tang, Y., Yool, A., Wiltshire, A., O'connor, F., Stringer, M., Hill, R., Palmieri, J. & Woodward, S. (2019). UKESM1: Description and evaluation of the UK Earth System Model. *Journal of Advances in Modeling Earth Systems*, *11*(12), pp.4513-4558.
55. Song, Z., Qiao, F., Bao, Y., Shu, Q., Song, Y. & Yang, X. (2019). FIO-QLNM FIO-ESM2.0 model output prepared for CMIP6 CMIP historical. Latest version. Earth System Grid Federation. https://doi.org/10.22033/ESGF/CMIP6.9199
56. Stevens, B., Giorgetta, M., Esch, M., Mauritsen, T., Crueger, T., Rast, S., Salzmann, M., Schmidt, H., Bader, J., Block, K. & Brokopf, R. (2013) Atmospheric component of the MPI-M Earth system model: ECHAM6. *Journal of Advances in Modeling Earth Systems*, *5*(2), pp.146-172.
57. Stouffer, R. (2019). UA MCM-UA-1-0 model output prepared for CMIP6 CMIP historical. Latest version. Earth System Grid Federation. https://doi.org/10.22033/ESGF/CMIP6.8888
58. Swapna, P., Roxy, M., Aparna, K., Kulkarni, K., Prajeesh, A., Ashok, K., Krishnan, R., Moorthi, S., Kumar, A. & Goswami, B. (2015). The IITM earth system model: transformation of a seasonal prediction model to a long-term climate model. *Bulletin of the American Meteorological Society*, *96*(8), pp.1351-1367.
59. Swart, N., Cole, J., Kharin, V., Lazare, M., Scinocca, J., Gillett, N., Anstey, J., Arora, V., Christian, J., Jiao, Y., Lee, W., Majaess, F., Saenko, O., Seiler, C., Seinen, C., Shao, A., Solheim, L., von Salzen, K., Yang, D., Winter, B. & Sigmond, M. (2019a) CCCma CanESM5 model output prepared for CMIP6 CMIP historical. Latest version. Earth System Grid Federation. https://doi.org/10.22033/ESGF/CMIP6.3610

60. Swart, N., Cole, J., Kharin, V., Lazare, M., Scinocca, J., Gillett, N., Anstey, J., Arora, V., Christian, J., Hanna, S. & Jiao, Y. (2019b) The Canadian Earth System Model version 5 (CanESM5. 0.3). *Geoscientific Model Development*, *12*(11), pp.4823-4873.
61. Tatebe, H. & Watanabe, M. (2018). MIROC MIROC6 model output prepared for CMIP6 CMIP historical. Latest version. Earth System Grid Federation. https://doi.org/10.22033/ESGF/CMIP6.5603
62. Tatebe, H., Ogura, T., Nitta, T., Komuro, Y., Ogochi, K., Takemura, T., Sudo, K., Sekiguchi, M., Abe, M., Saito, F. & Chikira, M. (2019). Description and basic evaluation of simulated mean state, internal variability, and climate sensitivity in MIROC6. *Geoscientific Model Development*, *12*(7), pp.2727-2765.
63. Voldoire, A. (2018) CMIP6 simulations of the CNRM-CERFACS based on CNRM-CM6-1 model for CMIP experiment historical. Latest version. Earth System Grid Federation. https://doi.org/10.22033/ESGF/CMIP6.4066
64. Voldoire, A. (2019) CNRM-CERFACS CNRM-CM6-1-HR model output prepared for CMIP6 CMIP historical. Latest version. Earth System Grid Federation. https://doi.org/10.22033/ESGF/CMIP6.4067
65. Voldoire, A., Saint-Martin, D., Sénési, S., Decharme, B., Alias, A., Chevallier, M., Colin, J., Guérémy, J.F., Michou, M., Moine, M.P. & Nabat, P. (2019) Evaluation of CMIP6 deck experiments with CNRM-CM6-1. *Journal of Advances in Modeling Earth Systems*, *11*(7), pp.2177-2213.
66. Volodin, E., Mortikov, E., Gritsun, A., Lykossov, V., Galin, V., Diansky, N., Gusev, A., Kostrykin, S., Iakovlev, N., Shestakova, A. & Emelina, S. (2019a). INM INM-CM4-8 model output prepared for CMIP6 CMIP historical. Latest version. Earth System Grid Federation. https://doi.org/10.22033/ESGF/CMIP6.5069
67. Volodin, E., Mortikov, E., Gritsun, A., Lykossov, V., Galin, V., Diansky, N., Gusev, A., Kostrykin, S., Iakovlev, N., Shestakova, A. & Emelina, S. (2019b). INM INM-CM5-0 model output prepared for CMIP6 CMIP historical. Latest Version. Earth System Grid Federation. https://doi.org/10.22033/ESGF/CMIP6.5070
68. Volodin, E., Mortikov, E., Kostrykin, S., Galin, V., Lykossov, V., Gritsun, A., Diansky, N., Gusev, A., Iakovlev, N., Shestakova, A. & Emelina, S. (2018). Simulation of the modern climate using the INM-CM48 climate model. *Russian Journal of Numerical Analysis and Mathematical Modelling*, *33*(6), pp.367-374.
69. Volodin, E., Mortikov, E., Kostrykin, S., Galin, V., Lykossov, V., Gritsun, A., Diansky, N., Gusev, A. & Iakovlev, N. (2017). Simulation of the present-day climate with the climate model INMCM5. *Climate Dynamics*, *49*(11), pp.3715-3734.
70. Walters, D., Baran, A.J., Boutle, I., Brooks, M., Earnshaw, P., Edwards, J., Furtado, K., Hill, P., Lock, A., Manners, J. & Morcrette, C. (2019). The Met Office Unified Model global atmosphere 7.0/7.1 and JULES global land 7.0 configurations. *Geoscientific Model Development*, *12*(5), pp.1909-1963.

71. Wieners, K-H., Giorgetta, M., Jungclaus, J., Reick, C., Esch, M., Bittner, M., Legutke, S., Schupfner, M., Wachsmann, F., Gayler, V., Haak, H., de Vrese, P., Raddatz, T., Mauritsen, T., von Storch, J-S., Behrens, J., Brovkin, V., Claussen, M., Crueger, T., Fast, I., Fiedler, S., Hagemann, S., Hohenegger, C., Jahns, T., Kloster, S., Kinne, S., Lasslop, G., Kornblueh, L., Marotzke, J., Matei, D., Meraner, K., Mikolajewicz, U., Modali, K., Müller, W., Nabel, J., Notz, D., Peters, K., Pincus, R., Pohlmann, H., Pongratz, J., Rast, S., Schmidt, H., Schnur, R., Schulzweida, U., Six, K., Stevens, B., Voigt, A. & Roeckner, E. (2019). *MPI-M MPI-ESM1.2-LR model output prepared for CMIP6 CMIP historical*. Latest version. Earth System Grid Federation. https://doi.org/10.22033/ESGF/CMIP6.6595
72. Williams, K., Copsey, D., Blockley, E., Bodas-Salcedo, A., Calvert, D., Comer, R., Davis, P., Graham, T., Hewitt, H., Hill, R., Hyder, P., Ineson, S., Johns, T., Keen, A., Lee, R., Megann, A., Milton, S., Rae, J., Roberts, M., Scaife, A., Schiemann, R., Storkey, D., Thorpe, L., Watterson, I., Walters, D., West, A., Wood, R., Woollings, T. & Xavier, P. (2017). The Met Office global coupled model 3.0 and 3.1 (GC3.0 and GC3.1) configurations. *Journal of Advances in Modeling Earth Systems*, *1*0, pp.357–380. https://doi.org/10.1002/2017MS001115.
73. Wu, T., Chu, M., Dong, M., Fang, Y., Jie, W., Li, J., Li, W., Liu, Q., Shi, X., Xin, X., Yan, J., Zhang, F., Zhang, J., Zhang, L. & Zhang, Y (2018) BCC BCC-CSM2MR model output prepared for CMIP6 CMIP historical. Latest version. Earth System Grid Federation. https://doi.org/10.22033/ESGF/CMIP6.2948
74. Wu, T., Lu, Y., Fang, Y., Xin, X., Li, L., Li, W., Jie, W., Zhang, J., Liu, Y., Zhang, L. & Zhang, F. (2019) The Beijing Climate Center climate system model (BCC-CSM): The main progress from CMIP5 to CMIP6. *Geoscientific Model Development*, 12(4), pp.1573-1600.
75. Xin, Y., Dai, Y., Li, J., Rong, X. & Zhang, G. (2019) Coupling the common land model to echam5 atmospheric general circulation model. *Journal of Meteorological Research*, 33(2), pp.251-263.
76. Yu, Y. (2019). CAS FGOALS-f3-L model output prepared for CMIP6 CMIP historical. Latest version. Earth System Grid Federation. https://doi.org/10.22033/ESGF/CMIP6.3355
77. Yukimoto, S., Kawai, H., Koshiro, T., Oshima, N., Yoshida, K., Urakawa, S., Tsujino, H., Deushi, M., Tanaka, T., Hosaka, M. & Yabu, S. (2019b). The Meteorological Research Institute Earth System Model version 2.0, MRI-ESM2. 0: Description and basic evaluation of the physical component. *Journal of the Meteorological Society of Japan. Ser. II*.
78. Yukimoto, S., Koshiro, T., Kawai, H., Oshima, N., Yoshida, K., Urakawa, S., Tsujino, H., Deushi, M., Tanaka, T., Hosaka, M., Yoshimura, H., Shindo, E., Mizuta, R., Ishii, M., Obata, A. & Adachi, Y. (2019a). *MRI MRI-ESM2.0 model output prepared for CMIP6 CMIP historical*. Latest version. Earth System Grid Federation. https://doi.org/10.22033/ESGF/CMIP6.6842

79. Zhang, J., Wu, T., Shi, X., Zhang, F., Li, J., Chu, M., Liu, Q., Yan, J., Ma, Q. & Wei, M. (2018) BCC BCC-ESM1 model output prepared for CMIP6 CMIP historical. Latest version. Earth System Grid Federation. https://doi.org/10.22033/ESGF/CMIP6.2949
80. Ziehn, T., Chamberlain, M., Law, R., Lenton, A., Bodman, R., Dix, M., Stevens, L., Wang, Y. & Srbinovsky, J. (2020) The Australian Earth System Model: ACCESS-ESM1.5. *Journal of Southern Hemisphere Earth Systems Science*, 70(1), pp.193-214.
81. Ziehn, T., Chamberlain, M., Lenton, A., Law, R., Bodman, R., Dix, M., Wang, Y., Dobrohotoff, P., Srbinovsky, J., Stevens, L., Vohralik, P., Mackallah, C., Sullivan, A., O'Farrell, S. & Druken, K. (2019) CSIRO ACCESS-ESM1.5 model output prepared for CMIP6 CMIP historical. Latest version. Earth System Grid Federation. https://doi.org/10.22033/ESGF/CMIP6.4272